WIRELESS CLOSED-LOOP FEEDBACK SYSTEMS FOR AUTOMATIC DETECTION AND SUPPRESSION OF NOCICEPTIVE SIGNALS

by

AYDIN FARAJIDAVAR

Presented to the Faculty of the Graduate School of

The University of Texas at Arlington in Partial Fulfillment

of the Requirements

for the Degree of

DOCTOR OF PHILOSOPHY

THE UNIVERSITY OF TEXAS AT ARLINGTON

AUGUST 2011

ACKNOWLEDGEMENTS

I would like to express my appreciation and gratitude to my supervising mentor Dr. J.-C. Chiao. This thesis could not have been accomplished without his wise guides, restless enthusiasm and support throughout my doctoral study, which have always encouraged me through the discovery of unknowns. I would like to express my deepest gratitude to: Dr. Y. B. Peng for his patience and supports in training me as a neuroscientist; Dr. K. Behbehani for teaching me fundamentals of signal processing and consistent advising during these years; Dr. M. Romero for teaching me principles of physiology and helping me in the experiments; Drs. S. Sparagana, M. R. Delgado and H.F. Tibbals for their constructive suggestions.

My sincere appreciation extends to C. E. Hagains, J. W. He, and J. Seifert, for their kind assistance in the animal facility and all the other students who worked with me during these years: P. G. McCorkle, T. W. Wiggins, S. M. Athar, R. M. Askari. Thanks to all of my friends in iMEMS group for their constructive suggestions during 110 meetings.

Last but not least, I would like to thank my parents, my sister and specially my lovely wife for their endless love and carefulness during the thesis progress.

This project was sponsored by the NSF, ECS Division, IHCS Program, Texas Norman Hackerman Advanced Research Program (003656-0071-2009) and Intel Corp.

April 8, 2011

ABSTRACT

WIRELESS CLOSED-LOOP FEEDBACK SYSTEMS FOR AUTOMATIC DETECTION AND SUPPRESSION OF NOCICEPTIVE SIGNALS

Aydin Farajidavar, PhD

The University of Texas at Arlington, 2011

Supervising Professor: Jung-Chih Chiao

Chronic pain is an important public health issue. Several approaches have been implemented for management of chronic pain, including surgical implantation of neurostimulators. Neurostimulators have been used in clinics for spinal cord implantation and they have been suitable for relieving certain types of pains, such as neuropathic pain in leg or arm, complex regional pain, and refractory angina. The stimulation at spinal cord has little relieving effects on syndromes such as facial pain, cluster headache, phantom limb pain, and post stroke pain. For treating such syndromes, electrical stimulation of deep brain structures such as thalamic nuclei (e.g. ventroposterolateral (VPL) or ventroposteromedial (VPM)), periaqueductal gray (PAG), periventricular gray (PVG), anterior cingulate cortex (ACC) and other regions near the central gray has been clinically suggested.

After implantation of neurostimulators in the spinal cord or brain, physicians adjust the stimulation parameters based on the patients' verbal description of pain at the time or their own judgment of the pain suppression effect during the trial period. Doctors do not have a way to physiologically document the pain signals in a quantitative way. Hence, from the hardware

perspective, the currently available neurostimulators perform in an open-loop fashion. This type of open-loop, continuously-operating stimulators are not adaptive and do not consider continuous neural feedback from the patient. Therefore, they are not always effective, and can give rise to stimulation-induced side effects. In contrast, several researchers have proposed the need for a closed-loop real-time system in neurostimulation to overcome these problems. A closed-loop feedback approach can provide a higher efficiency in terms of reduction in battery power consumption that will allow the implant to stay longer time in the patient's body, and reduction of side effects or syndromes such as excitotoxicity, leading to apoptosis.

In order to maximize the desired outcomes, we designed and developed wireless systems and indices that can detect the nociception automatically based on neurological signals. The developed wireless system for acquiring ECoG signals included a front-end that could be worn by small laboratory animals, and a back-end that could be connected to a computer and interface with the user through a graphical user interface (GUI). The front-end included an analog based and a 2.4 Ghz transceiver (nRF24Le1, Nordic Semmiconductor) that included an analog to digital converter (ADC), a microcontroller and a transceiver. Furthermore, the platform was utilized to develop new applications of wireless technology for acquiring transcranial motor evoked potentials (TcMEP) and slow wave gastric electrical activity. These two systems were characterized and evaluated on animal models.

We utilized extracellular single unit action potential signals from wide dynamic range (WDR) neurons in dorsal horn spinal cord and thalamus to detect nociception and make a closed-loop system. In addition, we have exploited electrocorticography (ECoG) in somatosensories and motor cortices to establish indices for objective detection of pain. Results showed that the WDR neurons in the spinal cord can be used to differentiate between graded mechanical stimuli, while WDR neurons in the thalamus can only be used to differentiate between the low and high intensity mechanical stimuli. Investigation of ECoG signals in rodent models showed that sharp pain caused by thermal stimulus leaves a peak signature in the time-

domain signal and a difference in both Delta and Gamma band frequencies while; the dull pain caused by chemical stimulus only increases the Gamma frequency bands.

WDR neurons in the spinal cord were utilized to develop a closed-loop feedback system that could acquire single-unit extracellular neuronal signals from the dorsal horn spinal cord in real-time and distinguish between the graded mechanical stimuli, i.e. brush (non painful), pressure (border between non-painful and painful) and pinch (painful). After setting, the system could automatically distinguish between the painful and non-painful signals and generated electrical stimulation during the painful signals. The indirect evidence of the decrease in the mean rate of the action potentials suggested that the system was able to inhibit the nociceptive signals.

I conducted the majority of the work in this dissertation and received minor assistance from other students including Christopher E. Hagains, Philip G. McCorkle, Timothy W. Wiggins Jennifer L. Seifert, Ramin M. Askari, Shariq M. Athar, Greg O'grady and Leo K. Cheng to whom I am grateful and have acknowledged their contribution in my manuscripts which I first-authored. However, all the results and figures (except Figs. 1.1 and 3.1) in this dissertation are original and generated by me and they are not published in any other manuscript, dissertation or thesis.

TABLE OF CONTENTS

LIST OF ILLUSTRATIONS

LIST OF TABLES

CHAPTER 1

INTRODUCTION

1.1 Why Pain

The primary role of the sensory systems in animals is to inform the brain about the state of the external and internal environment of the organism. Pain is one of the prominent outputs of the sensory system and defined as a perception advantaged by only highly evolved animals. The primary goal of this perception is to help the organism to protect itself against environmental perils [1.1] through triggering reactions and inducing learned avoidance behaviors, which may decrease whatever is causing the pain and, as a result, may limit the potentially damaging consequences. The complexity of pain network often addressed as nociceptive systems, has augmented during evolution as a result of the pressure to avoid organic lesions or their exacerbation [1.2].

According to the International Association for the Study of Pain (IASP), pain is defined as “An unpleasant sensory and emotional experience associated with actual or potential tissue damage, or described in terms of such damage” [1.3]. Generally, pain is divided into acute and chronic pain. Although unpleasant, acute pain is not considered as an important public health problem, while chronic pain causes major impacts on public. More than 50 million Americans are partially or totally disabled from their pain. Medical economists estimated that the total direct and indirect cost of pain in the US exceeds 100 billion dollars annually [1.4]. Chronic pain often produces various psychosocial problems such as fear, depression, isolation and anxiety, which further interferes with sleep quality, work, self-esteem, marital and family relationships. The impacts of pain suffering are not only on individual’s life quality [1.5] but also on the family [1.6-8], society [1.9] and national economics [1.10-12]. Chronic pain is also the most common cause of long-term disability.

Furthermore, the inability to communicate verbally from an animal does not negate the possibility that a subject is experiencing pain. In 1986, Zimmermann re-defined the IASP definition of pain so that it could be applied to animals: “an aversive sensory experience caused by actual or potential injury that elicits progressive motor and vegetative reactions, results in learned avoidance behavior, and may modify species specific behavior, including social behavior” [1.13]. Because of the subjectiveness nature of the pain, researchers perceive pains in animals throughout specific behaviors such as motor responses (withdrawal, jumping, contractures, etc.), licking and vocalization [1.14, 1.15]. Since animals cannot verbally communicate, the understanding of the behavioral mechanisms caused by pains has been lacking compared to clinical studies in human [1.2]. Therefore, an objective criterion for quantification and evaluation of pains in animals seems critical for animal behavior studies.

According to the National Institutes of Health (NIH), outcomes for individuals experiencing chronic pain can be improved by **predicting** the onset of pain, **personalizing** pain management strategies, and **preempting** the long-term adverse effects of intense, prolonged, or chronic pain [1.16]. All of the current approaches for pain treatments including, medications (muscle relaxants, narcotics and other analgesics), physical therapies, injections, behavioral treatments, surgery, neurostimulation (peripheral nerve, spinal cord and deep brain), implanted pumps, and nerve ablation, fail to satisfy predicting and personalizing criteria required by NIH. However, neurostimulation has several significant advantages among the treatments. First, it can be very effective for certain conditions with little side effects. Second, the implanted device can be controlled by patients or doctors with little risk of addiction or overdose. Third, the implant could be removed if it does not achieve the desired level of pain or symptom relief. Still neurostimulations cannot satisfy the first two required criteria of NIH. The reason is that they perform in an open-loop fashion hence; they cannot ***predict*** the pain occurrence of pain or ***personalize*** the pain management strategy. After implantation, physicians tune the stimulator based on patient’s subjective understanding of pain and doctors cannot physiologically

document the pain signals in a quantitative way. Furthermore, physicians have to use trial and error method to find an appropriate therapeutic electrical stimulation parameter (dose) among several thousand combinations of electrical stimuli [1.17] to inhibit pain. Hence, the therapeutic effect among patients varies dramatically from 24-100% which yields the the current procedure depends on the patient's or physician's skill in tuning the neurostimulator. The consequence results in inefficient neurostimulator that delivers non-optimized electrical stimulus for pain treatment.

1.2 Pain Physiology

We know the world through our sensory systems, one of which is the somatosensory (touch, temperature and pain). Somatosensory is controlled by the sophisticated nervous system. Any disturbance of the system at any level will cause dysfunction of the sensory perception, including pain. Harmful stimuli to the skin or subcutaneous tissue (joints or muscle), are received by nociceptors (thermal, mechanical, and polymodal). This nociception travels to the dorsal horn of the spinal cord through Aδ and C fibers. The response of the spinal cord dorsal horn neurons are typically classified as low threshold (LT), high threshold (HT), and wide dynamic range (WDR) neurons according to their response to graded mechanical stimuli [1.18]. Among these types of neurons, WDR neurons are the only ones that respond to both Aδ and C fibers. In addition, WDR neurons have the capacity to precisely encode the intensity of a nociceptive stimulus [1.19]. Therefore, they can be used effectively to recognize the nociceptive signal.

After the pain signal reaches to the spinal cord, it transmits to the brain through five major paths, known as pain pathways [1.20]. Among these pathways, spinothalamic tract is the most prominent ascending nociceptive pathway in the spinal cord. It comprises the axons of nociceptive-specific and WDR in laminae I and V-VII of the dorsal horn. Spinomesencephalic tract is the other prominent pathway that comprises the axons of neurons in laminae I and V. It projects to the periaqueductal gray matter, and via the spinoparabrachial tract, it projects to the

parabrachial nuclei. In turn, neurons of the parabrachial nuclei project to the amygdala, a major component of the limbic system, involved in emotion. Thus, the spinomesencephalic tract is thought to contribute to pain recognition. In addition, using local field potentials, Green et al. [1.21] have shown neural signatures of neuropathic pain in thalamus and PAG. Midbrain periaqueductal gray matter (PAG) is also a crucial component of the descending pain inhibition system. It has been well documented that the activation of this system inhibits behavioral responses to painful stimuli and the activity of nociceptive neurons in the dorsal horn of the spinal cord [1.22].

As mentioned in the background section, there are five major pathways in the pain and many structures of the brain are involved in pain perception. Figure 1.1 shows different brain structures and their possible interaction. These structures include primary and secondary somatosensory cortices (S1, S2, red and orange), anterior cingulate cortex (ACC, green), insula (blue), thalamus (yellow), and prefrontal cortex (PF, purple), primary and supplementary motor cortices (M1 and SMA), posterior parietal cortex (PPC), posterior cingulate (PCC), basal ganglia (BG, pink), hypothalamus (HT), amygdala (AMYG), parabrachial nuclei (PB), and periaqueductal gray (PAG) [1.23]. Among these structures, PAG and thalamus are also well

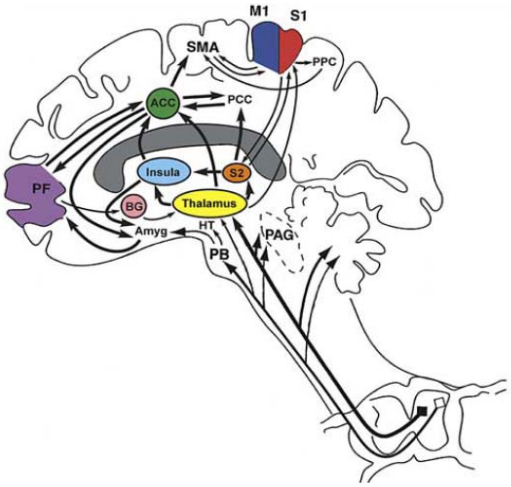

Figure 1.1 Schematic diagram of the main anatomical components of the ‘pain matrix’, and their possible functional significance [1.23].

known for inhibiting the pain if electrically stimulated [1.24, 1.25, 1.26]. Furthermore, there are evidences of neural signatures of pain in both thalamus and PAG in humans that directly correlates to the subjective reporting of pain intensity [1.27]. Therefore, these areas (thalamus and PAG) can be targeted for both pain recognition and inhibition.

The PAG comprises heterogeneous cell populations surrounding the cerebral aqueduct. It extends rostrally from the pericoerulear area of the pons to the opening of the third ventricle. As described above, electrical stimulation of the PAG produces behaviorally measurable antinociception. A substantial body of evidence supports the view that the PAG play critical roles in integrating the somatic, autonomic and antinociceptive components, which characterize the distinct emotional coping reactions evoked by pain of different tissue origins and/or durations [1.28].

Thalamus has been recognized to play a very important role in the higher-level processing of nociceptive inputs. As mentioned before, the major pathway involved in the relay of nociceptive information is the STT. Although the STT is frequently described as a single tract, nociception terminates in two of thalamic components, lateral and the ventral. The lateral STT originates largely from lamina I of the superficial dorsal horn and contains many neurons responding specifically to noxious stimuli and innocuous termoreceptive neurons. In contrast, the ventral STT originates largely from neurons in deeper layers (IV and V), most of which respond to innocuous tactile and proprioceptive input in addition to nociceptive inputs. Overall, there are six major regions of termination of the STT within the primate thalamus: the ventroposterior nucleus (VP), the posterior portion of the ventomedial nucleus (VMpo), the ventrolateral nucleus (VL), the central lateral nucleus (CL), the parafascicular nucleus (Pf) and the ventrocaudal portion of the medial dorsal nucleus (MDvc) [1.20, 1.26, 1.29]. Among these nuclei VP, which comprises ventroposterior lateral (VPL) and ventroposterior medial (VPM), is well established for both pain recognition and inhibition in human [1.27, 1.30, 1.31] and rats [1.32, 1.33]. VP is considered the main relay nucleus for nociceptive inputs involved in

mediating the sensory aspects of pain. In the rat, both nociceptive-specific (NS) and WDR neurons are reported throughout VP [1.34], which can facilitate the recognition task (similar algorithms of aim 2). Furthermore, it has been revealed that the main source of STT in VP is from the neurons in the deep dorsal horn (laminae IV and V) [1.26]; the same laminae we are recording WDR neurons in aim 2. In rats, VP is located approximately 3.6 mm caudal from bregma, 3 mm lateral left from the midline, and 6 mm deep from the brain surface [1.35].

1.3 Neuronal Signaling

The purpose of the nervous system is to perceive the information through peripheral nervous system (PNS) and transfer them to the central nervous system (CNS), process the information in the CNS, and send back information to the PNS. This transfer of information from the external environment, through neurons, and back again to the external environment is known as neuronal signaling. Neurons utilize various ions (e.g. Na^+, K^+, Cl^- and Ca^{2+}) for propagating and processing the information and overall constitute an electro-chemical mean for signaling. Scientists record neuronal signaling in different ways two of which are called extracellular single-unit recording and electrocorticography [1.20].

1.3.1 Extracellular Single-unit Action Potentials

An action potential is a short-lasting (about 1 ms) event in which the potential of the cell membrane rises and falls rapidly, following a stereotyped trajectory. Action potentials are generated by special types of voltage-gated ion channels embedded in the cell's membrane. These channels are closed when the membrane potential is near the resting potential of the cell, but they rapidly begin to open if the membrane potential increases to a precisely defined threshold value. When the channels open, they allow an inward flow of sodium ions, which changes the electrochemical gradient. In order to record this potential change, researchers insert microelectrodes – very fine wires usually made from tungsten or platinum-iridium alloys – in the extracellular environment of neurons. The microelectrode detects electrical activity generated by the neurons adjacent to the electrode tip [1.20].

1.3.2 Electrocorticography

A summation of the synchronous activity of thousands or millions of neurons of the brain, can be detected through electroencephalography (EEG) or electrocorticography (ECoG). Both EEG and ECoG show oscillations at a variety of frequencies. Several of these oscillations have characteristic frequency ranges, spatial distributions and are associated with different states of brain functioning (e.g., waking and the various sleep stages). EEG and ECoG have conventionally provided valuable information on the mechanisms of brain activities and their relation to subject behaviors [1.36, 1.37]. EEG records signals from the surface of the skull while ECoG acquires signals from the surface of the Dura of the brain, hence, provide a better spatial resolution, broader bandwidth and higher characteristic amplitude than EEG; hence, more robust to motional noises, which are due to the freely behaving subject [1.38].

1.4 Technologies in Pain Management

Several approaches for the pain treatment have been used including, medications (muscle relaxants, narcotics and other analgesics), physical therapies, injections, behavioral treatments, surgery, neurostimulation (peripheral nerve, spinal cord and deep brain), implanted pumps, and nerve ablation. However, all of these approaches failed to meet the three criteria defined by NIH. Among the treatments, neurostimulation has several significant advantages. First, it can be very effective for certain conditions with little side effects. Second, the implanted device can be controlled by patients or doctors with little risk of addiction or overdose. Third, the implant can be removed if it does not achieve the desired level of pain or symptom relief.

Depending on the location of the stimulations, there are five major types of electrical stimulations: transcutaneous, peripheral nerve, epidural spinal cord, motor cortex and deep brain. The following briefly describes each of these techniques:

Transcutaneous electrical nerve stimulation (TENS) is the application of electrical stimulation of various frequencies, amplitudes (intensity) and pulse durations to the skin of the subject for the purpose of pain relief [1.39]. TENS has been used for many years to manage a

range of acute and chronic pain problems and it is generally believed to be a safe, non-invasive procedure which may produce significant analgesia in patients with moderate pain associated with a range of conditions [1.40]. It is used in a variety of clinical settings to treat diverse acute and chronic pain conditions, and although clinical studies of its long-term efficacy have yielded variable results, it has become popular with both patients and health professionals of different disciplines, including physiotherapists, midwives, nurses and doctors. The most commonly types of TENS used in clinics are high-frequency, low-intensity (conventional) TENS and low-frequency, high-intensity (acupuncture-like) TENS [1.41, 1.42]. Conventional TENS stimulates large-diameter (Aβ) afferent nerve fibers that modulate onward transmission input of afferent nociceptive in the dorsal horn of the spinal cord. High-frequency TENS that has been used in animal models of inflammatory pain, increased the extracellular concentration of gamma-aminobutyric acid in the spinal cord and decreased central sensitization and primary hyperalgesia [1.43]. Acupuncture-like TENS (AL-TENS) mostly stimulates Aδ fibers and cause analgesia by modulating the descending pain inhibitory pathways in the spinal cord [1.42]. Overall, there are insufficient evidences to draw any conclusions about the effectiveness of TENS for the treatment of chronic pain in human [1.44].

Peripheral nerve stimulation (PNS) which was started in 1960s, showed promise in the management of neuropathic pain that cannot be relieved with other forms of neurostimulation or pharmacological treatments [1.45]. The main limitation to efficient treatment relies on the availability of specific electrodes that conform to the size and morphology of the target nerves and are highly reliable. Unfortunately, the early experiences of PNS failed because of the unreliable equipments, however, PNS has evolved recently due to the development of the the electrodes and equipments. Food and Drug Administration (FDA) has approved the procedure for PNS in association with a radio frequency receiver-transmitter system. Treatment parameters for PNS commonly range from 0.5-2 V intensity, 120-180 ms pulse width and 50-90 Hz frequency [1.46].

Spinal cord stimulation (SCS), was first reported in humans in 1967 by Shealy and colleagues [1.47]. Similar to PNS, this technique slowed down because of the hardware limitations in 1970's. However, with the improvement in hardware and simplification of procedure with introducing epidural approach in 1980's, the SCS became popular and it is now routinely practiced in clinics to treat many chronic pain conditions [1.48]. The SCS is particularly beneficial in relieving pain in patients with neuropathic pain in leg or arm and complex regional pain syndrome (CRPS) [1.49, 1.50]. The stimulation at spinal cord has little relieving effects on syndromes such as facial pain, cluster headache, phantom limb pain, and post stroke pain [1.51, 1.52]. The hardware for SCS includes of leads, extension and implantable pulse generator (IPG). The leads are placed in the epidural space usually in thoracic and cervical spine for leg and arm pain coverage, respectively. The actual stimulation happens from electrodes, placed at the tip of the lead. An electrical field resulted from the electrical stimulation from IPG, reaches the dorsal columns of the spinal cord and modulates the pain transmission. In a comprehensive study, Cameron reported the pain reduction percentage of 26-88% among 616 patients with Back and leg pain and 57-100% among 260 patients with CRPS [1.53].

Motor cortex stimulation (MCS) and deep brain stimulation are the two other techniques used to treat chronic pains that are not curable with more conservative procedures. For treating syndromes such as facial pain, cluster headache, phantom limb pain, and post stroke pain, electrical stimulation of deep brain structures such as thalamic nuclei (e.g. ventroposterolateral (VPL) or ventroposteromedial (VPM)), periaqueductal gray (PAG), periventricular gray (PVG), anterior cingulate cortex (ACC), motor cortex and other regions near the central gray has been clinically suggested [1.24, 1.54, 1.55, 1.56]. The surgical techniques for implantation of the electrodes have been developed significantly due to the neuronavigation and application of computed tomography (CT) or magnetic resonance imaging (MRI). The success rate of the procedure ranges from 44-88% depending on the cases [1.45].

Still none of the neurostimulation methods mentioned above can predict or personalize pain treatment automatically. The main reason is that the currently available stimulators perform in an open-loop fashion. After implantation, physicians tune the stimulator based on patient's subjective understanding of pain [1.57] and doctors cannot physiologically document the pain signals in a quantitative way. Obviously, this procedure does not work for infants, children, patients with brain stroke who cannot describe the type, degree, or location of pain they are experiencing. In contrast, several researchers have proposed the need for a closed-loop real-time system in deep brain stimulator (DBS) treatments [1.24, 1.57]. The closed-loop approach can potentially satisfy all three required criteria by NIH. Furthermore, the closed-loop approach can provide more efficient stimulations with fewer side effects than the indiscriminate methods currently used [1.24]. The efficiency of the system can be increased in terms of reduction in battery power consumption that will allow the implant to stay longer in the patient's body and reduction of side effects or syndromes such as excitotoxicity, which causes the death of neurons [1.58, 1.59].

1.5 Wireless Technologies for Acquiring Neuronal Signals

For the past few decades, the field of neural recording systems has drawn many attention and interest. We have divided the developed systems into the systems for acquiring single-unit action potentials form the extracellular environment and electrocorticography or electroencephalography systems for recording signals from the surface of the cortex or skull. A summary of the efforts to make these systems are explained below.

1.5.1 Extracellular Single-unit Action Potentials

Prior to the 1990s, there were few experiments conducted with meaningful wireless extracellular neural recordings. At the time, it was a major challenge to develop robust telemetry systems to acquire extracellular signals because of the low amplitude of the signals (50-500 μV), and high frequency band (upto 10 kHz). In 1994, Akin and Najafi developed an inductively powered implantable neural recording system with CMOS interface circuitry and telemetry. The

system could handle neural recordings of ± 500 μV signals from regenerated peripheral nerve axons. The ASIC was dissipating 15 mW of power from a 5V supply, and sized 4 × 4 mm^2 on chip [1.60]. Later in 1998, they developed an implantable, fully integrated, multi-channel extracellular neural recording system [1.61]. Their new system including the RF interface circuitry contained over 5000 transistors, had two front-end neural amplifiers, and sized 4 × 6 mm^2 on chip. However, a big problem of this system is the 90 mW power consumption and the limited recording sites from two simultaneous channels. In 1997, Song et al. also reported a single-chip system for the acquisition, digitization, and wireless telemetry of biological signals [1.62]. The problem with this single-channel system was that it consumed 10 mW of power, which was not quite efficient. In 2005, P. Mohseni et al. developed an 8-ch system with the total size of 2.1 × 2.1 × 0.16 cm^3 that was operated at 94~98 MHz carrier frequency, powered with two 1.5 V batteries, and consumed a 2.05 mW power, however, the system suffered huge channel crosstalk (more than 37.1% crosstalk), the bandwidth was only 150 kHz and their front-end amplifier had large input referred noise (~10μVrms) [1.63].

In 2006, Harrison et al. developed a wireless recording system with 100 electrodes which interfaced Utah Microelectrode Array [1.64]. The 433MHz FSK wireless transmitter provided 330kbps data rate. The complete system was implemented in the 0.5 μm 3-metal 2-poly standard CMOS process, sized 4.7 × 5.9 mm^2, and consumed a total power of 13.5 mW. However, the system had only low bandwidth, could only transfer a single channel high resolution data at a time and the transmitting distance was only 2 cm. In 2008, Chae et al. developed a 128 channel wireless system with 6-9 bits of resolution per channel [1.65]. The system utilized ultra-wide-band (UWB) wireless link that transmitted upto 90Mbps data. The entire system was implemented in a 0.35 μm 4-metal 2-ploy CMOS process and consumed 6mW power. The total chip area for this system was reported to be 8.8 × 7.2 mm^2, however, no in vivo recording results reported for this system.

1.5.2 Electrocorticography

One of the leading wireless systems for acquiring EEG/ECoG was developed by Modareszadeh and Schmidt in 1997. The system was low power, had 32 channels, utilized ISM-band RF (902-928 MHz) system for real-time monitoring and evaluations of epilepsy [1.66]. However, the system was bulky (6.4 × 5.1 × 1 cm^3) and weighted 68g. Irazoqui-Pastor et al. reported *in vivo* EEG recordings from un-tethered rodents using an inductively powered implantable wireless neural recording device in 2003 [1.67]. The disadvantage of that system is it only has one channel. In 2008, Mollazadeh et al. presented a 16-channel wireless system that was powered by a separate telemetry chip, which harvested power from a 4 MHz inductive link. The telemetry module was also used to transmit data over the same link to the base station across 4 cm distance at up to 32 kbps. Obviously this system was limited by the transmitting distance and data rate [1.68]. Lapray et al. presented a single channel ECoG system that could be implanted in the small laboratory animals and used for long-term acquisition of signals in freely moving animals [1.69]. Recently, Charvet and colleagues developed a low power, 64-channel system for recording Electrocorticogram (ECoG). The system utilizes a custom integrated circuit (ASIC) for conditioning and digitizing the analog signals and commercial components for wireless transmission. It supports the RF transmission of 32 channels (among 64 channels available) sampled at 1 kHz per channel with a 12-bit resolution. The wireless communications utilizes 402-405 Mhz. which is within the MICS band (Medical Implant Communication Service) and can achieve a data rate of 480 kbps. This system is powered through an inductive link at 13.56 MHz able and can provide up to 100mW (30mA at 3.3V). However, the size of this system is not suitable to be either implanted or worn by the animal [1.70].

CHAPTER 2

WIRELESS MULTICHANNEL PLATFORM

2.1 Introduction

Electroencephalography (EEG) and electrocorticography (ECoG) have conventionally provided valuable information regarding brain activities. ECoG acquires signals below electrodes placed on the surface of the brain making contact with the dura mater. Such contact is able to provide better spatial resolution, broader bandwidth and higher characteristic amplitudes than EEG [2.1, 2.2]. Recording either signal in animal models has traditionally been done via wired equipments, which not only restricts locomotion, but may also add stress factors to animals' current physiological state [2.3]. Thereby, wireless technology that has positively affected a number of medical fields [2.4] has been deployed to solve this dilemma. Furthermore, the telemetric recordings of the EEG/ECoG signals in freely moving mammals helps to recognize the different brain waves associated with various motor reactions as well as vegetative reactions [2.5, 2.6].

Several systems have previously been proposed for wireless recording of either EEG or ECoG. Telemetric systems with appropriate size and weight have been developed for acquiring the signals in rodents [2.7, 2.8, 2.9]; however, they are designed to record signals from only one active electrode and they do not provide sufficient communication bandwidth to acquire signals from multiple active electrodes. On the other hand, wireless systems capable of acquiring signals from multi active electrodes have been developed more recently [2.10, 2.11, 2.12]. However, because of the bulkiness, they could not practically be used to study small animal models. Therefore, a multichannel system that can acquire ECoG signals from multiple electrodes in small animals with high fidelity and low power consumption is desired.

A number of required characteristics for telemetric recording systems suitable for long-term data acquisition in small freely moving animal models under stress-free conditions have been suggested by [2.6, 2.7, 2.13]. We have concluded that the criteria include: (1) The size and weight of the telemetric front-end transponder on the animal should be small and light enough to be carried by the animal without adding stress or pain. (2) The energy consumption of the front-end should be as low as possible and the battery should be easily accessible for replacement. (3) The wireless transmission range should be at least a few meters so the animals can easily explore their environment. (4) The wireless communication bandwidth and module sampling rates should be sufficient for recording signals in several brain regions. (5) The total cost of the system should be reasonable so it can be used for recording a large population of animals to gain statistical accuracy.

We have developed a prototype system that can acquire ECoG signals from small laboratory animals according to the aforementioned criteria. The characteristics of the system were evaluated in bench top settings and compared to a commercially-available wired system. The wireless system was then tested on rats in various experimental settings to make sure that it can practically be used for animal behavioral studies.

2.2 Materials and Methods

The system is comprised of a front-end transmitter that can be worn and carried by a small animal and a back-end receiver connected to a computer via a custom-made graphical user interface (GUI). The front-end acquires the signals from implanted electrodes on the animal's brain and transmits them wirelessly to the back-end through a 2.4-GHz transceiver. The back-end receives the data packets and feeds them through a universal asynchronous receiver/transmitter (UART) serial port to a GUI developed in LabVIEW (National Instrument). Figure 2.1 shows the block diagram of the system.

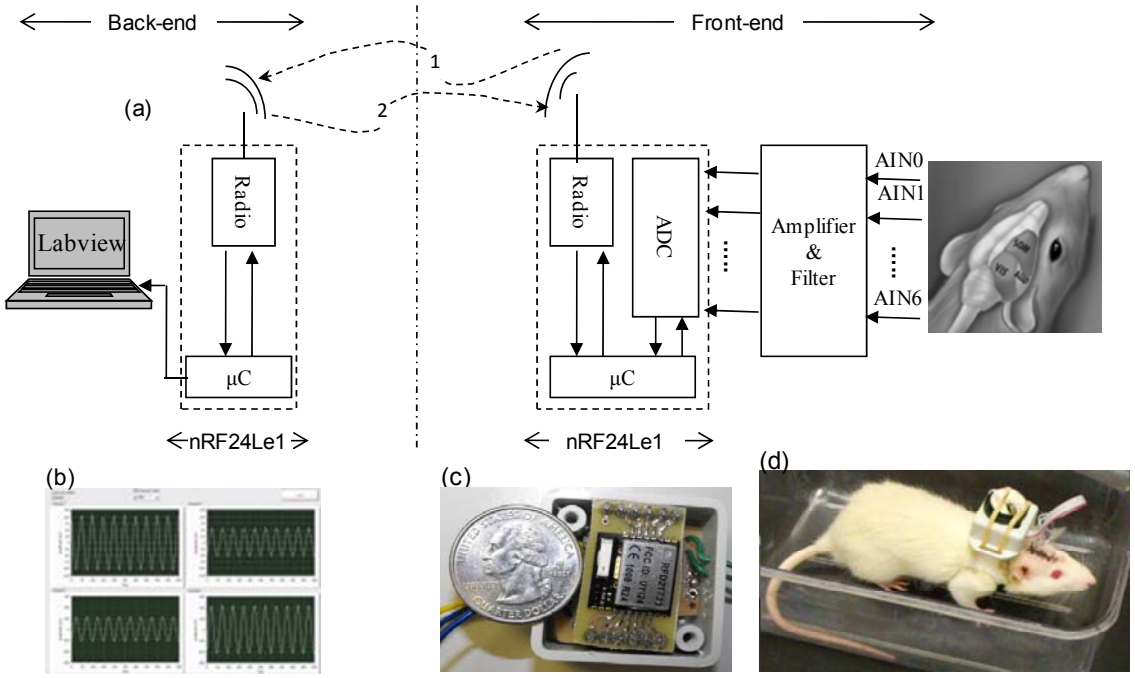

Figure 2.1 (a) The block diagram of the telemetric system developed for acquiring ECoG signals that includes a front-end and a back-end. (b) The front panel of the graphical user interface (GUI) developed in LabVIEW showing acquired ECoG signals. (c) The fabricated front-end module. (d) The front-end on a roaming animal after the animal recovered from surgery.

2.2.1 Front-end Design and Fabrication

The front-end includes an analog board, an analog to digital converter (ADC), a microcontroller and a transceiver. The analog board, which includes seven identical channels, is designed to amplify and filter out unwanted signals. Each channel utilizes an instrumentational amplifier (INA333, Texas Instruments) with a gain of 10 and an operational amplifier (TLV2464, Texas Instruments) with a gain of 500. A band-pass filter with passband cut-offs at 1 Hz and 170 Hz is used to eliminate the DC offset and undesirable high-frequency signals. The output of the op-amp is fed to an ADC that is controlled by the microcontroller. Signal is sampled at a rate of 1 ksps per channel and digitized with a resolution of 8 bits. The microcontroller acquires the signals from the ADC and loads them into a 2.4-GHz transceiver. Therefore, at any given moment, one sample from each channel is acquired and loaded into a payload with a size of 7 bytes. The payload is then transmitted to the receiver back-end and turned into the receiving

mode. The back-end transceiver received the payload, turned into the transmitting mode, and sent an acknowledgement to the front-end. If an acknowledgement is not received by the front-end, the same payload is retransmitted once again. This retransmission function is designed to increase the fidelity of the wireless communication. Figure 2.2 shows the flow chart in both μCs of front- and back-ends. In the front-end, after the μC acquired data from ADC (step 1) and loaded it into the radio (step 2), the radio turned into the transmitting mode, which took 130 μs, and transmitted the data packets (step 3). Then the radio took another 130 μs returning back to the receiving mode (step 4). At the same time, the radio in the back-end that was in the receiving mode looked for the data (step 5). If it received the packet, it turned into the transmitting mode and sent back an acknowledgement to the front-end (step 6) while loading the data on the UART (universal asynchronous receiver/transmitter, at 500 kBaud) to be sent to the computer (step 7) as the μC on the front-end loaded the next set of data into the radio. If the data packet was not received by the back-end, without the acknowledgement packet the radio on the front-end re-transmitted the data packet to the back-end (back to step 3) until attainment was verified. The re-transmitting procedure mainly depended on the sampling rate of the μC and the time for each packet to travel in air, which varies between the three systems.

Each packet is composed of 1 preamble byte, 3 to 5 address bytes, up to 32 bytes of payload and 1 to 2 bytes for cyclic redundancy check (CRC). The time on air TOA can be calculated from TOA = (Packet length)/(Air data rate). The air data rate was chosen to be 1 Mbps and the packet length differed in each application. The following explains the detailed specifications on each system [2.14].

An nRF24LE1 (Nordic semiconductor) that combines an ADC, an 8051 microcontroller and a 2.4-GHz transceiver with a maximum transmitting rate of 2 Mbps is used to interface the analog board. We specifically utilize a 4×4 mm QFN24 package integrated with a chip antenna available through RFD21731, RFDigital Corp. on a PC board. The front-end is encased in a plastic enclosure, provided by Hammond Manufacturing, 35×35×20mm, and powered by a 3 V,

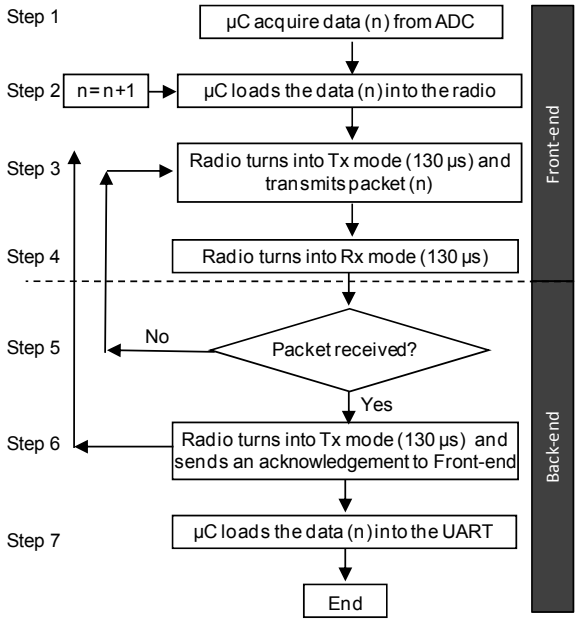

Figure 2.2 The flow chart for the µC in the front and back-ends to ensure reliable communication.

560 mAh, coin cell battery, Panasonic, (23×5.4mm). The battery lies on top of the plastic box that may be replaced conveniently without opening the enclosure. The overall size and weight of the front-end (including electronics, battery and plastic enclosure) is 35×35×27mm and 30 g, respectively. These parameters allow ease in encasing the device within a jacket to be worn by a freely-moving rat (Fig. 2.1 (c) and (d)).

2.2.2 Back-end Design and Fabrication

The back-end is also composed of a microcontroller and a 2.4-GHz transceiver combined in one chip, the nRF24LE1. The transceiver radio on the back-end is in the listening mode by default and only converts to a transmitter mode to send back an acknowledgement packet to the front-end. It receives packets (that include 7-bytes) from the front-end transmitter and the microcontroller put the data on a UART interface with a maximum baud rate of 500 k. Therefore, each 7-byte packet, with each byte representing one sample from the recording channels, is received by the custom-made GUI developed in LabVIEW (Fig. 2.1 (b)). In the computer, each packet is split into seven arrays. Therefore, the first packet constitutes the first sample of each array and the second packet is the second sample of each array, and so forth.

The GUI displays individual plots of current samples (up to 1000) of each channel as well as a plot containing current data from all channels integrated together. An additional graph is designed to show all of the channels and keep the traces in the graph accumulatively. This graph provides the user the ability to scroll back and forth to observe changes in the signals in on- and off-line. The data acquired from all channels can be saved individually at the end of the experiment.

2.2.3 Experimental Procedures for Acquiring ECoG

In one experimental setting, ECoG signal was acquired for an hour from the left S1HL of the anesthetized animal with both a commercial instrument (CED 1401Plus, Cambridge Electronic Design) and our developed wireless module. It was then saved for further comparison to ensure that the characteristics of the wireless and wired system are essentially identical.

Afterward, in another experimental setting, five-minute signal recordings were acquired from all four regions of interest during three different conditions: under anesthesia, twenty minutes after anesthesia (wakefulness) and after injecting a 3% solution of formalin to the animal's right paw. All of the experiments were in accordance with the guidelines published by the Committee for Research and Ethical Issues of the International Association for Study of Pain [2.15].

2.3. Results

2.3.1 Performance in Bench-top and Anesthetized Animal Set up

Bench-top experiments were performed using sinusoidal waveforms produced by a function generator at amplitudes ranging from 10 to 300 μV. Spectral responses of the analog board were measured in the frequency range from 0.1 to 1000 Hz. The 3dB-band passed was obtained in the range of 1-170 Hz for all the various amplitudes. Figure 2.3 (a) shows a typical frequency response at 100 μV. The same pass band was obtained for each individual channel after combining the analog board with the nRF24Le1, yielding no distortion in the wireless

communication. Various sinusoidal waveforms with different amplitudes and frequencies were produced and simultaneously fed to all of the channels (up to seven) of the wireless system and recorded to verify that the system is capable of concurrent acquisition of signals from multiple channels. The wireless communication range of the system was measured to be 30 m outdoors and 10 m indoors. The power consumption of the transponder front-end was observed to be 21 mW at 3 V at full load (i.e. 7-channels). Thus, the system is capable of continuously recording signals for up to 80 hours with the designated coin cell battery (560 mAh).

ECoG signals were simultaneously recorded by both the wired and wireless systems for an hour. The top and bottom traces in Figure 2.3 (b) show seven seconds of the retrieved data for the wired and wireless recordings respectively. Some of the characteristic peaks present in both systems are identified with dashed arrows. For further comparison, the relative power spectrum of each of these signals is plotted in Figure 2.3 (c) and (d) for the wired and wireless systems. A few critical peaks distinguished with numbers 1-3 and the ratios between the peaks were measured. This fraction between peaks 1/2, 2/3 and 1/3 were measured to be 1.01, 0.72 and 0.79 in both the wired and wireless systems.

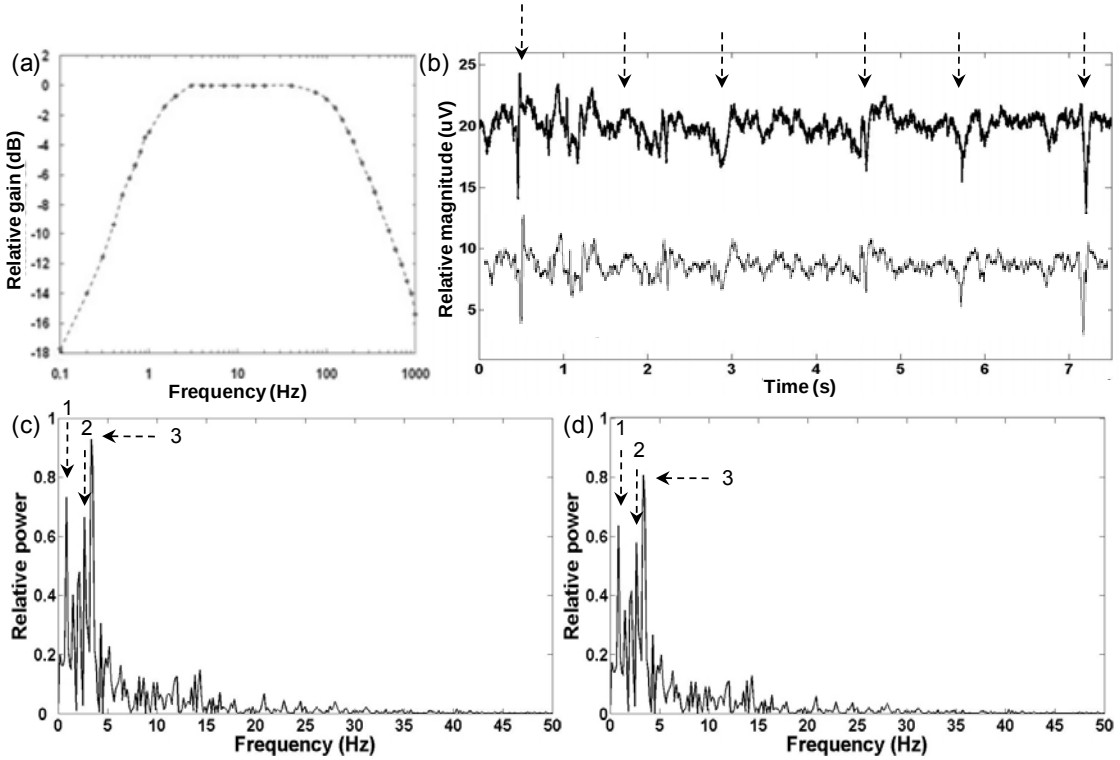

Figure 2.3 (a) The frequency response of the analog board in response to sinusoidal waveforms with 100 μV amplitude, (b) seven seconds of a one hour recording simultaneously acquired by both wired (top panel) and wireless (bottom panel) systems with some characteristic peaks emphasized by dashed arrows. The relative power spectrum is plotted in (c) for the wired system and (d) for the wireless system. A few characteristic peaks that essentially match in (c) and (d) are numbered from 1 to 3.

2.3.2 Performance in Lightly Anesthetized and Freely Roaming Animal Set up

ECoG signals were simultaneously recorded from the left and right S1HL and M1 during three different conditions. In the first setting, signals were acquired from the animal under light anesthesia for five minutes. Figure 2.4 (a) shows one second of the typical signal during this period and 2.4 (b) shows the power spectrum of the same section. One hour after the animal recovered from anesthesia, ECoG signals were acquired for another five minutes while the animal was wandering in its cage. One second of the typical time-domain signal and associated power spectrum of this period are plotted in figures 2.4 (c) and (d) respectively. Finally, ECoG signals were recorded after 0.05 ml of 3% formalin was injected into the right hind paw. The one-second signal plotted in figure 2.4 (e) and the relevant power spectrum (Fig. 2.4

(f)) were taken from an additional five-minute recording acquired twenty minutes after formalin injection.

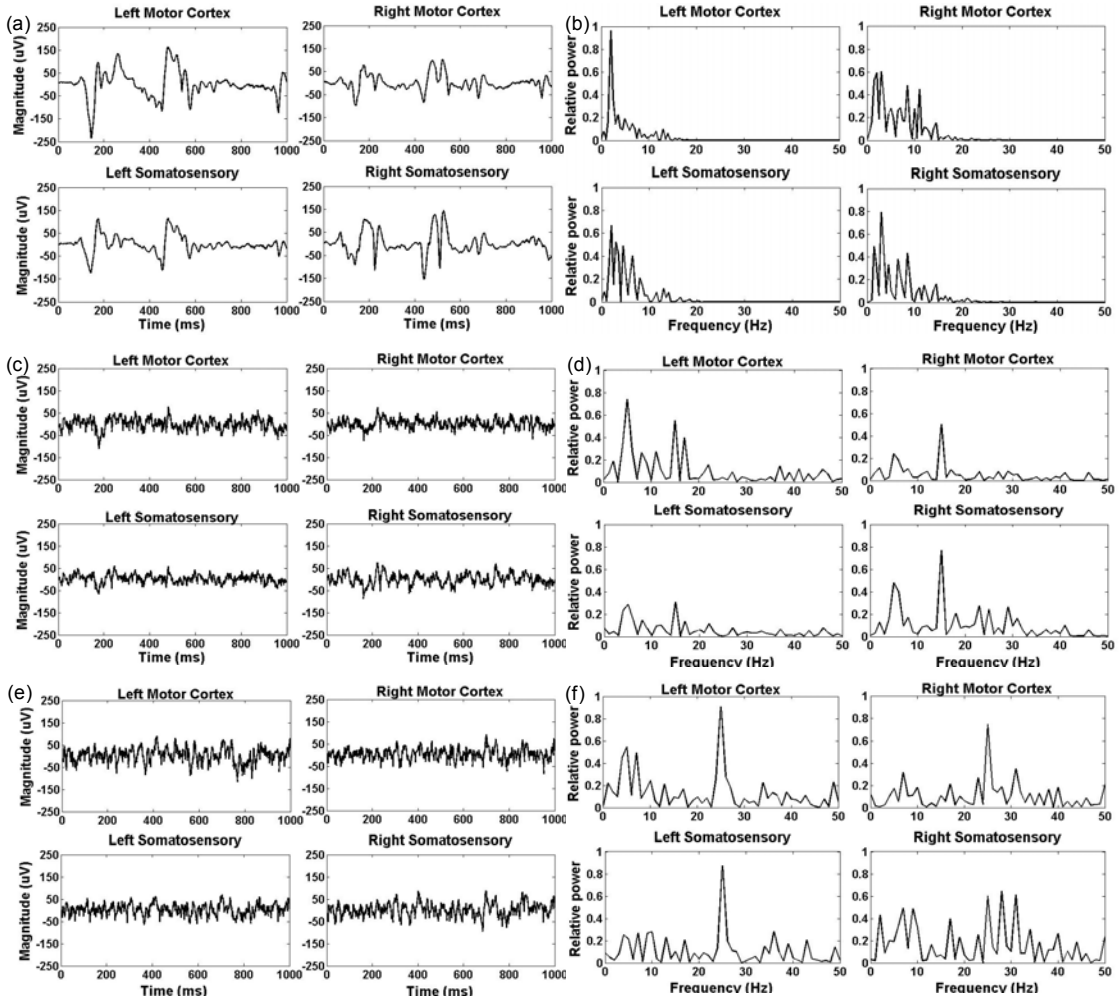

Figure 2.4 (a) The one-second period of the signal taken from left and right S1HL and M1 of the rat during periods of (a) light anesthesia (c) wakefulness and (e) bearing pain (after formalin injection) on left column and their associated power spectrum plotted respectively in (b), (d) and (f) on the right column.

2.4. Discussion and Conclusion

A telemetry system was designed and fabricated to record and transmit ECoG and EEG signals from up to seven channels in freely behaving animals within an acceptable range for various experimental procedures in laboratories. The small size and light weight of the transmitting front-end provides the advantage of using the system in both small and large

laboratory animals. The power consumption of the front-end transponder is reasonable and could work consistently for 80 hours based on a 560-mAh coin cell rechargeable battery, which is sufficient to provide valuable information. All of the components utilized to fabricate the system are commercially available within a reasonable range; hence, it is affordable for all the researchers to use this platform. The performance of the system was examined in both bench-top and a rodent model.

In the bench top setting, the system was able to accurately record various waveforms of different amplitudes and frequencies produced by a signal generator. Various signals were fed simultaneously to different channels and recorded successfully, proving that that the channels are perfectly isolated and are not affected by one another. The 3 dB-pass band of the system shown in Figure 2.3 (a) provided an acceptable range for acquiring ECoG signals. The comparison between the time-domain signal of the wired and wireless systems did not show any sensible difference and, as indicated by the arrows, most of the peaks present in both signals are identical in both systems. The slight difference between the signals may be due to the difference in the sampling rate and filtering set up. However, the power spectral density of the two systems did not show any difference in either shape or ratio of the essential peaks.

Furthermore, the retransmit function is designed to guarantee wireless communication between the front-and back-end. The maximum number for re-transmission is determined by the sampling rate of the ADC on the front-end. The lower the sampling rate, the higher the number of retransmission can be performed by the transceiver and microcontroller. With the current sampling rate of 1ksps, the transponder retransmits the packet 2 times upon request. Since there is no need for deep implantation of the ECoG system, two retransmissions guarantees the fidelity of wireless communication.

In order to prove the capability of this system in concurrent recording of ECoG signals from different brain regions in a behaving animal, signals were acquired from both left and right somatosensory and motor cortices during three different conditions of anesthesia, wakefulness

and pain. Figures 2.4 (a), (c) and (e) illustrate that the system was able to acquire ECoG signals simultaneously under these varying conditions without suffering distortion from the animal locomotion, since the signals recorded during the anesthesia had even higher magnitudes in general when compared to the signals recorded while the animal was awake and moving around. Considering the amplitude and frequency criteria, the recorded signals are in good agreement with previous studies [2.16, 2.17]. Furthermore, the power spectral density plotted in figures 2.4 (b), (d) and (f) showed distinct frequency bands of less than 10 Hz for the anesthesia condition, between 10-20 Hz during wakefulness, and 20-30 Hz for the pain condition. These frequency bands obtained during anesthesia and wakefulness conditions are also compatible with other studies conducted by [2.18] and [2.19, 2.20]. Nevertheless, more statistical experiments need to be conducted to confirm these obtained results.

CHAPTER 3

METHODS TO DETECT NOCICEPTION

Considering the Spinothalamic pathway for pain, nociception was detected through three different methods: 1- single-unit recording of wide dynamic range neurons of dorsal horn spinal cord, 2- single-unit recording of wide dynamic range neurons located in ventral posterior (VP) nucleus of the thalamus and 3- electrocorticography from somatosensory of hind limb (S1HL) and motor cortices of both right and left side. Each method and related results are explained in the following.

3.1 Utilizing Extracellular Single- unit Signaling from Spinal Cord

The objective in this experiment was to establish a reliable a criteria to detect nociceptive signal through spinal cord. In the following the methodology, animal experiments and obtained results have been described.

3.1.1. Methodology

3.1.1.1 Recording sites

A tungsten microelectrode (10–12 MΩ, FHC) was used for single-unit extracellular electrophysiological recordings in the spinal cord dorsal horn, where nociceptive primary afferent fibers terminate. The electrode was connected to the wireless head stage. Neurons in the left L5 region were targeted, and it was tried to include at least one WDR neuron in each experiment, however, other neurons firing with smaller action potential amplitudes were also recorded, due to the nature of the recording. The raw signals were digitized through 1401plus CED (Cambridge Electronic Design), fed and stored into a computer in which the Spike2 program analyzed and separated the main cell signals from those fired by other cells off-line after each experiment. The off-line signal processing took a significant amount of time so this

task could not be done in real time. Each recording included at least one WDR neuron to make use of its graded responses to innocuous and noxious stimuli. In other words, innocuous stimuli (less intense) evoke a low rate of neuronal firing, whereas noxious stimuli (more intense) evoke a high rate of neuronal firing [3.1, 3.2]. The neuronal responses to each mechanical stimulus were measured as the number of action potentials (APs) per second in Spike2.

3.1.1.2 Mechanical stimuli

Graded mechanical (brush, pressure and pinch) stimuli were applied to a receptive field in the left hind paw to evoke neuronal responses in the spinal cord. Brush was applied by a camel hairbrush moving over the receptive fields in a rhythmic fashion for innocuous stimulation. Pressure was applied by a venous bulldog clamp (6 cm long, straight, serrated jaws), which bordered innocuous and noxious. Pinch was applied by an arterial bulldog clamp (3 cm long, straight, serrated jaws) as a noxious stimulus. Each mechanical stimulus was applied once for 10 seconds with an inter-stimulus interval (rest) of 20 seconds as a 90-second sequence of (brush-rest-pressure-rest-pinch-rest). Totally three sets of stimuli were applied to the hind paw in each experiment: the first one for control, the second one with electrical stimulation, and the last one for recovery with one minute between each segment. In order to quantitatively analyze the pain level we measured the applied force (F) as a function of displacement (x) of the clamp. The results shown in Figure 3.1 demonstrate that the spring constant of the clamp follows the Hooke's law F=kx, where the slope k is. The slopes were obtained as 31.17 N/m for the pressure and 57.3 N/m for the pinch stimuli. The rat's paw was pressed within the area of 25-mm^2 (A), and the clamp opened by 3 mm, therefore the mechanical pressures were obtained as 0.54 psi for the pressure stimulus and 0.99 psi for the pinch stimulus, respectively, calculated by P = F/A = kx/A [3.3]. According to several studies [3.4, 3.5], applying a force of 140 to 600 g/mm^2 (0.81 to 3.51 psi) (with arterial clip) to the rat's paw, causes nociception. In human, pain threshold with a comparable compression stimulus has been shown to be ~80 g/mm^2 (~0.46 psi) [3.6].

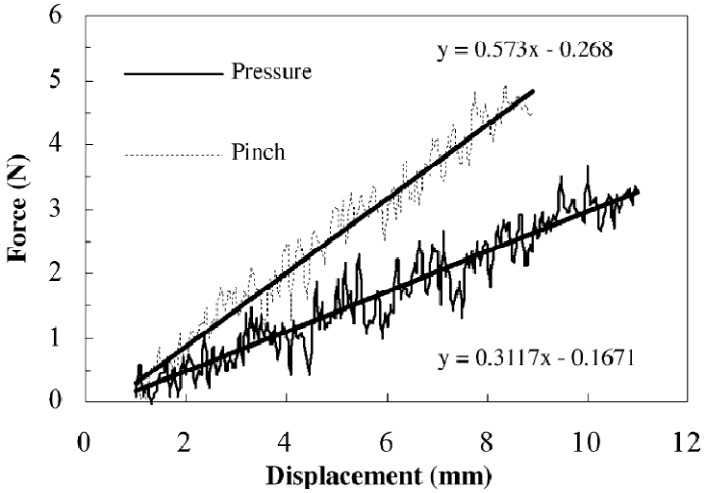

Figure 3.1 Measured force as a function of displacement for the clips used for mechanical stimuli [3.3].

3.1.2. Animal Experiment

Seven male Sprague–Dawley rats (450 and 550 g) were used for the experiments. Mechanical stimuli were applied to the left hind paw, neuronal signal were acquired from the left lumbar section of the spinal cord and electrical stimulations were applied to the right PAG for each rat. All surgical procedures were approved by the University of Texas at Arlington Institutional Animal Care and Use Committee. The procedures were in accordance with the guidelines published by the Committee for Research and Ethical Issues of the International Association for Study of Pain [3.7].

Animals were anesthetized using sodium pentobarbital (50 mg/kg, i.p.). A 3–4 cm laminectomy was done over the lumbosacral enlargement. A jugular vein cannulation was performed so that anesthesia could be maintained by intravenous administration of sodium pentobarbital at a rate of 5 mg/ml per hour. A cannula was inserted into the trachea for artificial respiration as needed. The pupil reflex was monitored periodically to ensure a proper depth of anesthesia. Following surgery, the spinal cord was fixed in a stereotaxic frame. The dura mater was removed to expose the nerves and covered with mineral oil to preserve moisture. Finally, a

craniotomy was done to expose the brain for stimulation. The end tidal CO2 was maintained at around 30mmHg and the body temperature was kept at 37 ºC using a feedback controlled heating pad and a rectal thermal sensor probe.

3.1.3. Results

Fifty-three neurons were recorded from the dorsal horn of the spinal cord from seven rats. The mean rate of action potentials per second ± standard error of the mean is plotted in figure 3.2. The responses for (control and recovery) obtained as follow: (1) brush: (8.20 ± 1.06, 8.69 ± 1.27); (2) pressure: (25.10 ± 3.05, 27.46 ± 3.86); and (3) pinch: (35.01 ± 3.98, 33.08± 3.91). A 3 x 3 repeated measure Analysis of variance (ANOVA) revealed the following effects: mechanical stimulation, $F(2, 106) = 46.1$, $p < 0.001$; electrical stimulation, $F(2, 106) = 18.5$, $p < 0.001$; and mechanical stimulation x electrical stimulation, $F(4, 212) = 11.3$, $p < 0.001$. ANOVA followed by *post-hoc Tukey* test was conducted between the control and recovery series did not show any significant differences between the two series among each mechanical stimulus suggesting that the mean rate of action potentials did not change during the time from control series to recovery. ANOVA was conducted between the brush, pressure and pinch in each series showed that the mean rate of action potentials during the pinch were greater than the pressure and the pressure were greater than the brush (p-value <0.001). In order to certify the results, ANOVA was followed by Wilcoxon rank sum and Kruskalwallis nonparametric tests, which both showed that the mean rate of action potentials during the pinch and pressure were greater than the brush. However, the mean rate of action potentials during the pinch stimulus was greater than pressure only during the control (P-value< 0.05) group and not the recovery (p-value = 0.12). Overall, this experiment showed that the wide dynamic range neuron in the dorsal horn of spinal cord could be used for detecting graded mechanical stimuli.

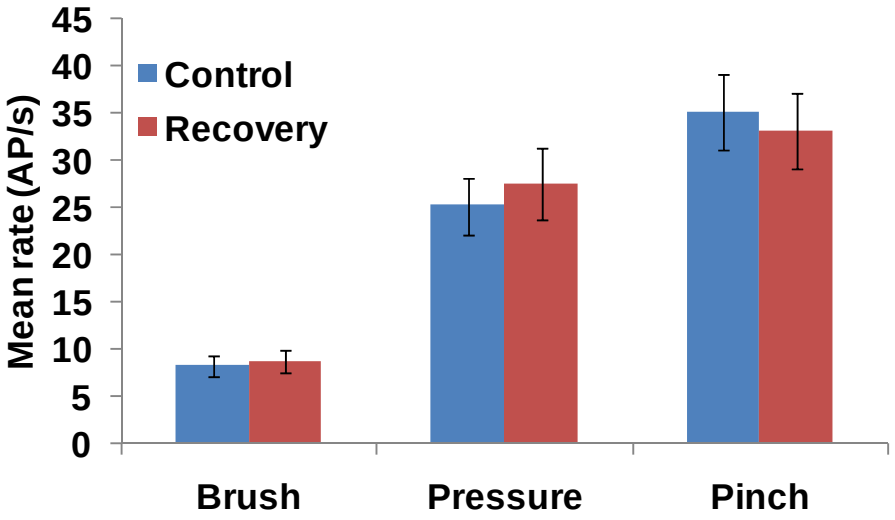

Figure 3.2 Mean rate of Action potentials per second ± Standard error of mean recorded from spinal cord dorsal horn in response to different mechanical stimuli from fifty-three neurons from seven rats.

3.2 Utilizing Extracellular Single-unit Signaling from Thalamus

3.2.1. Methodology

Extracellular single unit action potentials were recorded from ventroposterolateral (VPL) and ventroposteromedial (VPM), thalamic nuclei. The electrode type and other recording equipment were followed by the procedure explained in section 3.1.1.

3.2.2. Animal Experiment

Five male Sprague–Dawley rats (420 and 530 g) were used for this experiment. Animals were anesthetized using sodium pentobarbital (50 mg/kg, i.p.). A jugular vein cannulation was performed so that anesthesia could be maintained by intravenous administration of sodium pentobarbital at a rate of 5 mg/ml per hour. A cannula was inserted into the trachea for artificial respiration as needed. Head of the animals were fixed in the sterotaxic frame. A circular craniotomy of 5 mm diameter was done over the coordinates of –3 mm anterior and 3.5 mm lateral (right) to the Bregma. The dura matter over the brain was removed. Utilizing a micromanipulator, an electrode was inserted into the brain and searched the area from 5 to 6 mm depth for finding WDR neurons. The end tidal CO2 was maintained at

around 30mmHg and the body temperature was kept at 37 ºC using a feedback controlled heating pad and a rectal thermal sensor probe. Mechanical stimuli were applied to the left hind paw. All surgical procedures were approved by the University of Texas at Arlington Institutional Animal Care and Use Committee. The procedures were in accordance with the guidelines published by the Committee for Research and Ethical Issues of the International Association for Study of Pain [3.7].

3.2.3. Results

Forty neurons were recorded from the VPL and VPM of the thalamus from five rats. The mean rate of action potentials per second ± standard error of the mean is plotted in figure 3.3. The responses for (control and recovery) obtained as follow: (1) brush: (19.17 ± 2.58, 20.20 ± 2.40); (2) pressure: (24.81 ± 3.44, 25.36 ± 2.96); and (3) pinch: (27.52 ± 3.54, 27.20± 2.92). A 3 x 3 repeated measure Analysis of variance (ANOVA) revealed the following effects: mechanical stimulation, $F(2, 80) = 7.5$, $p < 0.001$; electrical stimulation, $F(2, 80) = 21.5$, $p < 0.001$; and mechanical stimulation x electrical stimulation, $F(4, 160) = 9.5$, $p < 0.001$.

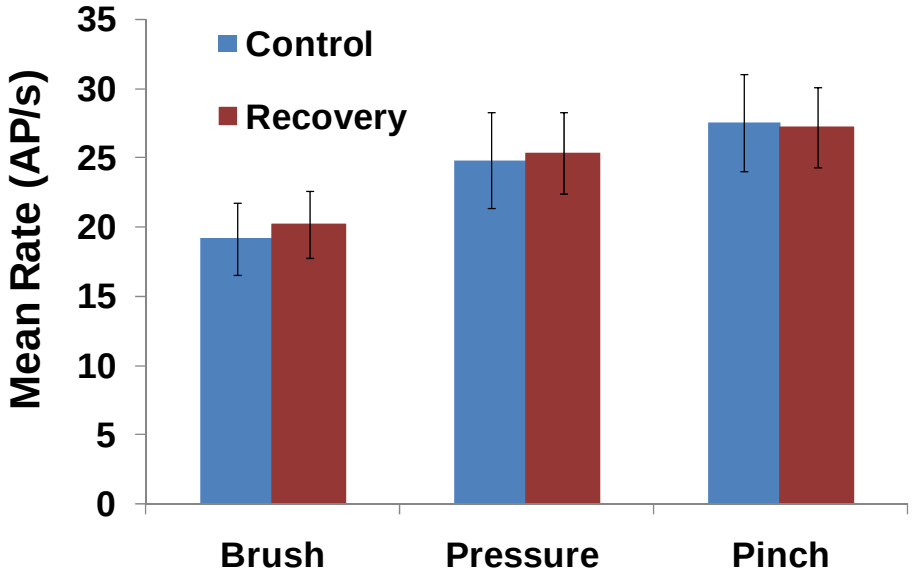

Figure 3.3 Mean rate of Action potentials per second ± Standard error of mean recorded in VPL of thalamus in response to different mechanical stimuli from forty neurons from five rats.

ANOVA followed by *post-hoc Tukey* test was conducted between the control and recovery series did not show any significant differences between the two series among each mechanical stimulus suggesting that the mean rate of action potentials did not change during the time from control series to recovery. ANOVA was conducted between the brush, pressure and pinch in each series showed that the mean rate of action potentials during the pinch were greater than the pressure and the pressure were greater than the brush (p-value <0.05). However, in the recovery series the mean rate of action potentials during the pinch was not significantly greater than the pinch (p-value = 0.67). In order to certify the results, ANOVA was followed by Wilcoxon rank sum and Kruskalwallis nonparametric tests, which only showed significant difference between the mean firing rate of pinch and brush (p-value < 0.05). This experiment showed that the wide dynamic range neuron in the VPL and VPM could only differentiate between high and low intensity mechanical stimuli and not medium stimulation. Therefore, they may not provide an appropriate index for detecting graded mechanical stimuli.

3.3 Utilizing ECoG from Somatosensory and Motor Cortex

3.3.1. Methodology

It has been shown that noxious stimuli cause changes in the electroencephalogram (EEG) and electrocorticogram (ECoG) in human [3.8] and in rodent models [3.9, 3.10]. In addition, researchers have tried to quantify the intensity of nociception in rodent models using single unit microelectrodes recordings in recent years [3.3, 3.11, 3.12]. However, to our best knowledge, all of these studies have been conducted on anesthetized animals; hence, they cannot be associated to the behavioral perception of pains. Specifically there are evidences that anesthesia reduces the responses of the neural systems to noxious stimuli [3.13]. Furthermore, microelectrode implantation is categorized as an invasive method [3.14] that can potentially modify the behavior of the animal. Considering numerous evidences that have used either ECoG or EEG signals to evaluate pains [3.10, 3.15, 3.16, 3.17], ECoG seems to be a better candidate for objective quantification of the behavior in animal under painful stimuli. One main

issue for using ECoG on the freely behaving animal until now has been the lack of a light-weight, low-power wireless system that is capable of acquiring ECoG signals from several areas of the brain. We have designed, fabricated, and successfully examined such a system on the rodent models.

In this study, we will collect ECoG signals in the somatosensory and motor cortices of a freely roaming rat during different behavioral states related with pain perception. We analyzed the signals in both time and frequency domains to associate the pain characteristic behaviors such as tail or paw withdrawal to thermal and mechanical stimuli to certain features of the ECoG signal.

The ECoG signals in response to right and left paw stimulus were separated considering baseline, low, medium and high filament categories. The signals that were saturated at any point were taken out from the analysis. The power spectrum was calculated for different segment size, depending on the experiment. The segment size for each experiment has been clarified in the result section. The power of the frequencies was categorized as well-know ECoG bands: Delta (0-4 Hz), Theta (4-8 Hz), Alpha (8-13 Hz), Beta (13-30 Hz), and Gamma (30-100 Hz). Student t-test was conducted between frequency bands of each different stimulus to reveal any significant difference.

3.3.2. Animal Experiment

Adult male Sprague-Dawley rats were anesthetized with sodium pentobarbital (50 mg/kg, i.p.) and placed in a stereotactic frame. Two ECoG screws (stainless steel, 1.58 mm length and 0.53 mm shaft diameter, provided by Small Part Inc.) were located on the somatosensory of the hind limb (S1HL) at anterior–posterior (AP) −1.5 mm, medial–lateral (ML) 2.5 mm bilaterally to bregma and two other screws were placed bilaterally on motor cortex (M1), at AP 2 mm, ML 2.5 mm. Two additional screws serving as ECoG reference and ground were placed bilaterally over the cerebellum (AP -11.5 mm, ML 1.5). Three other screws (stainless steel, 1.58 mm length, 1.5 mm diameter, Plastics one Inc.) were utilized as the support for

cement that covered the skull afterward (Fig. 3.4). The electrodes were connected to male socket and embedded in the cement. All surgical procedures were approved by the University of Texas at Arlington Institutional Animal Care and Use Committee. Animals were provided with extra care and were maintained under conditions of controlled light and temperature for one week to heal. They were then taken out and placed in a plastic chamber and isoflurane 4–5% was delivered until the animals were lightly anesthetized. On removal, isoflurane (2–3%) was delivered via mask for about five minutes, until we mounted the front-end telemetric backpack on the animal. Thirteen animals were implanted with this procedure.

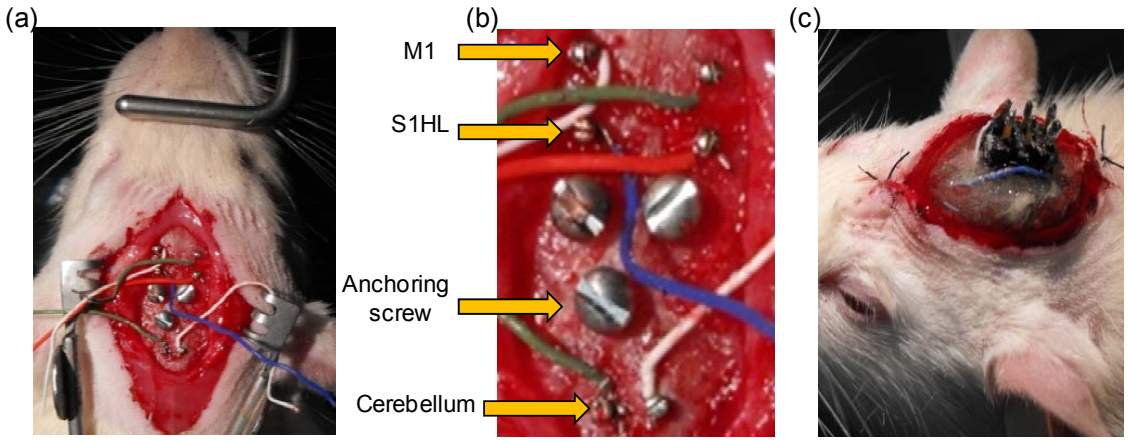

Figure 3.4 (a) Implanting the ECoG screws. (b) Recording sites (S1HL and M1), reference and ground electrodes (cerebellum), and anchoring screws. (c) The male socket on the cement.

In order to correlate the ECoG signal with the behaviors of the animals, noxious thermal, mechanical, chemical, and combination of mechanical and chemical stimuli were applied to the hind limbs (both paws and tale) of the animals.

In order to evaluate the correlation of ECoG signals and behaviors of the animal to mechanical stimuli, animals were placed on a grid and von Frey filaments (Fig. 3.5), which are series of nylon monofilaments of different thickness, were pressed against the skin to the point where they bent [3.18]. Three different filaments of low (8 g.), medium (26 g.) and high (100 g.) pressures were applied to the animal hind paws, while the behaviors of the animal were observed and filmed. The procedure initiated with 15 seconds of baseline, followed by the 15

seconds of stimulation of right paw with low intensity. 15 seconds of baseline recording and then stimulating the left paw with the same filament. Waiting for 15 seconds and stimulating the right paw with the medium filament and so on and forth.

After the mechanical test, animals were tested for thermal stimulus, which included the tail-flick, and paw withdrawal tests with radiant heat were used [3.19]. The application of thermal radiation to the tail or paws of an animal provoked the withdrawal of the tail or paws by a brief vigorous movement. The reaction time of this movement was recorded and correlated with the ECoG signals obtained from S1HL and M1 of the animal.

Figure 3.5 The animal on the grid and the Von Frey filament.

One week after the thermal experiments, another round of thermal tests was conducted. In these experiments, the left paw of the animal was injected with 0.05 ml of Saline and the right paw was injected with 0.05 ml of 2% lidocaine. Animals were placed on the heating pad and the reaction time for each paw was recorded. If the animal did not withdraw the paw, the machine stopped automatically at 32.1 s.

One week after the second thermal experiments, chemical stimulation test was conducted. For the chemical test, 0.05 ml of a 3% solution of formalin was injected into the rat's right hind paw to investigate the relation between the resulted ECoG signals and elicited behaviors (i.e. licking and nibbling) [3.20]. ECoG signals were generally recorded 20 to 30

minutes after the injection for about 3 minutes. Finally, Von Frey filaments were of low (2 g.), medium (8 g.) and high (26 g.) intensities were applied to both paws according to the mechanical stimulation procedures explained above.

3.3.3. Results

A typical ECoG signal that was recorded in response to Von Frey mechanical stimulus from left and right somatosensories and motor cortices is shown in Fig. 3.6. In this experiment, the first 15 seconds was recorded as baseline and then the left paw was stimulated with strong (100 g.) von Frey filament for 5 times (from 15-30 s). The animal withdrew the paw at the third poke, started to move around, and stopped moving before the fourth poke that caused a light paw movement. It did not respond to the last (5^{th}) stimulus. The red arrows show the stimulus incidents one to four.

The number of detected signature peaks in the time-domain signal and paw withdrawal behavior was correlated. In 88.9% and 92.1% of the withdrawal of the right and left paw a signature peak was detected in the signal, respectively.

The ECoG signals in response to right and left paw stimulus were separated considering baseline, low, medium and high filament categories. The power spectrum was calculated for each segment within the 15 seconds of baseline or stimulation for 6 animals. Fig. 3.7 and 3.8 show the ECoG bands that happened in response to various mechanical stimuli in right paw and left paw respectively. Tables 3.1 and 3.2 show the t-test results for right and left paws respectively. These results showed significant increase in the Delta band if either of the left or right paw is stimulated with the strong (high) mechanical stimulus in compare to baseline. In some of the comparisons, Theta and Gamma band showed significant increase in the high or medium stimuli in compare with baseline.

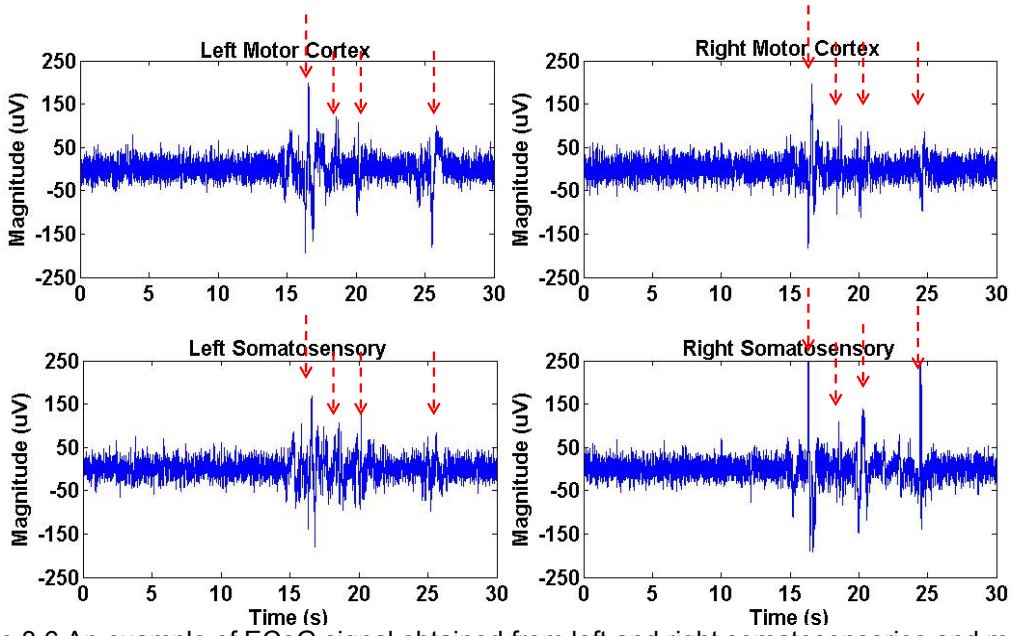

Figure 3.6 An example of ECoG signal obtained from left and right somatosensories and motor cortices in response to medium Von Frey filament. The stimulus incidents are highlighted with arrows.

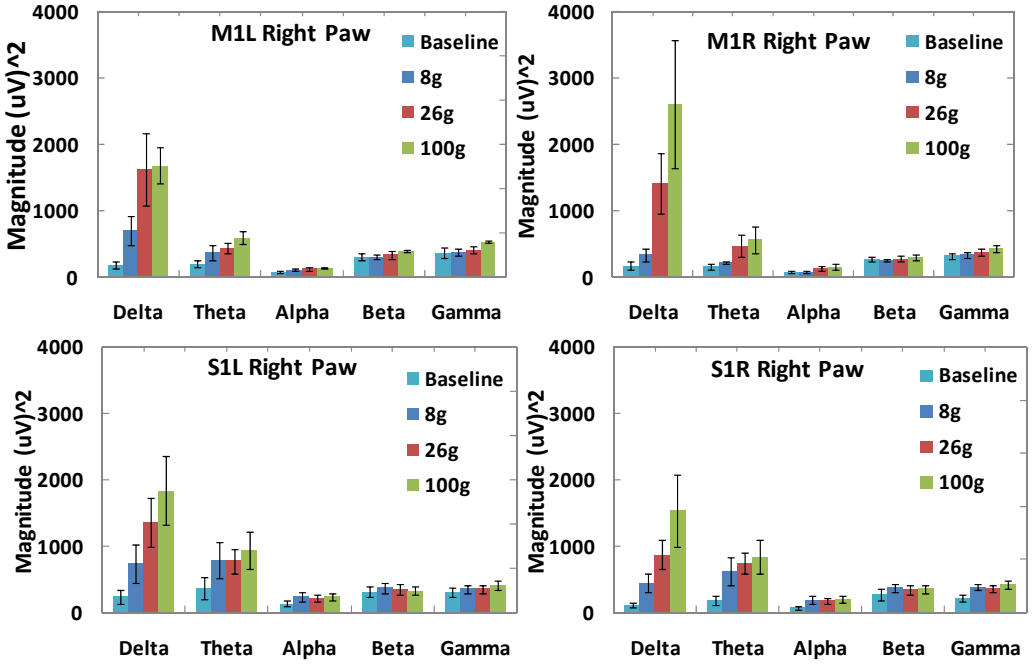

Figure 3.7 The average ± SEM of the power of various frequency bands of the ECoG signals (15 seconds segments) during baseline (no stimulation) and in response to graded mechanical stimuli. The stimulations were applied to the right paw. The top left plot shows the signal acquired in left motor cortex, top right: right motor cortex, bottom left: left somatosensory and bottom right is right somatosensory.

Table 3.1 T-test between the combinations of baseline (B), Low (L), Medium (M), and High (H) mechanical stimuli. Each comparison is categorized to specific frequency band and separated for left (L) and right (R) motor cortices (M1) and Somatosensories (S1).

	M1L						M1R					
	BvL	**BvM**	**BvH**	**LvM**	**LvH**	**MvH**	**BvL**	**BvM**	**BvH**	**LvM**	**LvH**	**MvH**
Delta	0.098	0.067	**0.018**	0.495	0.218	0.365	0.086	**0.033**	**0.044**	0.142	0.174	0.147
Theta	0.168	**0.014**	0.058	0.552	0.468	0.219	0.073	0.098	0.075	0.240	0.218	0.057
Alpha	0.422	0.114	0.174	0.594	0.764	0.278	0.243	0.122	0.117	0.227	0.194	0.183
Beta	0.079	0.897	0.771	0.156	0.217	0.846	0.746	0.629	0.205	0.559	0.305	0.343
Gamma	0.336	0.728	0.454	0.246	0.164	0.063	0.763	0.196	**0.049**	0.165	**0.036**	**0.006**
	S1L						S1R					
	BvL	**BvM**	**BvH**	**LvM**	**LvH**	**MvH**	**BvL**	**BvM**	**BvH**	**LvM**	**LvH**	**MvH**
Delta	0.062	**0.042**	**0.026**	0.511	0.212	0.347	0.380	**0.031**	**0.044**	0.353	0.231	0.172
Theta	**0.026**	**0.004**	**0.009**	0.470	0.111	0.185	**0.033**	**0.013**	**0.019**	0.320	0.087	0.462
Alpha	0.061	**0.015**	0.138	0.405	0.708	0.790	0.893	0.625	0.538	0.632	0.599	0.590
Beta	0.738	0.237	0.521	0.277	0.923	0.585	0.056	0.552	0.990	0.426	0.322	0.591
Gamma	0.803	0.343	0.102	0.189	0.068	**0.008**	0.638	0.432	**0.046**	0.561	**0.023**	**0.033**

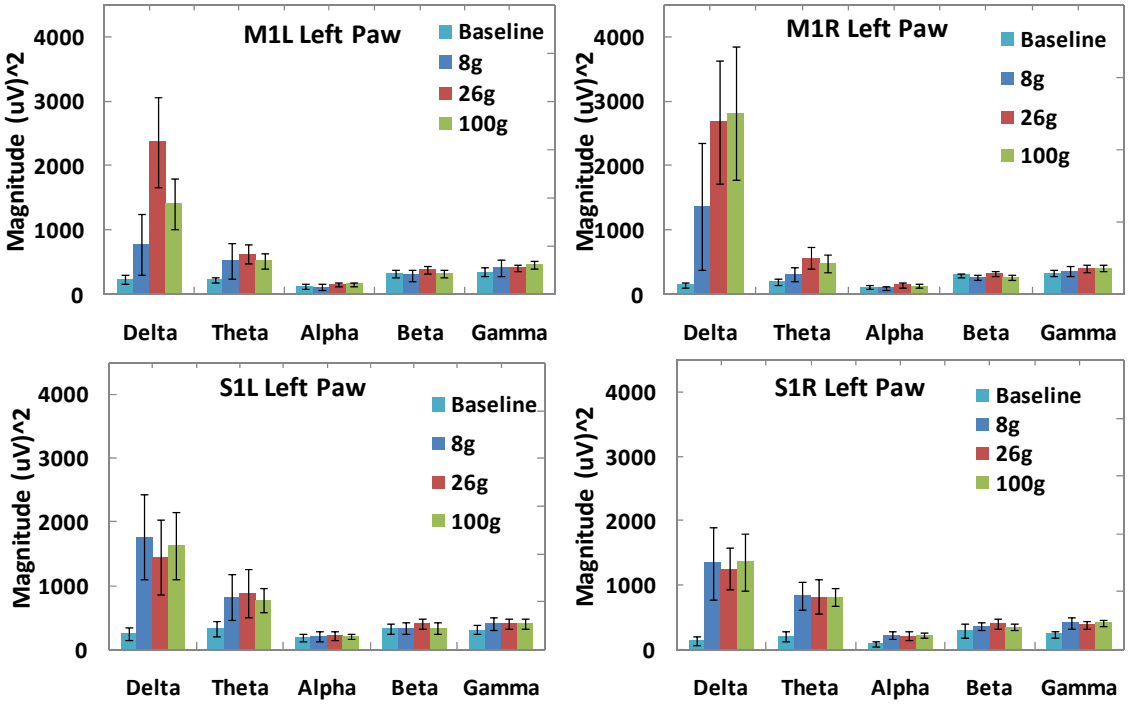

Figure 3.8 The average ± SEM of the power of various frequency bands of the ECoG signals (15 seconds segments) during baseline (no stimulation) and in response to graded mechanical stimuli. The stimulations were applied to the left paw. M1L and M1R are Motor cortex left and right, S1L and S1R are somatosensory left and right respectively.

Table 3.2 T-test between the combinations of baseline (B), Low (L), Medium (M), and High (H) mechanical stimuli. Each comparison is categorized to specific frequency band and separated for left (L) and right (R) motor cortices (M1) and Somatosensories (S1).

	M1L						M1R					
	BvL	**BvM**	**BvH**	**LvM**	**LvH**	**MvH**	**BvL**	**BvM**	**BvH**	**LvM**	**LvH**	**MvH**
Delta	0.321	**0.027**	**0.031**	0.391	0.749	0.271	0.282	**0.041**	**0.046**	0.927	0.303	0.829
Theta	0.347	**0.027**	**0.046**	0.896	0.707	0.175	0.131	**0.027**	0.069	0.580	0.486	0.557
Alpha	0.701	0.337	0.593	0.249	0.444	0.798	0.706	0.291	0.494	0.664	0.313	0.651
Beta	0.553	0.368	0.938	0.251	0.895	**0.038**	0.948	0.322	0.319	0.764	0.232	**0.040**
Gamma	0.199	0.285	0.122	0.647	0.845	0.087	0.527	0.429	0.385	0.176	0.080	0.476
	S1L						S1R					
	BvL	**BvM**	**BvH**	**LvM**	**LvH**	**MvH**	**BvL**	**BvM**	**BvH**	**LvM**	**LvH**	**MvH**
Delta	0.055	0.107	**0.048**	0.508	0.769	0.728	0.091	**0.019**	0.051	0.828	0.957	0.790
Theta	0.110	0.141	**0.003**	**0.033**	0.801	0.851	**0.013**	**0.039**	**0.006**	0.880	0.904	0.979
Alpha	0.731	0.989	0.644	0.474	0.974	0.971	**0.027**	0.150	0.078	0.540	0.992	0.767
Beta	0.806	0.572	0.778	0.063	0.980	0.161	0.564	0.180	0.642	0.207	0.743	0.269
Gamma	0.375	0.539	0.215	0.183	0.872	**0.041**	0.181	0.182	**0.023**	0.342	0.892	0.107

A typical ECoG signal for thermal experiment is shown in Figure 3.9. The first 10 seconds were baseline recording and the radiation started in the left paw at the 10^{th} second and continued until the animal withdrew the paw (21.0 s). Therefore, the reaction time was measured as 11.0 s. The withdrawal moment has been indexed with an arrow.

The number of detected signature peaks in response to paw withdrawal behavior was counted and correlated. In 84.0%, 87.5% and 79.17% of the withdrawal of the right paw, left paw and tale a signature peak was detected in the signal, respectively.

The first two seconds of the baseline, the two seconds of withdrawal and the two seconds right before the withdrawal were taken from the recorded signals of 5 animals. The power spectrum during each segment was obtained and divided into the ECoG bands. The mean of the power of each band ± standard error of mean has been plotted in Figures 3.10 and 3.11 for right and left paw radiation respectively. T-test was conducted between the baseline (B), Heating (H) and withdrawal (W) periods and results for right and left paw radiations are shown in table 3.3 and 3.4 respectively. T-test revealed that the power of the withdrawal segment was significantly higher than both the baseline and heating periods in Delta and Gamma bands. While no significant difference was found between the baseline and heating periods.

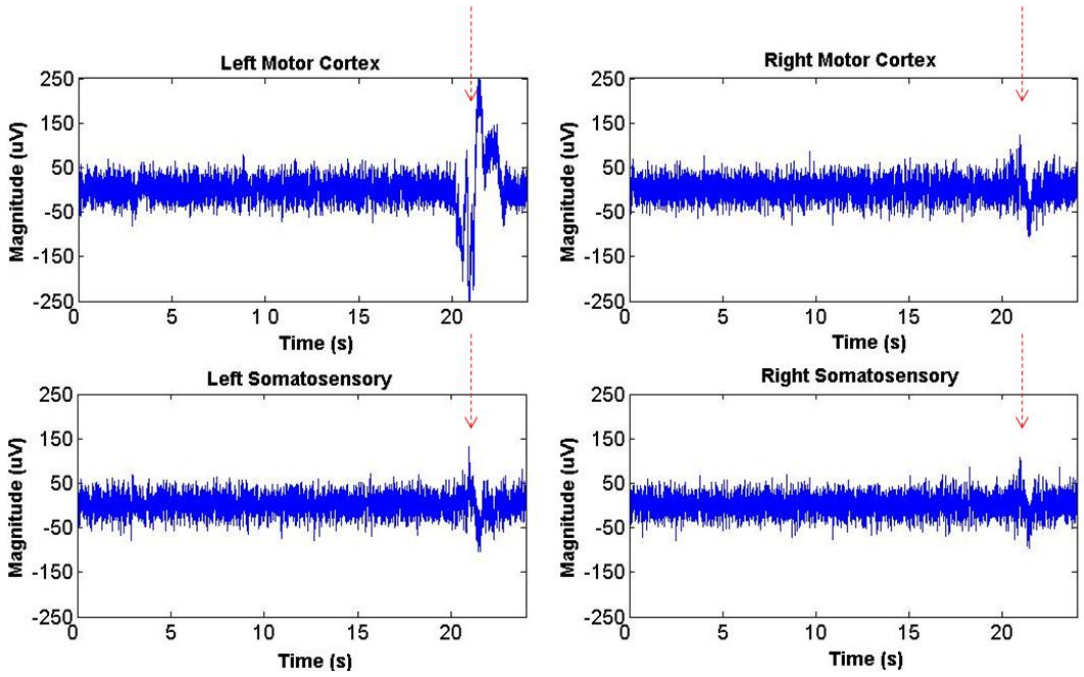

Figure 3.9 An example of the ECoG signal recorded from thermal experiment. The radiation started in the left paw at the 10th second and the animal withdrew the paw at the 21s.

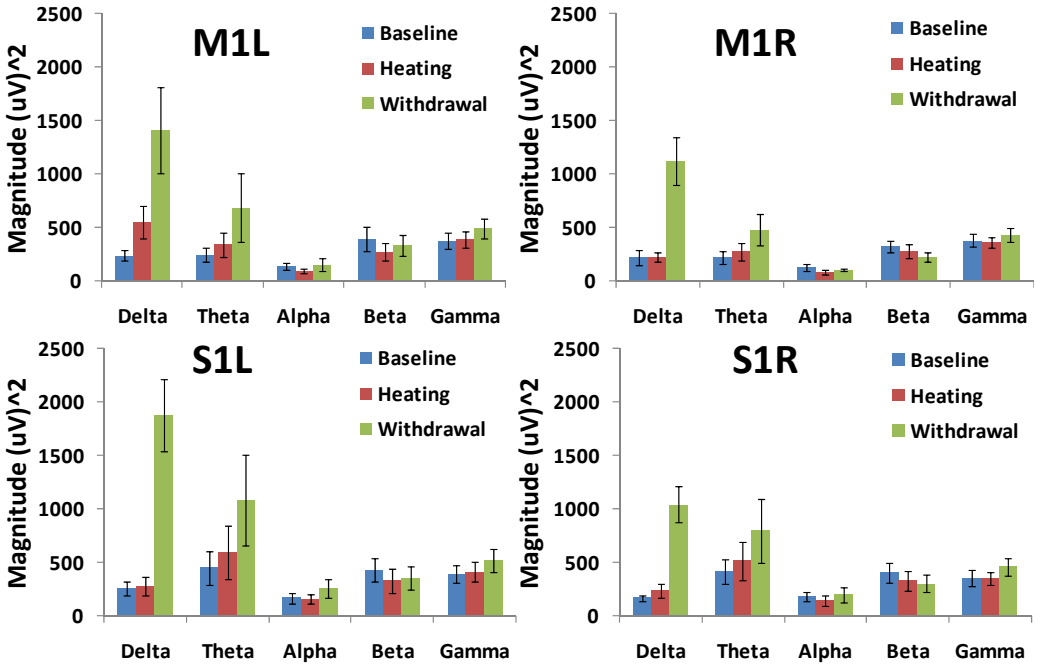

Figure 3.10 The mean power of different ECoG bands ± SEM has been plotted for the baseline, heating and withdrawal periods (each 2 s.). In these experiments, radiation was exposed to the right paw.

Table 3.3 T-test between the baseline (B), heating (H), and withdrawal (W) periods for different ECoG bands and four different electrodes in motor cortices and somatosensories of left and right sides. Right paw was exposed to radiation in these experiments. Most significant changes can be seen in the Delta band between the withdrawal and baseline/heating periods.

	M1L			M1R			S1L			S1R		
	BvH	BvW	HvW	BvH	BvW	HvW	BvH	BvW	HvW	BvH	BvW	HvW
Delta	0.069	0.053	0.032	0.954	0.025	0.015	0.621	0.006	0.005	0.211	0.004	0.004
Theta	0.283	0.232	0.197	0.506	0.143	0.039	0.222	0.101	0.086	0.241	0.126	0.114
Alpha	0.032	0.823	0.373	0.234	0.367	0.242	0.745	0.196	0.102	0.447	0.639	0.219
Beta	0.022	0.147	0.384	0.415	0.035	0.148	0.025	0.013	0.289	0.130	0.023	0.501
Gamma	0.442	0.185	0.339	0.554	0.095	0.077	0.284	0.019	0.083	0.849	0.079	0.023

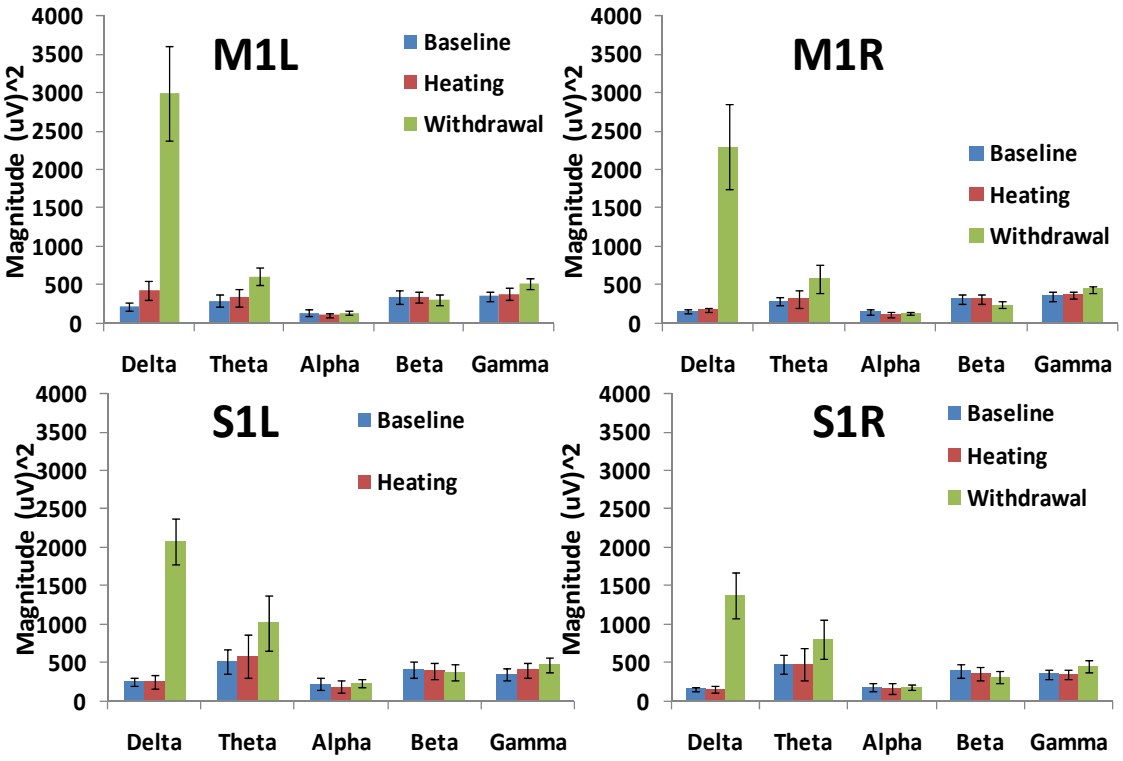

Figure 3.11 The mean power of different ECoG bands ± SEM has been plotted for the baseline, heating and withdrawal periods (each 2 s.). In these experiments, radiation was exposed to the left paw.

Table 3.4 T-test between the baseline (B), heating (H), and withdrawal (W) periods for different ECoG bands and four different electrodes in motor cortices and somatosensories of left and right sides. Left paw was exposed to radiation in these experiments. Most significant changes can be seen in the Delta band between the withdrawal and baseline/heating periods.

	M1L			M1R			S1L			S1R		
	BvH	**BvW**	**HvW**	**BvH**	**BvW**	**HvW**	**BvH**	**BvW**	**HvW**	**BvH**	**BvW**	**HvW**
Delta	0.252	0.022	0.024	0.241	0.020	0.019	0.841	0.006	0.009	0.938	0.018	0.017
Theta	0.749	0.155	0.076	0.815	0.182	0.110	0.580	0.110	0.133	0.951	0.163	0.192
Alpha	0.503	0.451	0.625	0.486	0.659	0.502	0.648	0.801	0.508	0.854	0.992	0.851
Beta	0.896	0.043	0.127	0.941	0.069	0.081	0.685	0.450	0.723	0.336	0.085	0.118
Gamma	0.193	0.011	0.015	0.155	0.012	0.006	0.142	0.036	0.053	0.646	0.029	0.026

The reaction time in eight animals for the left and right paw withdrawals were obtained as 13.97±0.88 s and 14.74±0.85 s. Student t-test did not show any significant difference between the reaction time of left and right paw. After injection of the saline to the left and lidocaine to the right paw, the reaction times were obtained as 16.7±5.2 s and 23.8 ± 6.1 s. Student t-test revealed that the lidocaine injection significantly increased the reaction time (p-value < 0.05). Figure 3.12 shows the mean of the thermal latency ± SEM in second for the right and left paw before and after the injections.

No signature peak was detected if the animal did not withdraw the paw. In addition, lidocaine caused the signature peak either disappear or happens in the later time according to reaction time.

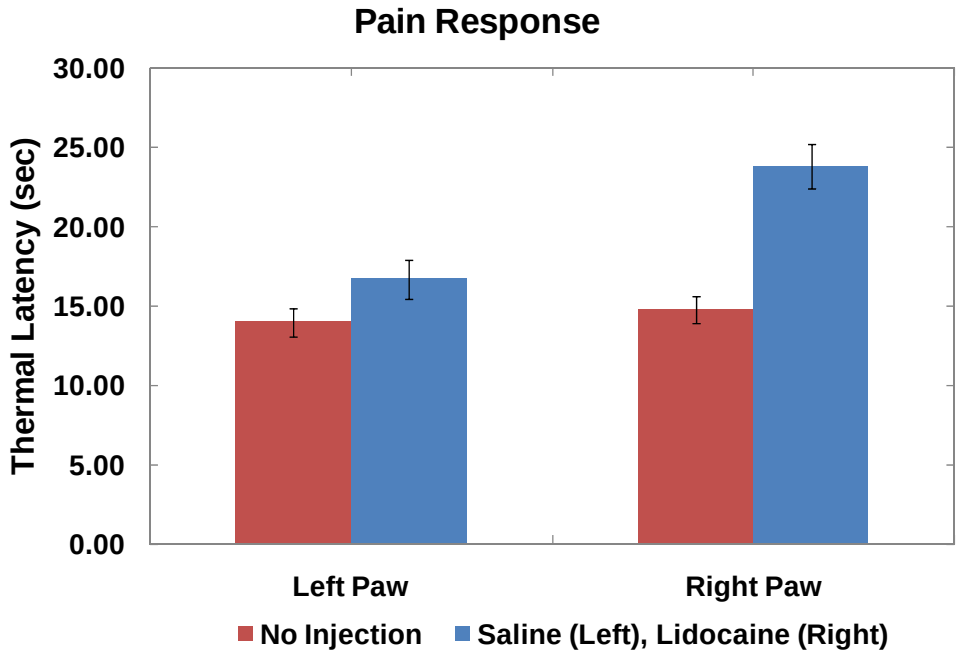

Figure 3.12 Thermal latency in second ± SEM for left and right paws, before injection and after injecting saline to the left paw and lidocaine to the right paw.

ECoG signal was recorded from 6 animals when the animals were under anesthesia, awake (and do nothing in the cage) and 20 minutes after formalin injection. One second of each of these conditions are plotted for the left and right motor cortices and somatosensories in figures 3.13, 3.14 and 3.15 for anesthesia, wakefulness and after formalin injection respectively.

The power of the signal during the three conditions (anesthesia, wakefulness, and formalin injected) was calculated for various bands and presented in figure 3.16 as mean of the power ± SEM. Since the mean of the power during the anesthesia condition is much larger than the other two conditions, figure 3.17 was plotted to better reveal the differences between the wakefulness and formalin injected conditions.

Student t-test was conducted over the different conditions and showed that the power of the signal is larger during the anesthesia in compare to the other two conditions. Also the post formalin condition showed higher power than the other two conditions in the Gamma band. The results for all the t-tests are showed in table 3.5.

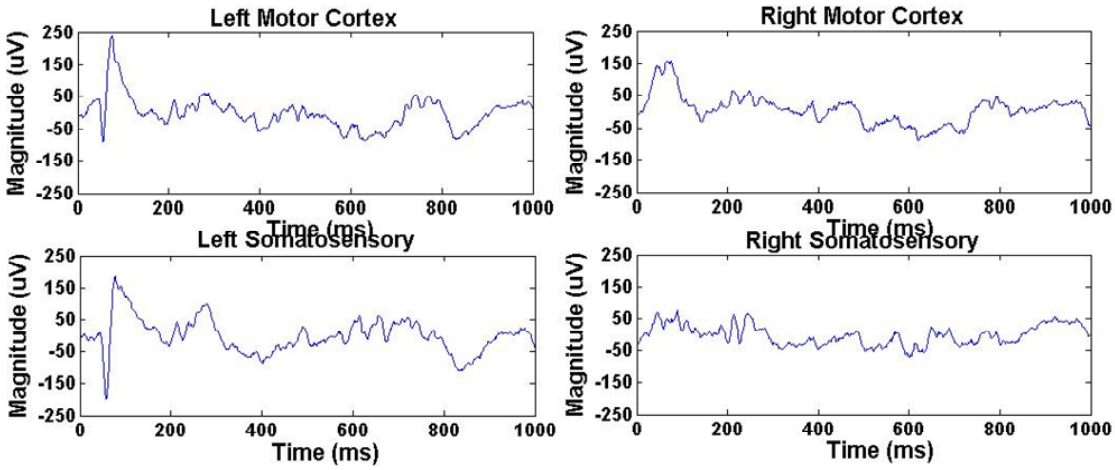

Figure 3.13 One second of ECoG signal while the rat was under anesthesia.

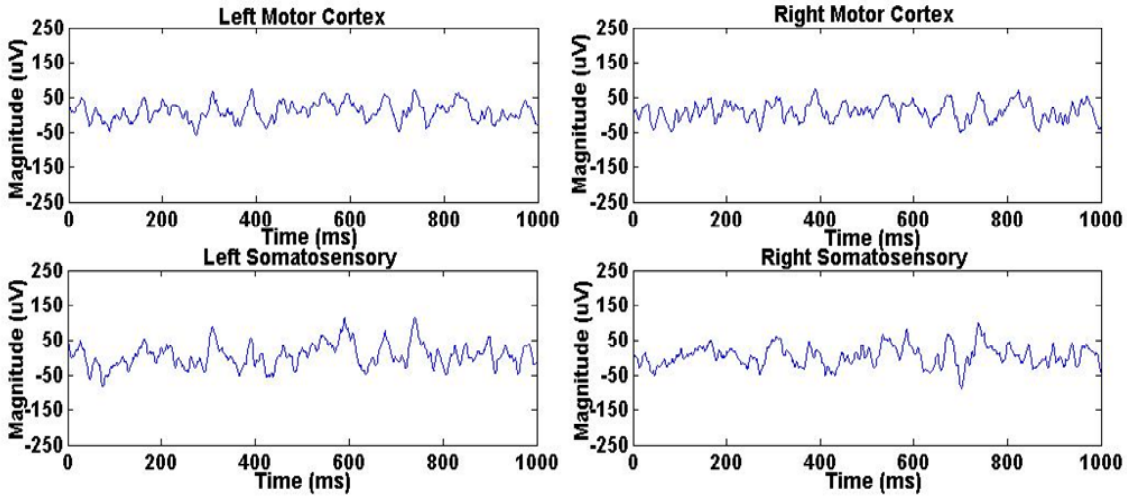

Figure 3.14 One second of ECoG signal while the rat was awake and sitting in the cage.

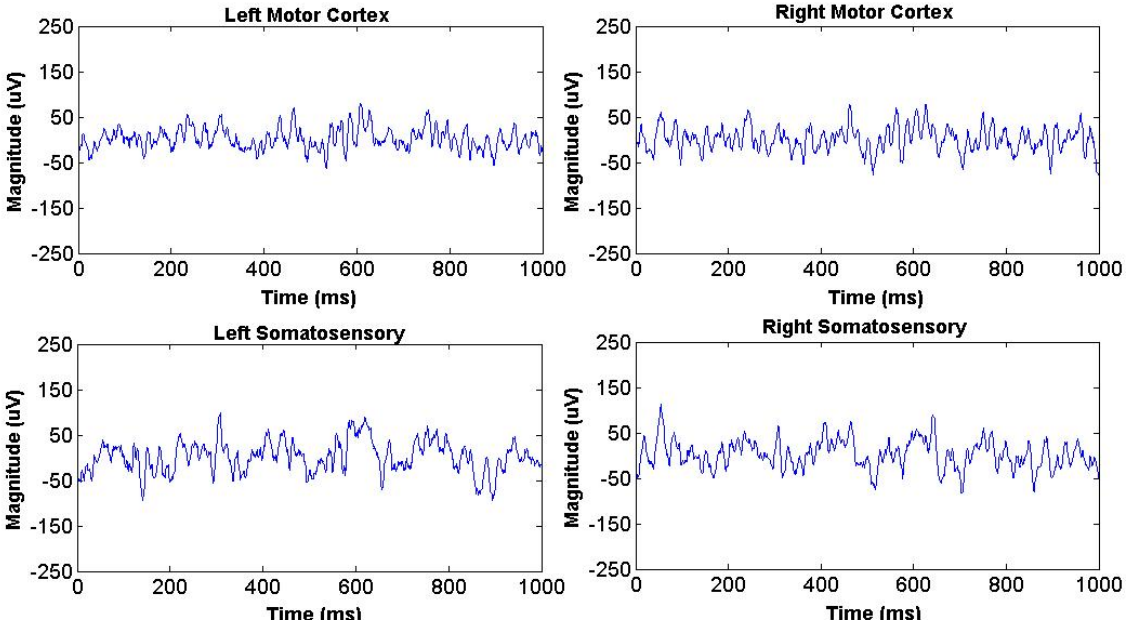

Figure 3.15 One second of ECoG signal after 20 minutes of injecting formalin to the rat's right paw.

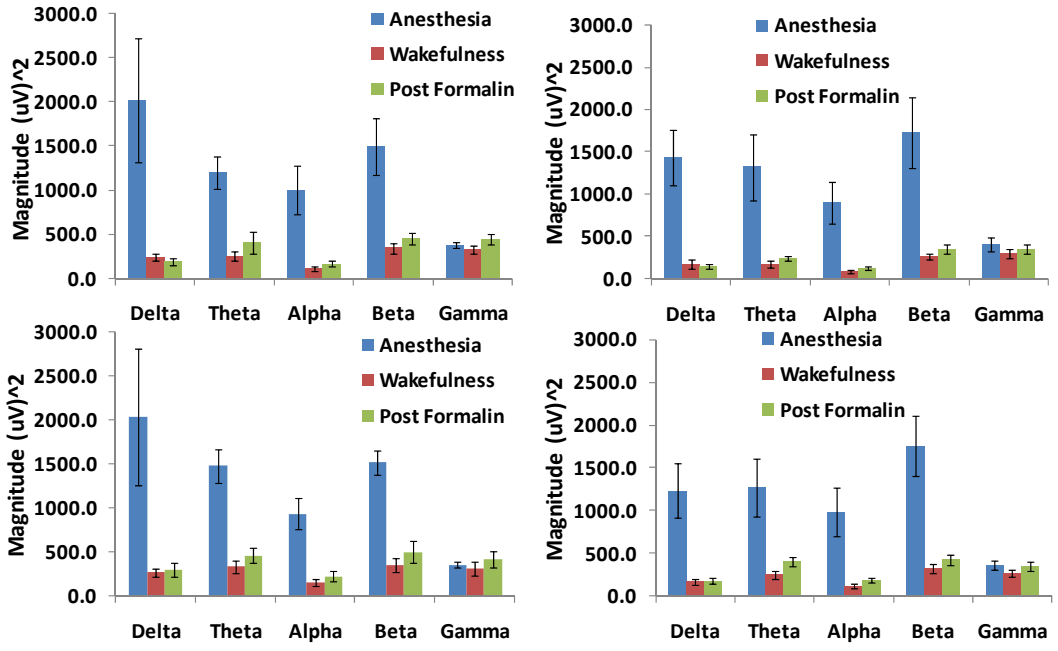

Figure 3.16 The mean power of different ECoG bands ± SEM has been plotted for the anesthesia, wakefulness and post-formalin condition for segments of 1 s.

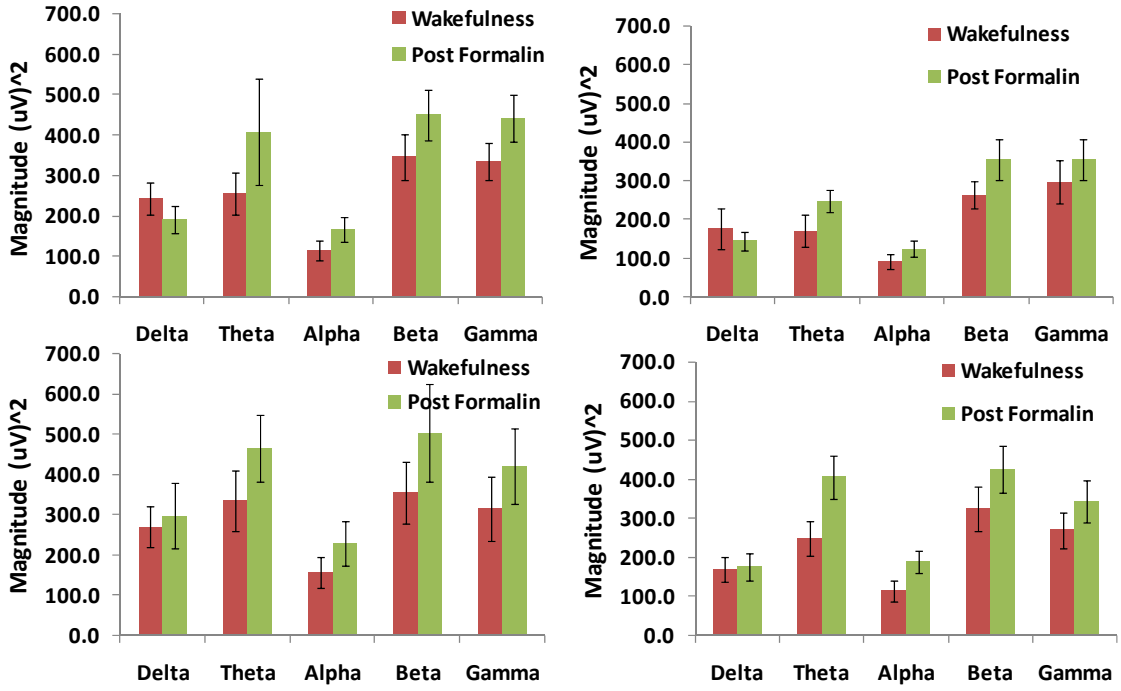

Figure 3.17 The mean power of different ECoG bands ± SEM has been plotted for the wakefulness and post-formalin condition for segments of 1 s.

Table 3.5 T-test between the anesthesia (A), wakefulness (W), and post-formalin (PF) periods for different ECoG bands and four different electrodes in motor cortices and somatosensories of left and right sides.

	M1L			M1R			S1L			S1R		
	AvW	AvPF	WvPF	AvW	AvPF	WvPF	AvW	AvPF	WvPF	AvW	AvPF	WvPF
Delta	0.055	0.050	0.132	0.019	0.013	0.426	0.072	0.084	0.640	0.024	0.023	0.861
Theta	0.003	0.012	0.326	0.029	0.038	0.052	0.001	0.003	0.037	0.027	0.044	0.005
Alpha	0.025	0.036	0.167	0.020	0.027	0.119	0.005	0.004	0.092	0.025	0.033	0.024
Beta	0.021	0.034	0.020	0.014	0.018	0.041	0.000	0.000	0.051	0.008	0.009	0.010
Gamma	0.568	0.523	0.005	0.234	0.563	0.019	0.709	0.616	0.003	0.229	0.765	0.013

In another experiment, the rats' right and left paws were stimulated with von frey filaments (2, 8 and 26 g.) 20-30 minutes after the formalin was injected to the right paw. The ECoG signals in response to right and left paw stimulus were separated considering baseline, low, medium and high filament categories. The power spectrum was calculated for each segment within the 15 seconds of baseline or stimulation for 5 animals. Fig. 3.18 and 3.19 show the power of the signal in different ECoG bands that happened in response to various mechanical stimuli in right paw and left paw respectively. Tables 3.6 and 3.7 show the t-test

results for right and left paws respectively. These results did not show a major trend in any of the ECoG bands that show significant difference between the effects of the various filaments.

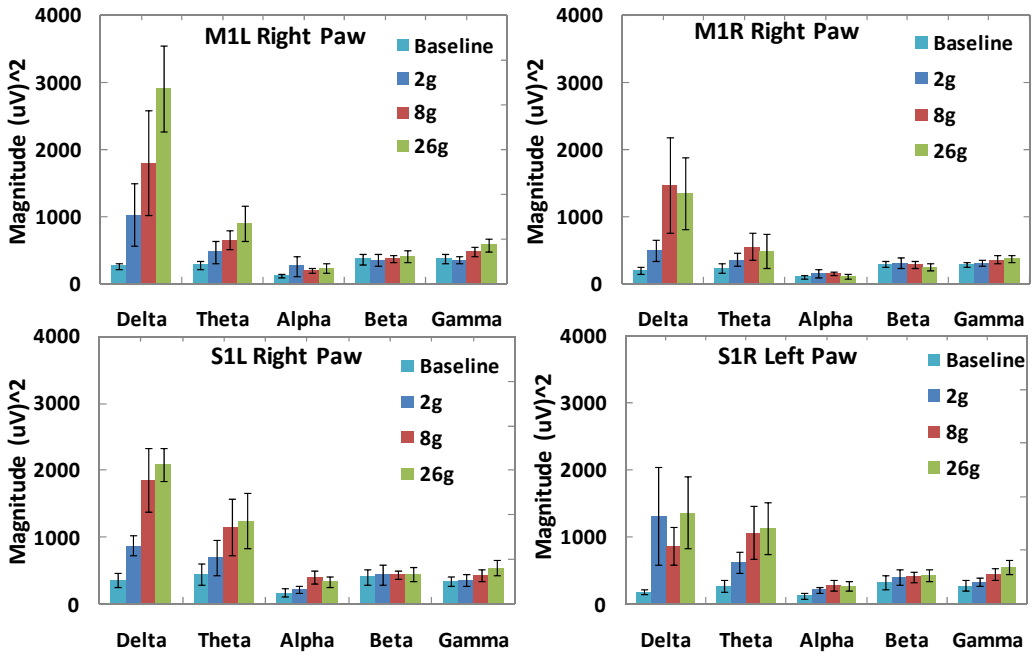

Figure 3.18 Mean power of different ECoG bands ± SEM has been plotted for various von frey filaments (2, 8, and 26 g.) and baseline. The stimulations were applied to the right paw of the animals. M1: Motor cortex, S1: Somatosensory

Table 3.6 T-test between the combinations of baseline (B), Low (L), Medium (M), and High (H) mechanical stimuli after formalin injection (in the right paw) obtained from right paw stimulation. Each comparison is categorized to specific frequency band and separated for left (L) and right (R) motor cortices (M1) and Somatosensories (S1).

	M1L						M1R					
	BvL	**BvM**	**BvH**	**LvM**	**LvH**	**MvH**	**BvL**	**BvM**	**BvH**	**LvM**	**LvH**	**MvH**
Delta	0.177	0.109	**0.013**	0.371	**0.028**	0.175	0.142	0.161	0.134	0.196	0.162	0.935
Theta	0.295	**0.034**	0.061	0.375	0.128	0.247	0.211	0.144	0.322	0.226	0.338	0.467
Alpha	0.448	0.085	0.134	0.576	0.569	0.432	0.522	0.211	0.377	0.917	0.615	0.462
Beta	0.985	0.963	0.483	0.587	0.975	0.223	0.994	0.475	0.623	0.595	0.956	0.657
Gamma	0.790	0.401	0.085	0.164	0.061	0.106	0.869	0.472	0.166	0.252	0.096	0.480
	S1L						**S1R**					
	BvL	**BvM**	**BvH**	**LvM**	**LvH**	**MvH**	**BvL**	**BvM**	**BvH**	**LvM**	**LvH**	**MvH**
Delta	0.155	**0.049**	**0.002**	0.114	**0.040**	0.578	0.239	0.084	0.097	0.311	0.526	0.149
Theta	0.186	0.090	**0.041**	0.195	0.087	0.646	0.106	0.119	0.083	0.385	0.277	0.484
Alpha	0.646	0.064	0.052	0.210	0.236	0.433	0.483	0.058	0.068	0.476	0.586	0.701
Beta	0.982	0.656	0.387	0.863	0.965	0.876	0.684	0.494	0.119	0.510	0.782	0.150
Gamma	0.739	0.303	0.084	0.165	0.120	0.098	0.846	0.173	**0.048**	0.226	0.098	0.082

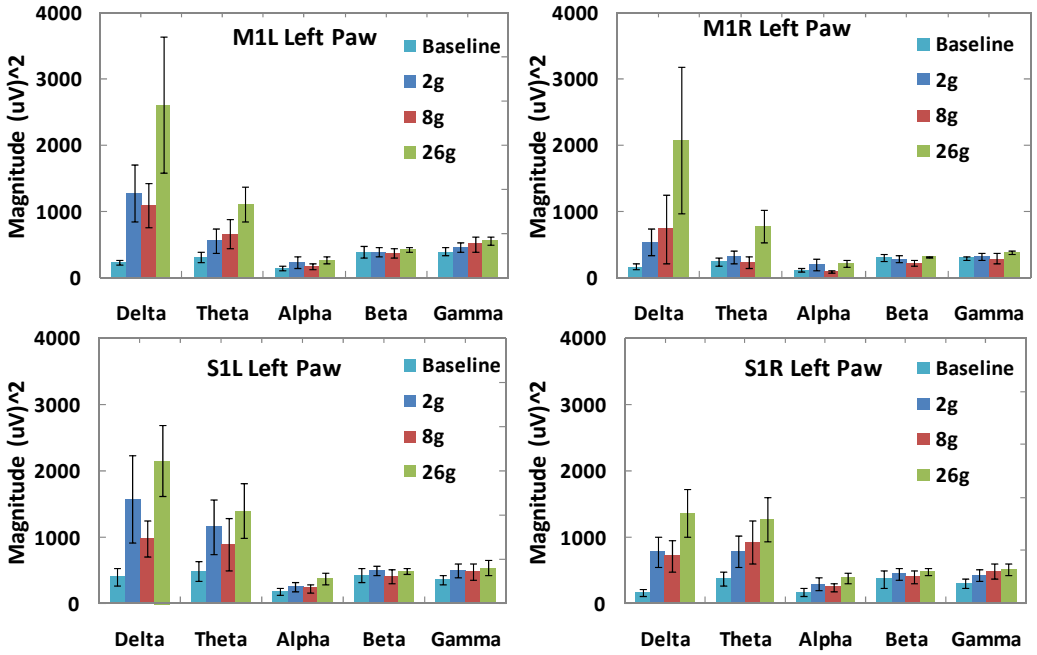

Figure 3.19 Mean power of different ECoG bands ± SEM has been plotted for various von frey filaments (2, 8, and 26 g.) and baseline. The stimulations were applied to the left paw of the animals. M1: Motor cortex, S1: Somatosensory

Table 3.7 T-test between the combinations of baseline (B), Low (L), Medium (M), and High (H) mechanical stimuli after formalin injection (in the right paw) obtained from the left paw stimulation. Each comparison is categorized to specific frequency band and separated for left (L) and right (R) motor cortices (M1) and Somatosensories (S1).

	M1L						M1R					
	BvL	**BvM**	**BvH**	**LvM**	**LvH**	**MvH**	**BvL**	**BvM**	**BvH**	**LvM**	**LvH**	**MvH**
Delta	0.077	0.058	0.086	0.780	0.340	0.153	0.161	0.366	0.178	0.532	0.268	0.289
Theta	0.107	0.095	**0.041**	0.350	0.140	0.127	0.276	0.631	0.105	0.848	0.165	0.194
Alpha	0.199	0.365	**0.022**	0.279	0.610	**0.020**	0.312	0.781	0.068	0.739	0.771	0.067
Beta	0.973	0.774	0.607	0.459	0.526	0.347	0.931	0.578	0.603	0.608	0.626	0.148
Gamma	0.512	0.381	**0.046**	0.342	0.089	0.507	0.563	0.910	0.053	0.850	0.301	0.147
	S1L						S1R					
	BvL	**BvM**	**BvH**	**LvM**	**LvH**	**MvH**	**BvL**	**BvM**	**BvH**	**LvM**	**LvH**	**MvH**
Delta	0.166	**0.042**	**0.038**	0.262	0.576	0.096	**0.044**	0.080	**0.033**	0.741	0.266	0.197
Theta	0.151	0.187	**0.029**	0.645	0.343	**0.019**	0.083	0.116	**0.029**	0.249	**0.038**	0.056
Alpha	0.341	0.199	**0.021**	0.321	0.079	**0.042**	0.171	**0.029**	**0.011**	0.518	0.330	**0.010**
Beta	0.904	0.760	0.579	0.674	0.693	0.457	0.347	0.994	0.259	0.491	0.573	0.264
Gamma	0.416	0.228	0.074	**0.045**	0.126	0.319	0.236	0.151	**0.027**	0.163	0.072	0.521

3.4 Discussion and Conclusion

Results in figure 3.2 showed that the single-unit extracellular action potentials from the spinal cord dorsal horn can be utilized to distinguish between the graded mechanical stimuli from non-painful (brush) to the border of painful and non-painful (pressure) and painful (pinch). These results are in good agreement with the ones obtained in [3.2, 3.3]. However, results in figure 3.3 showed that the single-unit extracellular action potentials from the thalamus can only be used to distinguish between painful (pinch) and non-painful (brush) signals. This might be due to the integration of other sensory modalities with the mechanical signals in the thalamus. Therefore, we utilized the extracellular signals from the spinal cord to distinguish between the graded mechanical stimuli to develop a closed-loop feedback system in chapter 4.

When mechanically stimulating rats' paws with von-Frey filaments, in 88.9% and 92.1% of the withdrawal of the right and left paw an evoked response was detected in the ECoG signals, respectively. This result shows a good correlation between the paw withdrawal and the evoked potential in ECoG signals. For the same mechanical stimuli, figures 3.7 and 3.8 and tables 3.1 and 3.2 showed that the power of Delta band during the mechanical stimuli was significantly higher than the baseline. However, no significant difference was observed among the graded stimuli. Therefore, ECoG signal can only be utilized to distinguish a withdrawal event or mechanical stimulation from a non-stimulation condition, however, it cannot be used to differentiate between the graded stimuli.

When rats' paws exposed to thermal stimulation, in 84.0%, 87.5% and 79.17% of the withdrawal of the right paw, left paw and tale an evoked response was detected in the ECoG signal, respectively and evoked response was detected in the signal until the animal withdrew the right paw, left paw or tale. For the same mechanical stimuli, figures 3.10 and 3.11 and tables 3.3 and 3.4 showed that the power of the frequency bands of Delta and Gamma were significantly higher during the withdrawal in compare to baseline and heating periods. Therefore, ECoG signal can only be utilized to detect a withdrawal event caused by thermal

stimulation and it cannot be used to differentiate between the gradually increasing temperature and non-stimulating condition.

Figures 3.16 and 3.17 and table 3.5 showed that the ECoG signals during the “Anesthesia” (or deep sleep) is significantly different with “wakefulness” and “post formalin” in all frequency bands except Gamma. “Wakefulness” and “post formalin” conditions are significantly different in high frequency bands (Beta and Gamma). As expected no evoked potential was detected in the time-domain of ECoG signals associated with these three conditions. Considering the amplitude and frequency criteria, the recorded signals are in good agreement with previous studies [3.13, 3.21]. Therefore, ECoG signal can be used to distinguish between the painful condition resulted from chemical stimulation with wakefulness and sleeping conditions.

CHAPTER 4

CLOSED-LOOP INHIBITION OF NOCICEPTION

4.1 Automatic Suppression Induced in Spinal Cord

4.1.1. Methodology

We utilized an integrated wireless system as a platform for recording and stimulating the nervous system [4.1]. The system is composed of a module that can be worn by rats, a receiver station and a transmitter station (see block diagram in Figure 4.1). The module acquires neuronal signals at the spinal cord, amplifies the signals and sends the modulated signals wirelessly to the receiver station that is connected to two different data acquisition units (CED 1401Plus, Cambridge Electronic Design, and USB-6008, National Instrument). The CED 1401Plus is connected to the computer #1, which acquires real-time signals through the software Spike2 (Cambridge Electronic Design). The data acquisition unit USB-6008 is connected to the computer #2 in which our program obtains the demodulated neuronal signals, processes the data, makes a decision on the triggering of stimulation and sends stimulation commands through the transmitter station wirelessly to the wearable module to initiate brain stimulation. The redundant data acquisition methods are to compare the signal recognition by Spike2 and by our own software based on the positive peak detection algorithm. The real-time processing of the recorded signals closes the feedback loop in the computer #2. LabVIEW (National Instrument) was used for programming our signal-processing algorithm in the computer #2. Since the developed system is an automatic real-time feedback system, it was called Automatic Pain Recognition and Inhibition System (APRIS).

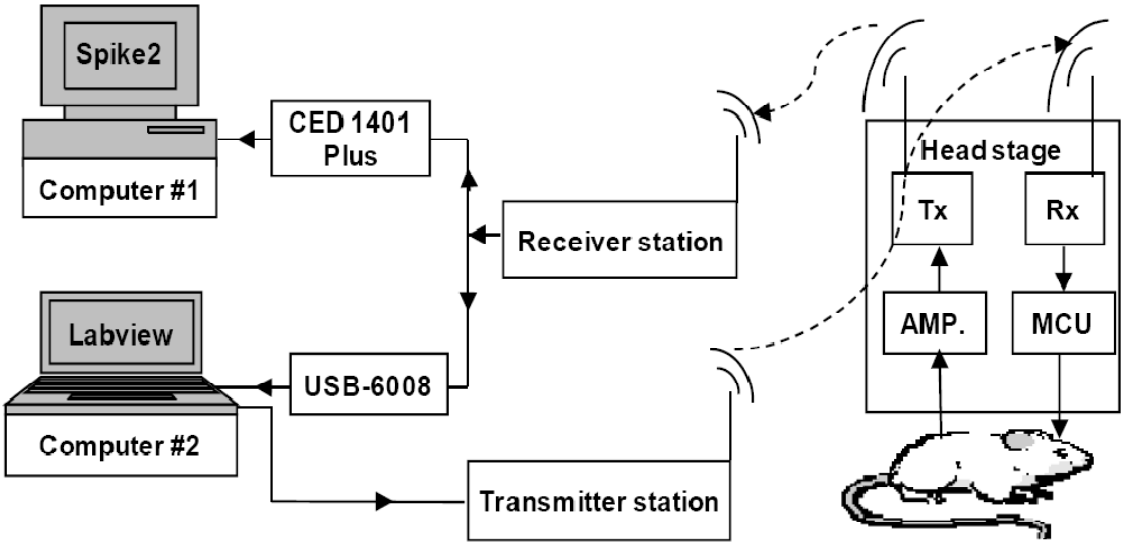

Figure 4.1 The block diagram of the system for automatic, real-time recognition and inhibition of the nociceptive signals. Action potentials were recorded from the spinal cord and transmitted wirelessly to the computers #2 where received signals were processed, and electrical pulses commands were initiated and transmitted to the wearable module on the rat to stimulate the PAG area. Computer #1, which also acquired neural signals in real-time, was used for further off-line processing and comparison of the signals.

4.1.1.1. Feedback mechanism

In order to implement a feedback loop that can continuously acquire neuronal signals, recognize nociception induced by different mechanical stimuli, and transmit proper stimulation commands, a custom-made program and graphics user interface was developed in LabVIEW. There were several design considerations for spike detection, consisting of features for discriminating types of neural activities, and a set of neurostimulation parameters for nociception inhibition.

4.1.1.2 Spike detection

A sampling rate of 10k samples/s was chosen to acquire the WDR neuronal signals assuming the duration of an action potential is in the millisecond range [4.2]. This guarantees detectable values on both positive and negative peaks of the signals. Different spike detection techniques were considered: simple threshold, energy based, matched-filter based [4.3], and template-matching [4.4]. The simple threshold (positive threshold) method was chosen due to its acceptable accuracy and simplicity of implementation [4.3]. The APRIS algorithm applies a positive threshold to the raw recorded data and detects action potentials above the threshold. Because the single microelectrode in the spinal cord may record from several neurons near the electrode and each firing with different amplitudes of spikes, the program user has a choice to set a proper threshold for recording action potentials from the desired neuron. Generally, the closer the microelectrode is to the recording cell, the higher the threshold should be set to detect the desired action potentials due to their larger amplitudes.

4.1.1.3 Neural Activity Detection

The detailed method we used for detecting different levels of neural activities was discussed extensively in our previous work [4.5] and only a brief description is given in this paper. In order to find different rates of neural activities, inter spike intervals (ISIs), which are the time differences between the detected action potential peaks, were used as the main feature [4.6, 4.7]. Detected with the preset signal amplitude threshold, ISIs of the recognized action potentials were saved in a floating numerical array called cluster. The cluster size (number of ISIs) could be set by the user to identify targeted nociceptive or other types of responses. The sum of ISIs within the defined cluster is called critical threshold. If the critical threshold exceeds the pre-determined level, the program recognized the series of action potentials as nociceptive. Depending on the signals from the recording cells, users could change the size and critical threshold of the cluster to calibrate correct detection of different neural activities related to various stimuli. In this work, the parameters (cluster size and critical

threshold) were set such that the system detected both pressure and pinch stimuli as noxious. As the noxious signals were identified, the program closed a feedback loop that initiated an electrical stimulation command and transmitted it wirelessly to the wearable module to trigger the neurostimulator.

4.1.1.4. Neurostimulation

Our system has the flexibility to generate different neurostimulation parameters called doses. These doses could be varied in frequency, amplitudes, and pulse widths of the stimulation pulses. APRIS generated stimulation commands for brain stimulation with one of these doses to inhibit nociceptive neural activities. If the firing rate returns below the threshold set for noxious activity, the program ceased commands for stimulation until the threshold was breached again. If the firing rates remained at the same level, the program triggered further stimulation with the same dose. Our pilot study showed that a series of electrical pulses with an amplitude of 1 V, a frequency of 100 Hz, and a pulse width of 100 μs were sufficient for inhibiting nociceptive neural activities. Similar stimulation doses have been used or suggested by other researchers [4.1, 4.8]. In order to effectively monitor the inhibitory effect of each delivered dose, a time delay of 1 s was considered between the dose deliveries according to the pilot studies.

4.1.1.5. Statistical Analysis

The stored digital record of unit activity was retrieved and analyzed off-line. Mean responses of dorsal horn neurons to graded mechanical stimuli (brush, pressure, and pinch) were compared for control, APRIS, and recovery. A 3 (mechanical stimulation) x 3 (electrical stimulation) repeated measure ANOVA followed by Tukey HSD post-hocs (STATISTICA, StatSoft, OK) were used to compare mean neuronal responses between when the electrical stimulation feedback was on (labeled as APRIS) and when it was off (labeled as control or recovery). Significant difference was defined at $p < 0.05$. All data were expressed in mean ± SEM.

4.1.2. Animal Experiment

In order to investigate the effect of the feedback mechanism between the nociceptive neuronal activity detected in the spinal cord and the brain stimulation, in vivo experiments were performed in seven male Sprague–Dawley rats (450 and 550 g). Brain stimulation was delivered to the periaqueductal gray (PAG) area. The rest of the procedure for recording the signal was followed similar to section 3.1.2.

4.1.2.1. Stimulating Sites

After craniotomy, a bipolar stimulating electrode (SNE-100, Science Products) was placed in the PAG, 7.04 mm caudal from bregma, 0.5 mm lateral right from the midline, and 5 mm deep from the brain surface [4.9]. The electrode was connected to the wearable wireless device for bipolar stimulation. After each experiment, the brain was extracted and immerged in 10% formaldehyde solution. Serial coronal sections of the brain were sliced in 80 μm thickness, stained with thionin, and mounted on slides for histological verification of the stimulating electrode track. The site of the stimulating electrode was localized and verified under a microscope.

4.1.3. Results

4.1.3.1. PAG and SC verified as two stimulation targets

Histological observations found that the electrode tips were placed in the right PAG for two animals and in the right SC deep layers (less than a millimeter above the PAG) in five other animals (Figure 4.2). Targeted areas for the PAG are distinguished in black circles, and SC targets are in gray squares.

Figure 4.2 Location of stimulating electrode tips in the periaqueductal gray (PAG; black circles) and superior colliculus (SC, gray squares).

4.1.3.2. Distinguishable clustering of ISIs for two neurons

Clustering of inter spike intervals (ISIs) was used to classify different levels of neural activities. Clusters of 15 and 25 ISIs during brush, pressure and pinch stimuli in the control state, for two different neurons are depicted in Figure 4.3a and 4.3b, respectively. In these two representative neurons, only two series of ISI clusters are illustrated in each figure. These two series of clusters for each neuron allowed us to conduct comparison (in the later discussion section). The details of choosing proper cluster sizes for identifying mechanical stimuli were discussed in our previous work [4.5]. In brief, after a cluster size (number of ISIs) was chosen (e.g., 15 ISIs), the first and second clusters were defined as the first 15 ISIs and subsequent 15 ISIs in response to a specific mechanical stimulus. In neuron #1, a cluster size of 15 was chosen and the sum of total ISIs of the first cluster for brush, pressure and pinch were 3.86, 0.26, 0.18s, respectively, and corresponding values for the second cluster were 3.45, 0.69 and 0.17s, respectively. Similarly for neuron #2 (Figure 4.3b), a cluster size of 25 was chosen and the sum of total ISIs of the first cluster for brush, pressure and pinch were 3.28, 0.40, 0.20s, respectively, and corresponding values for the second cluster were 4.11, 0.74, and 0.26s, respectively.

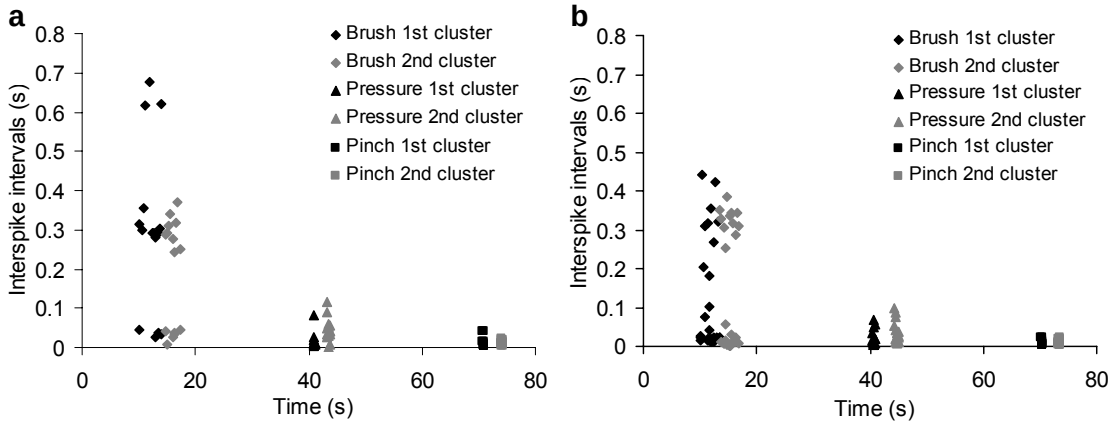

Figure 4.3 Representative two series of clusters of 15 ISIs for neuron #1 (a), and 25 ISIs for neuron #2 (b), in response to mechanical stimuli of brush, pressure and pinch.

4.1.3.3. Real-time recognition and inhibition of nociception

To illustrate the effects of APRIS on neuronal activities compared to those in the control and recovery periods, we have depicted three segments (each 90 seconds) in one experiment (Figure 4.4a, b and c) represent the control, stimulation (APRIS-on, cluster size of 25, and critical threshold of 0.7s), and recovery periods, respectively. The suppression of the neuronal activities during the electrical stimulation was obvious in Figure 4.4b. In this particular experiment, three and four trains of stimulation (1 V, 100 Hz, and pulse width of 0.1ms) were initiated by the APRIS for pressure and pinch, respectively. When pressure was applied to the receptive field, the response increased to 4.7 spikes/0.1s (at 166th–167th s). It reduced to 0.5 spikes/0.1s when the first stimulating pulses were initiated (at 167th–168th s), with an inhibition of 89%. One second following the termination of stimulation, the rate of APs rose back to 1.7 spikes/0.1s (at 168th–169th s). Then the second train of stimulation was triggered, resulting in an inhibition of 65%, and so on and so forth. The stimulus trains were terminated as soon as the mechanical stimuli were eliminated.

The time delay between the initiation of mechanical stimulation and delivering of electrical stimulations by APRIS were measured as 6.85s and 1.39s for pressure and pinch stimuli, respectively, for the cluster size of 25. In another experiment on the same neuron, a

cluster size of 15 with the same critical threshold (0.7 s) was chosen and the same experimental procedures were followed. The time delay between the initiation of pressure stimulation and the delivering of electrical stimulations by APRIS was reduced to 3.29 s (Figure 4.5).

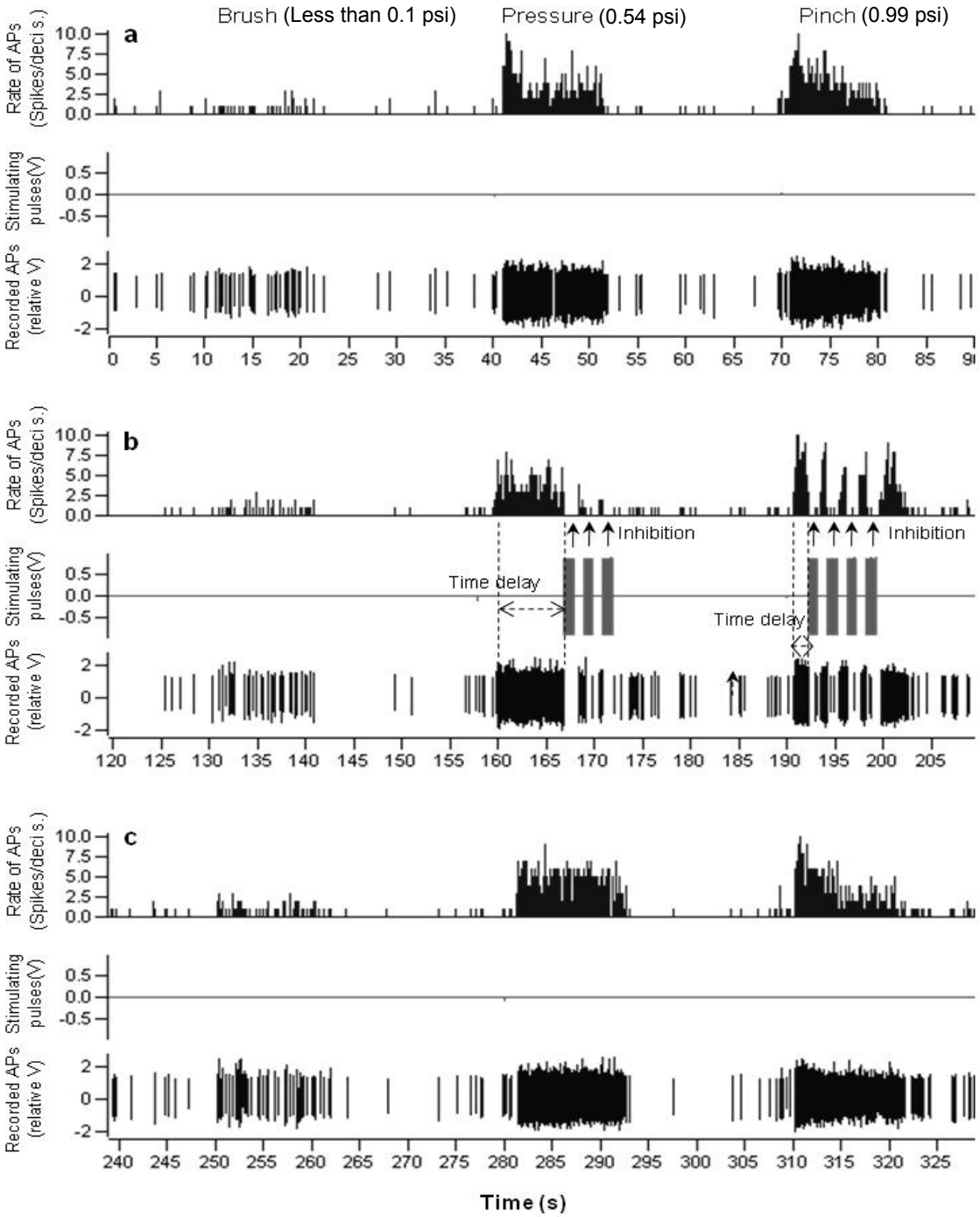

Figure 4.4 A representative dorsal horn neuron with APRIS. Neural activities during brush, pressure and pinch are shown in terms of both individual action potentials (lower panel) and the rate histogram in 0.1-s bins (upper panel) for the control (a), APRIS (b) and recovery periods (c), respectively. The initiation of electrical stimulations and inhibition of neuronal firings are indicated by vertical arrows. Time delays between the initiation of mechanical stimuli and triggering of electrical stimulation are indicated by horizontal dotted arrow.

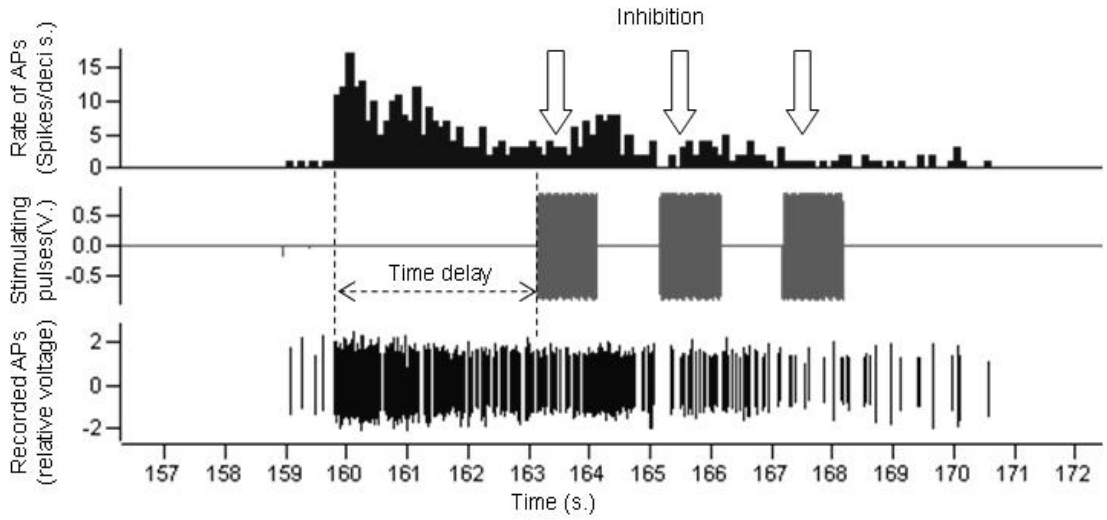

Figure 4.5 This recording was conducted on the same cell for the data shown in Figure 4b. Time delay between the initiation of pressure stimuli and triggering of electrical stimulation was measured as 3.29 s.

4.1.3.4. Performance of the APRIS system

As a measure for system responses, the number of electrical stimulation trains was obtained for each mechanical stimulus. For instance, in the experiment shown in Figure 4.4b, the numbers of stimulation trains during pressure and pinch were three and four, respectively. The average numbers of stimulations initiated by the APRIS algorithm in the PAG (n=13) and SC (n=12) areas are shown in Figure 4.6a. The numbers of electrical stimulations that were initiated during the brush stimuli were zero because the algorithm was set to recognize the brush stimulus as innocuous. When the stimulating electrodes were in the PAG, the numbers of stimulations triggered during the pinch stimulus were significantly greater than the stimulations initiated during pressure ($p < 0.01$, n=13). The same result was observed in SC-stimulated group ($p < 0.05$, n=12)

Furthermore, the time delay between the starting point of mechanical stimuli and the initiation of electrical stimulation by the APRIS was obtained for the responses to PAG stimulation (Figure 4.6b). Analysis showed the time delays for the pinch stimuli were significantly shorter than those for the pressure ($p < 0.001$) while PAG and SC were stimulated.

In addition, PAG stimulation had significantly shorter delay than SC stimulation during pinch period ($p < 0.05$).

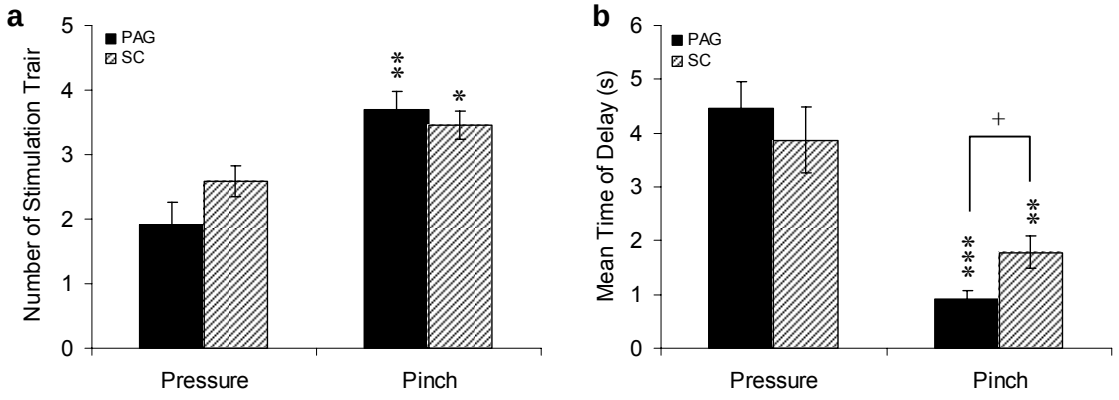

Figure 4.6 Summary of number of APRIS triggered stimulus (a) and time delay between the start of mechanical stimuli and start of electrical stimuli (b). Note: "*" $p < 0.05$, "**" $p < 0.01$, "***" $p < 0.001$, comparing between pressure and pinch; "+" $p < 0.05$, comparing between PAG and SC.

4.1.3.5. Significant inhibition for pressure and pinch stimuli with stimulation in PAG

Twenty-six WDR neurons from two rats were used for analyzing the effects of APRIS when the stimulation site was in the PAG. The responses (spikes/second) of the neurons to different mechanical stimuli during periods of control, stimulation, and recovery were: (1) for brush: 9.45 ± 1.74, 9.41 ± 1.8, 9.59 ± 2.11; (2) for pressure: 28.45 ± 4.90, 18.89 ± 3.15, 30.75 ± 5.88; and (3) for pinch: 41.10 ± 6.13, 24.51± 4.34, 37.61 ± 5.61 (Figure 4.7a). A 3 x 3 repeated measure ANOVA revealed the following effects for the mean responses of the neurons: mechanical stimulation, $F(2, 50) = 26.3$, $p < 0.001$; electrical stimulation, $F(2, 50) = 15.6$, $p < 0.001$; and mechanical stimulation x electrical stimulation, $F(4, 100) = 9.7$, $p < 0.001$. Following the omnibus test, a post-hoc analysis was done using the interaction effect (Figure 4.7a). The neuronal activities induced by the pressure stimulus were inhibited by electrical stimulation compared to those in control ($p < 0.001$) and then returned to an activity level similar to those in control during the recovery period, given that there were no significant differences in action potential rates between the control and recovery periods. The case of pinch stimuli showed the

same trend, such that the activities were inhibited by electrical stimulation ($p < 0.001$) and returned to the rates similar to those in the control case during the recovery period. There were no differences when comparing any of the brush cases, which were expected considering that the program defined brush as a non-responsive stimulus.

In addition, the mean percent changes of the APs during the stimulation (with the APRIS turned on) and the recovery periods in respect to the control were: (1) for brush: (13.48 ± 9.38, 8.52 ± 8.90); (2) for pressure: (-28.22 ± 6.08, 10.33 ± 9.09); and (3) for pinch (-40.98 ± 4.47, -9.44 ± 4.78) (Figure 4.7b). A repeated measure ANOVA revealed the following effects: mechanical stimulation, $F(2, 50) = 11.9$, $p < 0.001$; electrical stimulation, $F(2, 50) = 9.5$, $p < 0.001$; and mechanical stimulation x electrical stimulation, $F(4, 100) = 10.1$, $p < 0.001$. Following the omnibus test, a post-hoc analysis revealed that the mean changes in response to pressure ($p < 0.001$) and pinch ($p < 0.001$) stimuli were significantly lower during the stimulation in compare to the control. There were no significant differences observed between the control and recovery conditions for either pressure or pinch stimuli. There were also no differences when comparing any of the brush conditions. Overall, these results suggested that the APRIS program was able to suppress nociceptive neuronal activities originated from mechanical pressure and pinch.

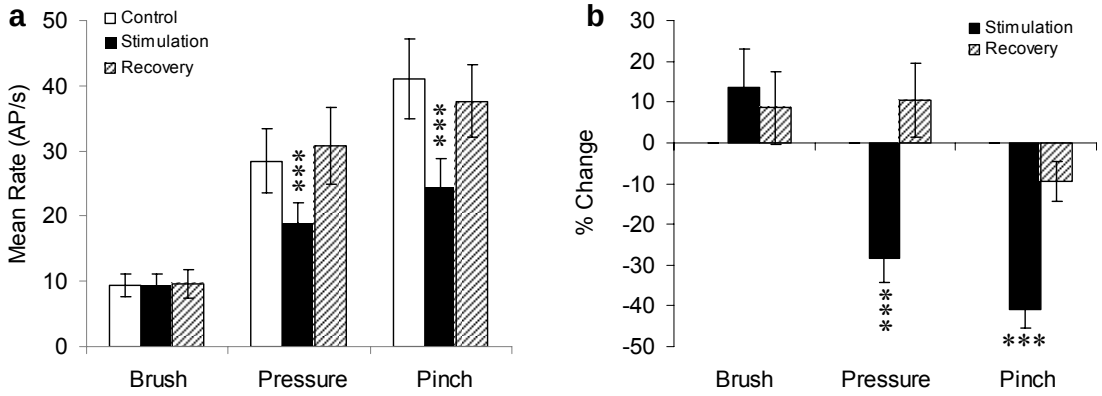

Figure 4.7 Summary of dorsal horn neuron responses to graded mechanical stimuli with or without APRIS-evoked PAG stimulation for raw (a) and percent change (b). Note: "***" $p < 0.001$.

4.1.3.6. Significant inhibition for pinch stimulus when deep layers in the SC were stimulated

For analyzing the effects of electrical stimulation initiated by APRIS on the deep layers of the SC, twenty-nine WDR neurons from five rats were examined. Accordingly, the responses (spikes/s) of WDR neurons to graded mechanical stimuli during the periods of control, stimulation, and recovery were: (1) for brush: (7.26 ± 1.15, 7.73 ± 1.12, 8.07 ± 1.39); (2) for pressure: (24.39 ± 3.95, 19.65 ± 3.76, 25.59 ± 4.83); and (3) for pinch: (32.18 ± 5.19, 26.30± 4.844, 30.69 ± 5.38) as shown in Figure 4.8a. A 3 x 3 repeated measure ANOVA revealed the following effects: mechanical stimulation, $F(2, 56) = 21.9$, $p < 0.001$; electrical stimulation, $F(2, 56) = 4.7$, $p < 0.05$; and mechanical stimulation x electrical stimulation, $F(4, 112) = 2.8$, $p < 0.05$. The omnibus test followed by a post-hoc analysis using the interaction effect did not show a significant difference between the control and stimulation periods, suggesting that there was no inhibition, for pressure stimuli ($p = 0.09$). The responses for pinch stimuli, on the other hand, were inhibited by electrical stimulation compared to the control ($p < 0.05$); there were also no differences when comparing any of the brush conditions, suggesting that the program defined brush as an innocuous stimulus.

Furthermore, the percent changes during stimulation and recovery) were 13.59 ± 10.30 and 10.56 ± 10.20 for brush; -15.89 ± 10.09 and 18.51 ± 17.30 for pressure; and -22.90 ± 5.47 and -9.77 ± 5.44 for pinch, respectively (Figure 4.8b). A repeated measure ANOVA revealed the effects for mechanical stimulation, $F(2, 56) = 3.0$, $p = 0.06$; electrical stimulation, $F(2, 56) = 2.2$, $p = 0.16$; and mechanical stimulation x electrical stimulation, $F(4, 112) = 4.5$, $p < 0.05$. Statistical analyses on the mean percent change revealed that there was a significant difference only between the stimulation (APRIS on) and control period during the pinch stimuli.

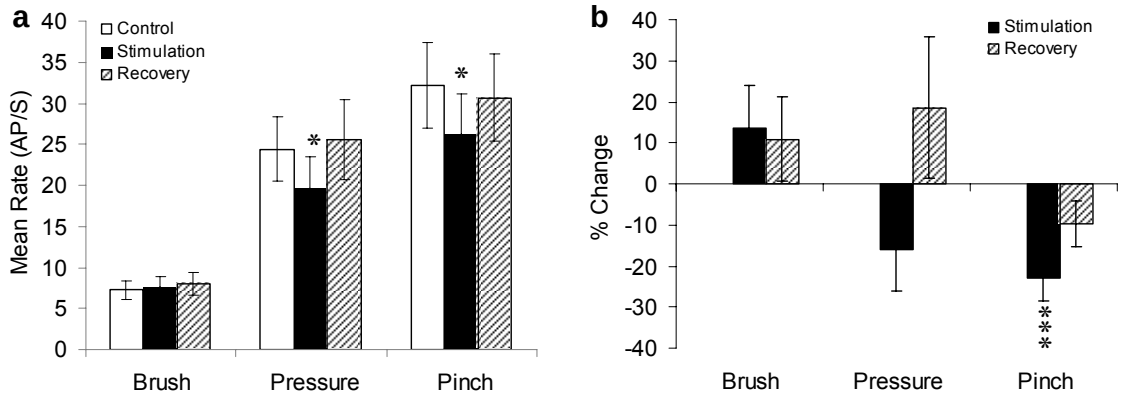

Figure 4.8 Summary of dorsal horn neuron responses to graded mechanical stimuli with or without APRIS-evoked SC stimulation for raw (a) and percent change (b). Note: "*" $p < 0.05$, "***" $p < 0.001$.

4.1.4. Discussion

In this study, we implemented a feedback system that can recognize dorsal horn nociceptive signals from three different mechanical stimuli (brush, pressure and pinch) and suppress nociceptive signals by initiating and delivering electrical stimulation in the brain. The system performance was demonstrated with our automatic pain recognition and inhibition algorithms. It was then verified through off-line analysis carried out by Spike2.

4.1.4.1. Strategies to determine cluster size and critical threshold in APRIS algorithm

It was assumed that the neuronal activities of WDR neurons in response to graded mechanical stimuli differ from low to medium and high, in which low corresponded to brush, medium represented pressure and high matched with pinch stimuli. Therefore, during

experiments, we looked for the WDR cells and each recording event included at least one cell that had graded neural responses. It was also assumed that ISIs of action potentials could be used as a feature to differentiate the mechanical stimuli. Figure 4.3a and 4.3b explain the theoretical roots for this assumption. For instance in Figure 4.3a, if the user sets the critical threshold (summation of ISIs inside the cluster) as 200 ms, most likely APRIS recognizes only pinch stimulus as noxious. However, if the critical threshold is set as 1 s, APRIS detects both pinch and pressure as noxious but not the brush. It should be noted that these critical thresholds are determined considering a cluster size of 15. Different cluster sizes would yield different critical thresholds. For example, the results in Figure 4.3b were from another neuron that fired more action potentials comparing to the neuron in Figure 4.3a in response to the same mechanical stimuli, a larger size of clusters (25) were chosen. When the critical threshold was set as 200 ms, APRIS would not recognize any noxious stimulus. In this case, the user had to set the critical threshold as 300 ms for accurate recognition of pinch, and 1 s for accurate recognition of both pressure and pinch.

For meaningful description, only two series of ISI clusters were illustrated. However, if we consider all of the clusters (during pinch stimuli) in Figure 4.3 (a), some of them may not meet the criteria of having a critical threshold of less than 200 ms; therefore, some of them would not be considered as noxious clusters. A user can increase the critical threshold to 400 ms to increase the chance of getting more noxious clusters. In this case, some of the clusters during the pressure stimuli could be recognized as noxious too. Considering the mean rate of APs, if one wants to set only the pinch stimulus as noxious and fixes the cluster size to be 15, on average the critical threshold has to be greater than 365 (15/41.10) ms and less than 527 (15/28.45) ms. If one aims to define both pressure and pinch stimuli as noxious while fixing the cluster size to be 15, on average the critical threshold has to be greater than 365 ms and less than 1.59 (15/9.45) s.

4.1.4.2. APRIS initiated more stimulation for pinch than for pressure

Because the firing rates during the pinch stimulus were more than those for pressure (Figure 4.4), it was expected to see more neurostimulation (doses) initiated by APRIS during pinch than pressure. The number of stimulation (PAG or SC) generated during pinch was significantly higher than the number during pressure (Figure 4.6a), suggesting that APRIS triggers more stimulation events to inhibit a more intense neuronal activity. One might expect to see more neurostimulation events initiated by APRIS when stimulating the SC area because it produced less inhibitory strength. This limitation is due to the experimental protocol, not our developed algorithm. The number of stimulation during any mechanical stimulus period cannot theoretically exceed a total of five times, considering the factors of (1) the 10-second mechanical stimulus period, (2) a minimum delay time of one second between stimulation triggers, and (3) the average delay time of one second that takes for the APRIS to detect the nociceptive activity and trigger the stimulation. Furthermore, two reasons also limit the maximum number of stimulations in the mechanical stimulus period: (1) Even without brain stimulation, the rate of action potentials in response to pinch stimuli naturally decayed during the ten-second periods (Figure 4.4), which is consistent with previous studies [4.10]; and (2) After triggering the electrical stimulation, the inhibition effect sometimes last beyond the time duration of electrical stimulation (Figure 4.4b) following the first electrical stimulation.

APRIS did not initiate any stimulation for the brush stimuli because brush was defined as innocuous in the algorithm. This feature helps to define painful signals and can potentially save battery life for a pain management implant in a patient since innocuous signals will not trigger unnecessary electrical stimulation.

4.1.4.3. APRIS initiated faster stimulation for pinch than for pressure

Ideally, the algorithm would detect the nociceptive activity immediately after initiation of the noxious stimulus. However, there is a time delay between the beginning of noxious stimulation and the initiation of electrical stimulation (Figure 4.6b). APRIS will take time to

recognize neuronal activities to determine the cluster size and depends on critical threshold set by user. It also takes time for the ISI array (cluster) to be filled and to judge if the sum of the array elements exceeds the critical threshold for nociception detection. The time to accumulate sufficient information contributes to the lag in the system. The cluster size also plays a key role in the accuracy of nociception recognition. In general, if the neuronal firing rate is high, the user needs to set a larger cluster size that will take more time to fill and so lead to a longer delay. In the case for the neuron measured in Figure 4.4b, a larger array size of 25 was set to detect the nociceptive activities; hence, a delay time of 6.85 s was obtained. In the same neuron (Figure 4.5), we decreased the cluster size to 15, the sensitivity of APRIS increased as the neuronal activities for pressure were recognized more quickly with a delay time of 3.29 s rather than 6.85 s. Further decrease in the cluster size will result in an increase in sensitivity; however, an excessively sensitive algorithm may mistakenly recognize a brush stimulus as noxious. Overall, because the goal for APRIS is to provide objective recognition of chronic pain signals, a few seconds of delay in recognition may not be as critical as a correct detection method.

4.1.4.4. Spinal dorsal horn neuron can be inhibited by using APRIS to trigger PAG or SC stimulation

The PAG is known for its descending inhibition [4.11, 4.12, 4.13], and our results (Figure 4.7) showed that the APRIS was able to monitor and recognize neural activities in order to elicit electrical stimulation to inhibit nociceptive input (i.e. PAG stimulation). The average reduction in dorsal horn neuronal responses in the PAG case was 28.22% and 40.98% for pressure and pinch stimuli, respectively, showing that the APRIS initiates sufficient intensities of electrical stimulation according to the real-time recording and recognition to suppress the nociceptive activities.

The SC is known for its prominent role in visual reflexes and the co-ordination of head, neck and eye movements [4.2]. A few studies have shown the anti-nociceptive effect of electrical stimulation in the SC in rats [4.14, 4.15], monkeys [4.16] and camels [4.17]. Our results (Figure 8) indicated that the stimulation in the SC has an antinociceptive effect. A possible descending pathway is most likely through the SC connections to the PAG [4.18] and NRM [4.19]. Both of these brain areas play a key role in descending inhibition [4.20]. An excitatory input from the SC has to the PAG, NRM, and LC could induce the inhibition in the spinal cord nociceptive activities (Figure 4.9).

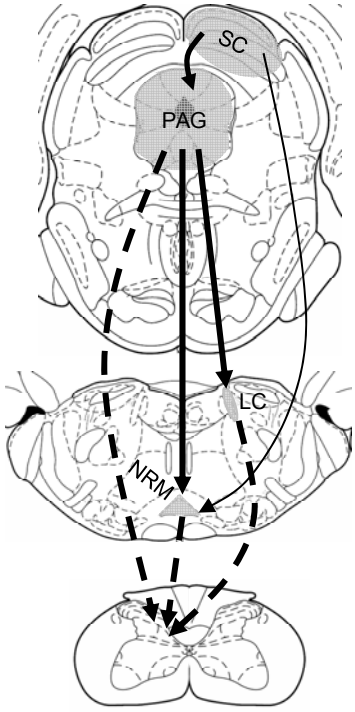

Figure 4.9 Possible mechanisms of the spinal cord dorsal horn neuron inhibition induced by superior colliculus stimulation. Filled arrow–excitatory input; dash arrow–inhibitory input; LC, locus coeruleus; NRM, nucleus raphe magnus; PAG, periaqueductal gray; SC, superior colliculus.

While SC-induced inhibition was less efficient than that of PAG-induced (Figure 4.7 & 4.8), this deficiency could potentially be improved by adjusting the electrical stimulation parameters in our system. As our algorithm initiates stimulation based on the level of neuronal activities, it further provides flexibility in adjusting stimulation parameters to optimize the

inhibition effect with the feedback mechanism. Since correct electrode placement through accurate stereotactic targeting is a key element to a successful result [4.21], this improvement could conceivably minimize the deficiency of misplacement of the stimulation electrodes in practical settings.

4.1.5. Conclusion

This real-time closed-loop feedback system has been demonstrated with integrated abilities to record action potentials, recognize nociceptive activities from a sensing area, and deliver electrical pulses to the targeted area. It opens up the possibility for more sophisticated software and hardware for neural implant applications, especially for chronic pains. Future works include extending the system that can find optimal stimulation parameters for pain inhibition in different brain areas.

4.2 Suppression Induced in Thalamus

4.2.1. Methodology

Since recording extracellular single unit action potentials from spinal cord in practical setting (i.e. in a freely behaving subject) is not feasible currently, due to the limitations in the current technology and the movement of spinal cord during signal acquisition, we investigated the thalamic neucli (VPL and VPM) as possible alternate. The objective of this experiment was to see whether the WDR neurons in the VPL and VPM nuclei are responding to the electrical stimulation delivered to PAG or not. Therefore, a recording electrode searched the thalamic area associated with VPL and VPM nuclei to find WDR neurons that are responsive to brush, pressure and pinch mechanical stimuli. More details on the recording procedure were provided previously in section 3.2.

Each experiment comprised of three sections: control, stimulation and recovery. The mechanical stimulus was applied once for 10 seconds with an inter-stimulus interval (rest) of 20 seconds as a 90-second sequence of (brush-rest-pressure-rest-pinch-rest) during each section, with control being first, stimulation the second and recovery to be last segment. During

stimulation segment, experimenter initiated five stimulation pulses during each mechanical stimulus. Each stimulation pulse lasted for one second and comprised of mono-polar pulses (1 V amplitude, 100 Hz, and 0.1 ms pulse duration). Therefore, five stimulation pulses were generated during brush, five during pressure and five during pinch for the stimulation segments.

4.2.2. Animal Experiment

Nine male Sprague–Dawley rats (430 and 520 g) were used for these experiments. Animal preparations for recording the signals were followed similar to the description in section 3.2.2. The procedures described in 4.1.2, were followed for animal preparations for stimulation of the brain. Mechanical stimuli were applied to the left hind paw, neuronal signal were acquired from the left VPL/VPM nuclei of thalamus and electrical stimulations were applied to the right PAG for each rat. All surgical procedures were approved by the University of Texas at Arlington Institutional Animal Care and Use Committee. The procedures were in accordance with the guidelines published by the Committee for Research and Ethical Issues of the International Association for Study of Pain [4.22].

4.2.3. Results

From the nine animals used for this experiment, five were verified through histology to have the stimulation electrode in the accurate location i.e. PAG. Forty neurons were recorded from these five animals. In some of the experiments, the action potentials were inhibited during the three mechanical stimuli (Fig. 4.10) and in some other experiments, only action potentials in response to pressure and pinch were inhibited (Fig. 4.11). Overall, the mean of the rate of action potentials per second ± SEM is presented in Figure 4.12.

Figure 4.10 shows the baseline (a) and stimulation (b) segments of a typical experiment. In each figure, bottom panel shows the action potentials that were fired, the middle panel shows the stimulating pulses that were initiated by the experimenter and the top panel shows the rate of action potentials that were generated during brush, pressure and pinch stimuli. In this specific experiment, neuron was also firing with a rate that was lower than the

rate during any of the mechanical stimuli. The neuron fired the most during the pinch stimulus and less during pressure and brush stimuli. Figure 4.10 (b) shows the same neuron during the stimulation period. As obvious in this figure, 5 trains of electrical stimulations were applied during each mechanical stimulus. The rate of action potentials decreased significantly while the stimulation triggered. Figure 4.11 shows another neuron during the stimulation period. As obvious in this figure, the neuron was not inhibited during brush, but some inhibition occurred during pressure and pinch.

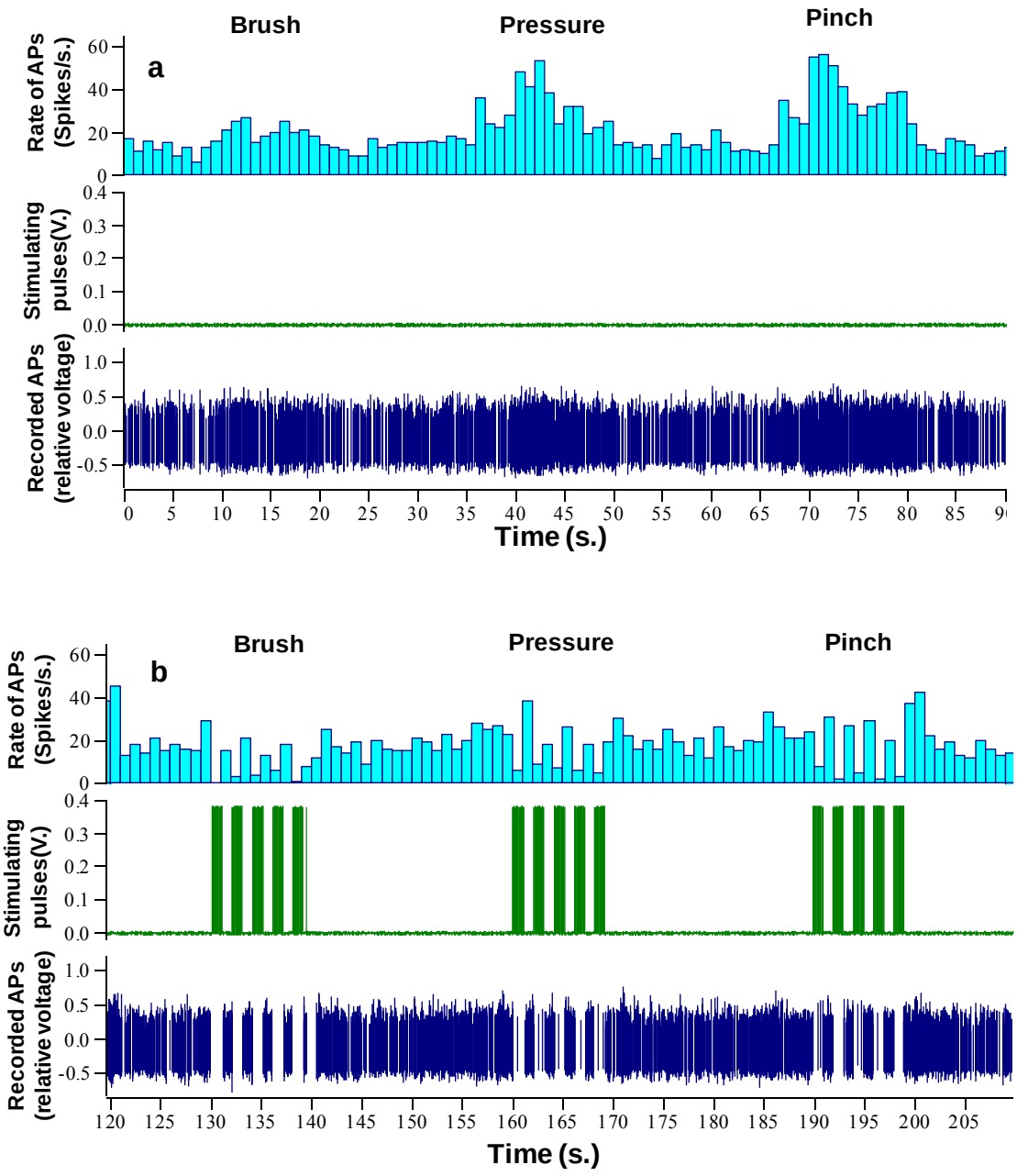

Figure 4.10 Response of a WDR neuron to various mechanical stimuli (brush, pressure and pinch), during the control (a) and stimulation (b) periods. The inhibition of the neuron during the electrical stimulations caused the decrease in the rate of action potentials.

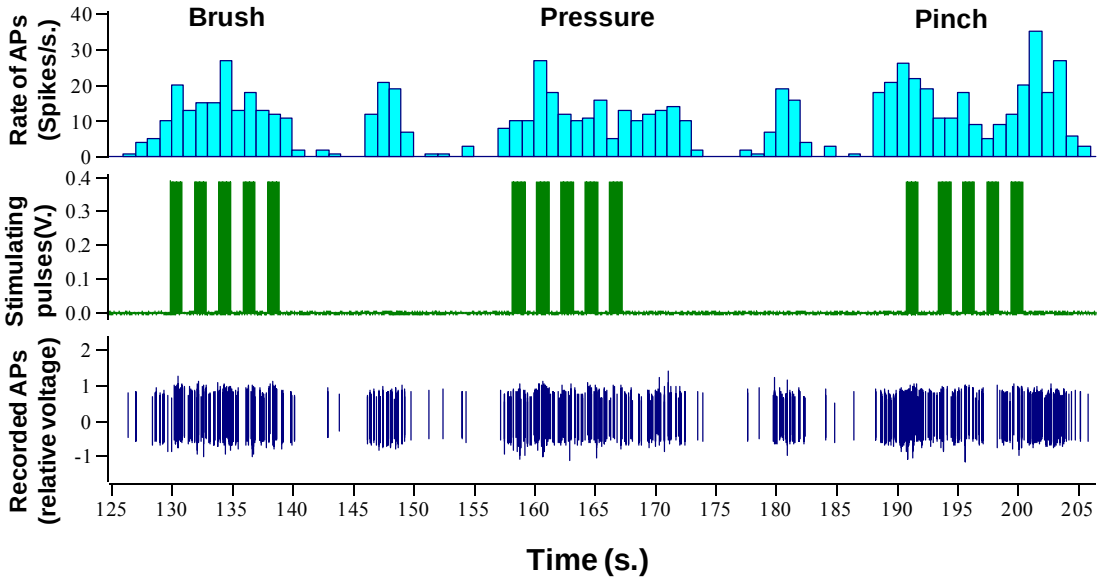

Figure 4.11 Response of a WDR neuron to various mechanical stimuli (brush, pressure and pinch), during the control and stimulation period. No inhibition was seen during the brush, while some inhibition during pressure and pinch.

Figure 4.12 shows mean rate of action potentials ± SEM for forty neurons. Student t-test that was conducted on the data showed no significant difference between the rate of action potentials in any of the control, stimulation and recovery for the brush stimulus. No significant difference was seen between the mean rate of action potentials of control and recovery periods during pressure and pinch stimuli, however, the mean rate decreased significantly (marked with *) during the stimulation periods of the pressure and pinch stimuli (p-value < 0.05). The mean rate of action potentials was decreased by 31% and 43% during stimulation period of pressure and pinch stimuli respectively.

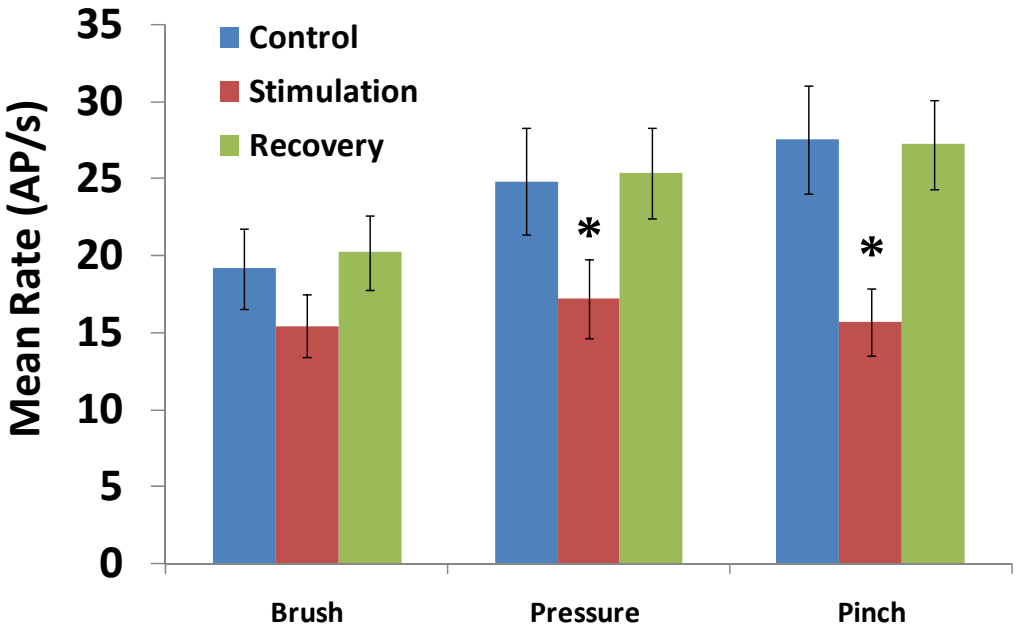

Figure 4.12 The mean rate of action potentials per second ± SEM for forty WDR neurons in response to graded mechanical stimuli (brush, pressure and pinch). The rate significantly decreased during the stimulation period in compare to control for pressure and pinch stimuli.

CHAPTER 5

FUTURE PERSPECTIVES

5.1 Novel Applications for the Wireless Platform

In this section, two novel applications of the developed wireless platforms and some preliminary results for each platform have been presented. These two applications include acquisition of transcranial motor evoked potentials and gastric electrical activity.

5.1.1. Transcranial Motor Evoked Potentials

5.1.1.1. Introduction

Intraoperative neurophysiological monitoring (IONM) is routinely used in neurological, orthopedic, and vascular surgeries to prevent unintended damage to the central and peripheral nervous system. IONM relies on transcranial motor-evoked potential (TcMEP) consisting of evoked descending neural signals from the motor cortex and recorded from the distal limb muscles, and on somatosensory-evoked potentials (SSEP) consisting of ascending sensory signals evoked in peripheral nerves and recorded from peripheral nerve, spinal cord and sensory cortex. In spine and thoracic surgery, IONM is of critical importance in order to detect early damage to the spinal cord in case of unintended insult, so that appropriate actions can be immediately taken to reverse the damage and prevent permanent neurological injury [5.1, 5.2]. Although the critical nature and need of IONM is well established, current monitoring systems have some important limitations. For instance, commercially-available IONM systems such as Digitimer (Digitimer Ltd., Welwyn Garden City, UK), Cadwell (Cadwell Lab Inc., Kennewick, WA, USA), Axon (Axon Inc. Hauppauge, NY, USA), and Nicolet (CareFusion Co., Madison, WI, USA) [4], often require up to 40 to 60 lead wires for stimulating and recording during spine surgery. The large number of electrodes, proportionally increases the IONM setup time needed

as a certain amount of time is required to verify all the accurate connections, which in turn, proportionally affects the time of anesthesia for the patients, which has been associated with possible deleterious effects [5.3].

In addition, most IONM systems use lengthy lead wires (i.e., 1.5 - 2.5 m), which despite the insulation, bear intrinsic antenna effects which affect the quality and sensitivity of the neural signals, due to electromagnetic interference (EMI) generated by other equipment in the operating room [5.4, 5.5]. Shielded wires and high common-mode rejection ratio (CMRR) techniques have been used to reduce the power-line interference. However, neither of these techniques can eliminate the power-line interference completely [5.6] since any part of the long connection wire can behave as an antenna coupling surrounding electromagnetic waves into the wire.

Together, the number and length of most IONM lead electrodes contribute to a cumbersome surgical area, in which the many wires unnecessarily crowd the operating room (OR), thus limiting the maneuverability of the surgeon and staff.

Wireless technology has positively affected a number of fields including medicine as wireless systems have been established for electroencephalography [5.7, 5.8], neural activity recordings [5.9, 5.10], electromyography, electrocardiography, and electro-oculography [5.11, 5.12]. This trend is predicted to continue growing as wireless systems add convenience to care providers and patients [5.13]. Since recording the TcMEP and SSEP signals are of high interest even in conscious subjects [5.14, 5.15], it would be more convenient for both patients and care providers to utilize wireless technology for acquiring these signals. According to our best knowledge, no wireless system has been developed for monitoring either TcMEP or SSEP signals.

We have developed a wireless method for acquiring IONM TcMEP signals. The communication range, sampling rate, amplification and filtering levels, as well as the reliability of

the system were defined and tested in a rodent animal model. In addition, the compatibility of our wireless system with a currently-available commercial recording system was evaluated.

5.1.1.2. Materials and Methods

Recording of transcranial motor-evoked potentials (TcMEPs) in IONM during surgery on human is accomplished by stimulation of the motor cortex with a train of 5–7 pulses, an amplitude of 100–300 V, a pulse width of 50–100 μs, and an inter-stimulus interval of 2–4 ms [5.16, 5.17, 5.18]. This stimulation paradigm evokes responses with amplitudes ranging from tens to several hundreds microvolts in the patient's limb muscles. Such signals are then evaluated according to an "amplitude criterion" and a "morphology criterion" [5.19]. The ''amplitude criterion'' is based on a decrease of more than 80% in one or more response amplitudes [5.20] and the "morphology criterion'' is based on changes in the waveform morphology of the TcMEP response [5.21]. We have adapted these evaluation methodologies for bench-top and animal trials of the wireless IONM system.

5.1.1.2.1 Wireless system for TcMEP acquisition

The wireless system is composed of a front-end module placed on the subject side and a back-end receiver placed on the recorder, in our case the Cadwell Cascade™ system (Fig. 5.1). The front-end includes multi-amplifying stages, a high-pass filter, and a 914 MHz-transmitter module (64 kbit/s) that can achieve a communication range up to 300 m in the industrial, scientific and medical (ISM) band. The amplifying stages on the front-end consist of an instrumentation amplifier (gain of 10.7) and two-stage amplifiers (with a gain of 15 each) creating a total gain of 2,407 for recording signals as low as 10 μV. AD620 (Analog Devices, Inc.), which has a common-mode rejection ratio (CMRR) of 80 dB, an input impedance of 1 GΩ, and an input bias current of 2 nA was used as the instrumentation amplifier. TLV2264 (Texas Instruments, Inc.) was used to make the two-stage non-inverting amplifiers. The amplified signals passed through a high-pass filter connected to a virtual ground to pull the signals to the 0–2.5 V level, which is in the analog input range of the wireless transmitter module (TX3A,

Radiometrix, Ltd.). The high-pass filter eliminates low frequency components in signals generated by the patient's movement. More details about the design of the front-end were described by Ativanichayaphong *et al.* [5.22].

The back-end receives signals and feeds them to a commercial (Cadwell Cascade™) IONM system. The back-end is composed of a 914 MHz receiver module (RX3A, Radiometrix, Ltd.) and an attenuator. Preliminary studies showed that a power attenuation of 26.5 dB was needed to match the scale of the amplitudes in the signals acquired with the wireless system (Ch. #2) to those acquired with Cadwell Cascade™ (Ch. #1) directly. The signal waveforms from the standard wired connection and the new wireless communication could then be compared directly to examine system performance.

5.1.1.2.2 Animals

Five adult female Long Evans rats (270-310 g) were used to test the wireless system performance. The animals were anesthetized with sodium pentobarbital (50 mg/kg, i.p.). Stimulating electrodes were placed subdermally over the motor cortex and recording electrodes (indicated by solid line in Fig. 5.1) were placed in the deltoid and gluteal muscles. Reference electrodes (dashed-line) were located in the paws and a ground electrode (dotted-line) inserted in the ventral thigh (Fig. 5.1). Subdermal needle electrodes (Viasys Healthcare Ltd., San Diego, CA, USA) were utilized for both stimulation and recording. The animals were maintained under conditions of controlled light and temperature. Institutional Animal Care and Research Advisory Committee regulations and protocols were followed for electrophysiology and care procedures. The University of Texas at Arlington Institutional Animal Care and Use Committee (IACUC) approved all the procedures.

5.1.1.2.3 Recording of TcMEPs

Transcranial motor evoked potentials were simultaneously obtained with conventional wires and our wireless device to perform comparison. The evoked potentials from a single electrode were split into two recording paths. Path #1 connected the electrode by wires to

channel #1 of the amplifying module of a Cadwell Cascade™ system (Cadwell Lab Inc., Kennewick, WA, USA) and path #2 connected the signals from the front-end module through wireless communication to a receiver (back-end) connected to channel #2 of the Cadwell amplifying module (Fig. 5.1). The Cadwell Cascade™ system was used to evoke motor activity in rat by applying a train of three stimulation pulses (6 V amplitude, 50 μs duration, and 2 ms interval) over the primary motor cortex. TcMEP signals were recorded at a rate of 21,500 samples per second. Low (lower than 100 Hz) and high (higher than 2 kHz) frequency components were filtered out, and the remaining was amplified, processed and stored.

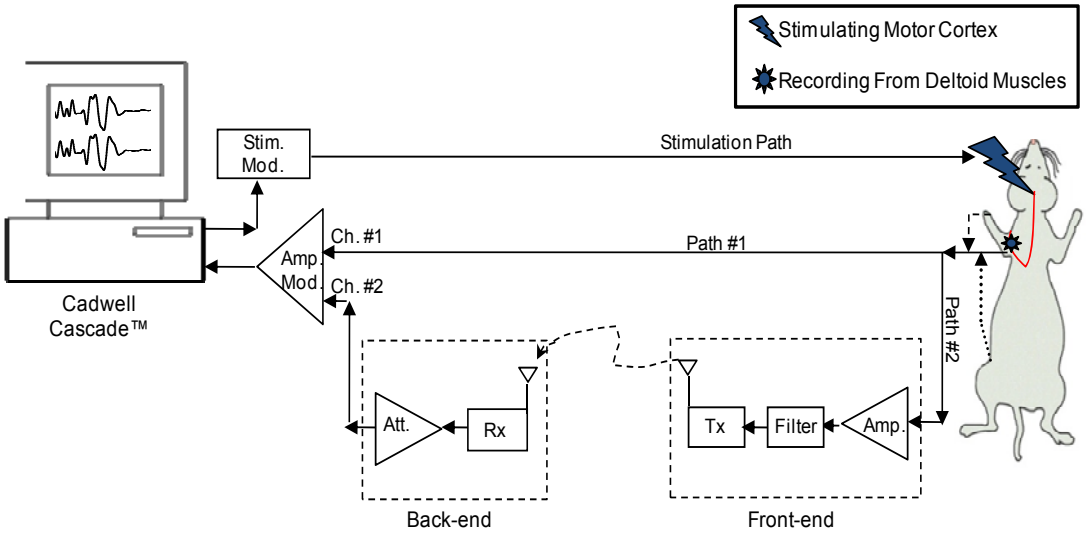

Figure 5.1 Block diagram of the animal experimental IONM setup. Channel #1 signals were acquired directly by the Cadwell Cascade™ through wires placed in the forelimb muscles (Path #1). In contrast, channel #2 signals were also acquired from electrodes connected from the forelimb muscles to the front-end module (Path 2), wirelessly transmitted to the back-end receiver, and subsequently imported to the Cadwell Cascade™. Recording, reference and ground electrodes are indicated by solid, dashed and dotted lines, respectively. Abbreviation in figure: stimulation module (Stim. Mod.), amplifying module (Amp. Mod.), amplifier (Amp.), transmitter (Tx), receiver (Rx) and attenuator (Att.).

5.1.1.3. Results

5.1.1.3.1. Improved frequency responses with wireless transmission

Bench-top experiments were carried out using sinusoidal waveforms produced by a function generator at amplitudes ranging from 100 μV to 1.6 mV. The spectral responses in the communication paths were measured in the frequency range from 100 Hz to 1,500 Hz at low (100 μV) and high (1.6 mV) signal amplitudes (Fig. 5.2). Both spectral responses at low and high amplitudes were similar in both the wired and the wireless systems, indicating the signals were not saturated or distorted in either communication path. Neither path contained recognizable nonlinear or amplitude-dependent components, which are specific to the amplifiers and transistors used in our module; hence, the responses do not depend on the amplitudes of input signals. The direct-wired connection has a flat passband from 400 Hz to 1 kHz while the wireless communication path has a flat passband from 200 Hz to 1 kHz. The improvement in passband bandwidth with the wireless system could be due to the elimination of the long wire connection, which added excessive inductance and resistance in the equivalent filter circuit of the communication channel resulting in an additional roll-off frequency at 400 Hz. This is further indicated by the fact that the roll-off slopes below 200 Hz in the Path #1 (wired) connection were doubled compared to those in Path #2 (wireless).

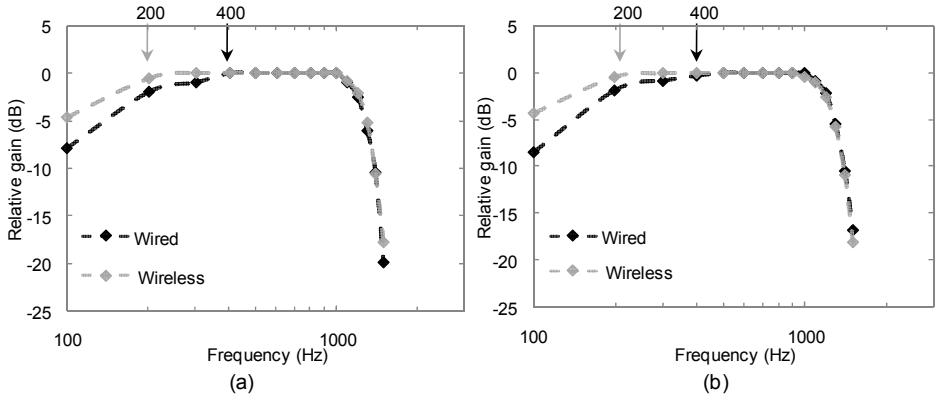

Figure 5.2 Frequency responses of communication channels for wired (Path #1) and wireless (Path #2) connections. Input signals with amplitudes of (a) 100 μV and (b) 1.6 mV were applied.

5.1.1.3.2. Wireless recording of TcMEP signals

TcMEPs elicited by a train of three electrical stimuli in the rat motor cortex and recorded through the wired and wireless systems according to Fig. 5.1, showed four specific peaks (Fig. 5.3). The first three peaks with an interval period of 2 ms represented the stimulation artifacts and the fourth peak was the acquired TcMEP signal. The TcMEP signal shapes (peak 4) recorded with the wired system (Fig. 3a, 234 μV, 6.98 ms) or with the wireless device (Fig. 5.3b, 231 μV, 7.07 ms) were indistinguishable. This demonstrates the fidelity in signal detection of the wireless system.

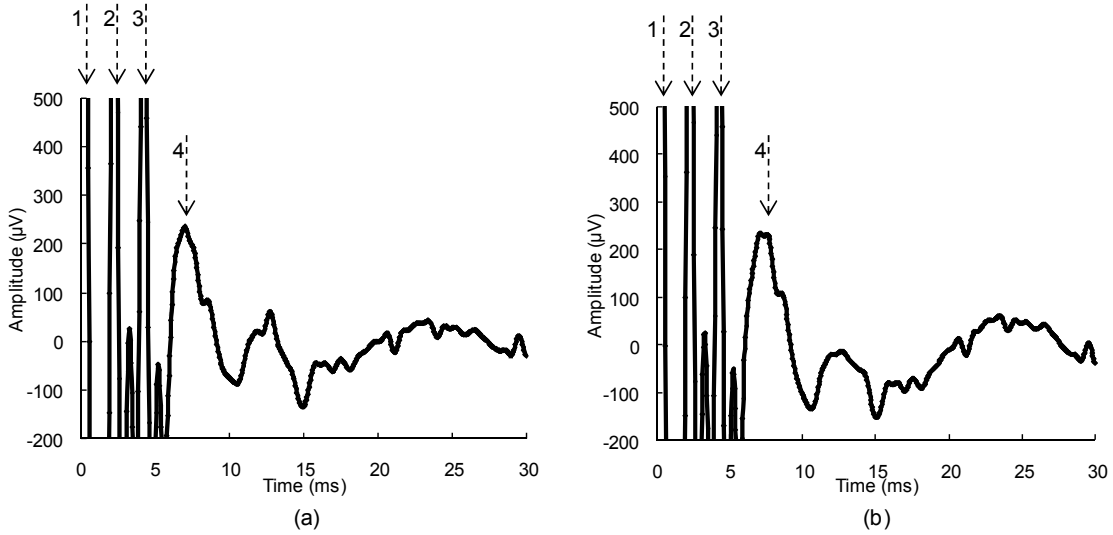

Figure 5.3 TcMEP signals obtained through (a) the wired (conventional) method and (b) the wireless communication methods. The peaks 1-3 represent stimulation artifacts and the peak 4 represents the TcMEP response.

To further investigate the commonalities between the wired and wireless signal acquisition systems, we performed a power spectral density (PSD) analysis (Fig. 5.4). Three major peaks (arrows in Fig. 5.4) for TcMEP signals were identified in both recording systems. The peaks for the wired acquisition method were at 250, 500 and 1000 Hz with relative powers of 111.3, 121.5 and 121.1 dB, respectively. The corresponding peaks for the wireless acquisition method were also detected at 250, 500 and 1000 Hz with relative powers of 111.7,

121.6 and 121.1 dB, respectively. The PSD analysis confirmed the similarity of the recorded signals.

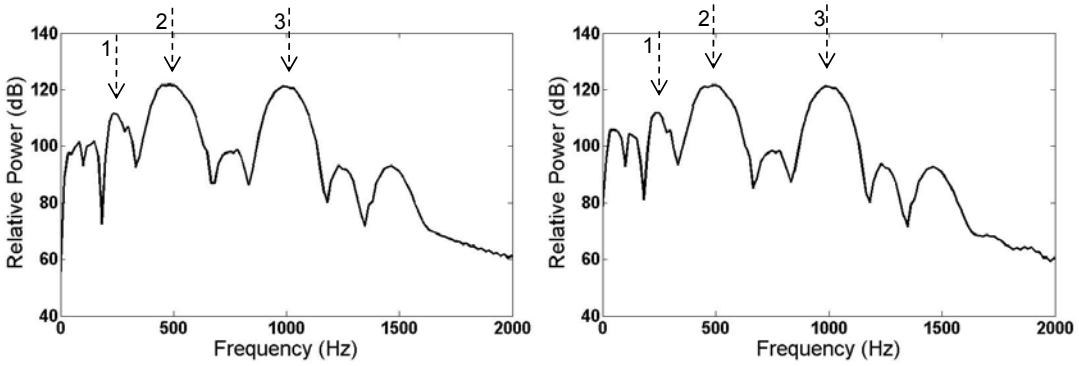

Figure 5.4 The power spectral densities (PSDs) of the signals through the (a) wired and (b) wireless acquisition methods. Major peaks as signatures were characterized for comparison.

5.1.1.3.3. Repeatability of the wireless recording

We evaluated the reliability of the wireless system recordings compared to the conventional wired method. A rat model was utilized in which the TcMEPs were elicited ten times consecutively with a 60-s resting time between the TcMEP stimulations. The cortical stimulation was achieved through the Cadwell Cascade™ system. Each of the ten events consisted of a train of three stimulus pulses with an inter-pulse interval of 2 ms as previously described. As the experimental setup in Fig. 5.1, the signals were recorded through both the wired and wireless methods. The obtained responses were aligned in time with respect to the trigger stimulation signals and spread out from top to bottom according to their chronological order, as shown in Fig. 5.5. As discussed before, the first three peaks represent stimulation artifacts and the peak #4 indicates the TcMEP response. Clearly, the 10 response traces obtained with both methods showed robust reproducibility, demonstrating the reliability of the wireless method.

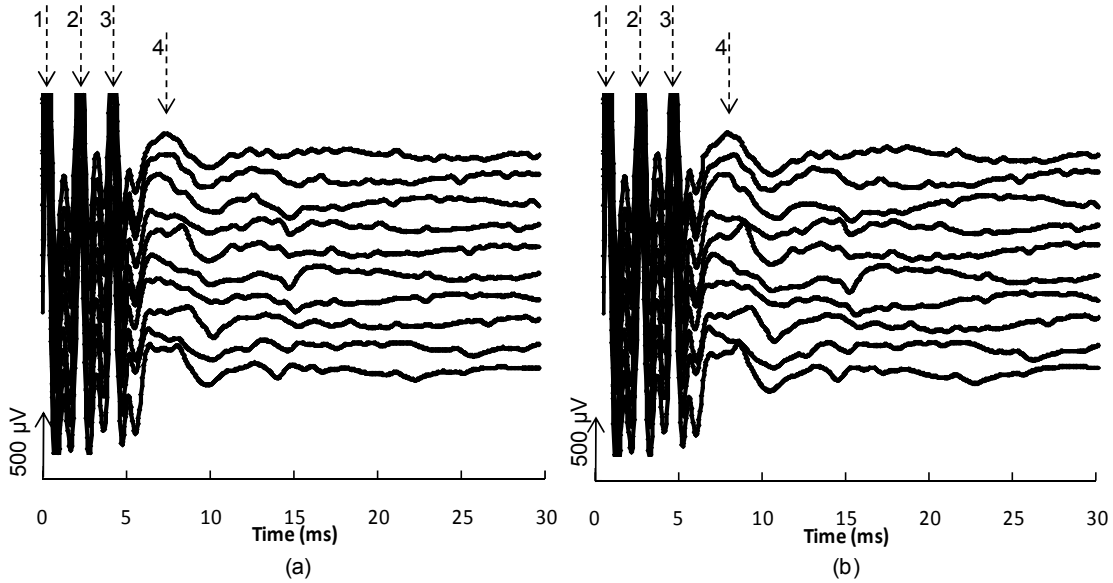

Figure 5.5 Ten successive TcMEP signals obtained through the (a) wired and (b) wireless methods. Traces were aligned in time according to the trigger stimulation signals and chronologically spread out in the vertical axis (from top to bottom) to show and compare the waveforms of individual responses. The peaks 1-3 represent stimulation artifacts and the peak 4 represents the TcMEP response.

5.1.1.4. Discussion

In this study, we developed and tested a method for wireless recording of transcranial evoked motor potentials (TcMEPs). The performance of the wired and wireless signal acquisition methods were compared in bench-top and animal experiments (Fig. 5.1). The frequency responses for both acquisition methods in response to sinusoidal waveforms at various frequencies were tested with low (100 µV) and high (1.6 mV) amplitudes (Fig. 5.2). Both acquisition methods showed similar recorded signals in the time domain. The experimental results demonstrated that the wireless method has a wider passband compared to the long-wire method. Importantly, the improved bandwidth produced less signal distortion, due to the elimination of excessive inductance and resistance inherited from the long metal connection wires. This signal distortion may be more pronounced in a hospital operating room where longer connection wires are commonly used due to the space or room/equipment layout. Using shield wires may not resolve this issue since the decrease of the passband bandwidth is due to the

inherited inductance and resistance, which are proportional to the length of metal wire. Hence, the wireless acquisition method will significantly improve the signal quality in an operating room since the signal quality does not depend on communication distance. Together, these results indicated that our developed wireless system was not only compatible with a commercially available intraoperative monitoring system, but also exceeded the performance of the wired conventional IONM methods. The animal experiments in this study confirmed the fidelity and reliability of the wireless TcMEP recording method. Typical TcMEPs waveforms recorded by both wired and wireless systems in the rat model are shown in Figs. 5.3 (a) and (b). Both methods produced very similar response traces in the time domain. The slight differences between these two figures may be due to the bandwidth differences (Fig. 5.2) discussed previously, which affect the low frequency components in the wired signals.

Overall, the wireless method provides a better-quality output in response to an input signal as more frequency components can pass through the wireless system without changes in the amplitude, which affects the morphology of the waveform. Measurement of the time differences between the corresponding peaks (the peaks 1 and 2 in the wired and wireless signals) revealed that the signal acquired through the wireless system has a 50-μs delay compared to the wired signal. This time delay is due to the communication delay and is small enough and most likely irrelevant for the intended clinical uses.

The power spectral densities of the same evoked responses through the two acquisition methods are similar, indicating that the wireless acquisition method does not significantly change the frequency response of the system. The differences in the power values of the signature frequencies, or the corresponding peaks, are small enough to be negligible.

Finally, we investigated the reliability of the wireless system, as results shown in Fig. 5.5 Comparison between traces from the paths 1 (wired) and 2 (wireless) of the same TcMEP signals revealed that the wireless system was able to record evoked potentials reproducibly over time with precise amplitude and morphology of each waveform.

In summary, we developed and examined a wireless system that can serve as a substitute for the long lead wires in a conventional IONM system. The performance of the system was tested in both bench-top and animal experiments. Comparison between the wired and wireless signal acquisition methods showed that the wireless system is able to preserve the amplitude and morphology of the TcMEP waveforms reliably and with high fidelity. Several potential advantages of wireless IONM system for human thoracic or spine surgery can be identified, such as (1) the reduction in the setup time in the OR prior to surgery as the wireless system eliminates the need to connect long wires and precisely identify them, (2) removal of the clutter of wires in the vicinity of the operation which will in turn increase freedom in mobility and convenience to the surgeon and staff around the operating room, and avoid accidental disconnection that create risks to the patient. The demonstrated fidelity and reliability of the wireless IONM system warrants evaluation of such device in the clinical setting. Our ongoing efforts are directed towards evaluating the reliability of the developed wireless system for IONM during human spine surgery.

5.1.2. Gastric Electrical Activity

5.1.2.1. Introduction

Myoelectric activity of the stomach consists primarily of very low amplitude and frequency signals termed slow waves [5.23]. Recording slow waves provides important information for evaluating gastric motility disorders including gastroparesis. For optimal data, electrodes are placed invasively on the gastric wall with wires connecting through an abdominal incision or via the mouth of the patient to an electronic recorder. We have designed, fabricated and examined a system for acquiring *in vivo* GEA signals using a commercially-available wireless transceiver nRF24Le1 that combines radio, microcontroller (μC) and analog to digital (ADC) converter all in a single chip. The design considerations for each transponder are addressed.

5.1.2.2. Materials and Methods

The analog board for the GEA system was designed to amplify signals at 65 dB and filter the undesired signals out of the range of 0.05 – 0.3 Hz. Since the slow wave signal occurs at very slow frequencies, it was sampled at a rate of 8 Sps and transmitted via the payload with a size of 4 bytes. Therefore, the T_{OA} was calculated as 0.096 ms at its maximum, which is much shorter than the sampling period. The detail for the wireless communications is similar to section 2.2.

5.1.2.3. Results

System was first examined via bench-top settings and then *in vivo* with appropriate animal models. All the procedures were approved by the relevant institution. For acquiring GEA signals, the anesthetized canine model was used in which signals were acquired from serosal membrane of the stomach using flexible PCB electrodes [5.23]. In bench top experiments, sinusoidal waves with different amplitudes and frequencies were fed into the transmitter and recorded at the receiver to determine the spectral characteristics of the communication channels. All of the pass-bands reside in the acceptable ranges of the respective signals. The reliable transmission range for each device was measured at 30 meters for GEA and ECoG

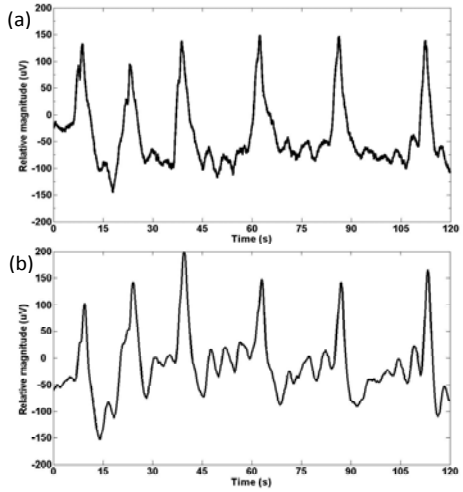

Figure 5.6. Two minutes of slow GEA wave signals recorded by (a) wired and (b) wireless systems.

transponders and 15 meters for TcMEP. The power consumptions for GEA, ECoG and TcMEP were 13.5, 21, and 30 mW, respectively, at 3V bias.

For GEA, slow wave signals were acquired for 80 minutes and the numbers of events recorded by both systems were identical. Figure 5.6 shows 2 minutes of slow wave signals recorded by (a) the wired Biosemi™ system and (b) our wireless system. The signals recorded by the wireless system preserved the critical steep peaks essential for tracking slow wave propagation across the stomach [5.23]. The differences between the trace shapes of the GEA signals recorded with wired and wireless systems (Figs. 5.6) are due to the unnecessary higher sampling rates in the wired systems and difference in pass-bands of the wired and wireless systems. This issue did not present a problem for diagnosis since the waveform characteristics (peaks) of the two methods did not show notable difference during 80 minutes of GEA recording.

APPENDIX A

MICROCONTROLLER CODE FOR TRANSMITTER

```
*/
#include <Nordic\reg24le1.h>
#include <stdint.h>
#include "hal_nrf_hw.h"
#include "MyCustom.h"


#define SAMPLING_INTERVAL_US 1000
#define CHANNEL_NUMBER 4
#define PAYLOAD_LUMPS 8
#define PAYLOAD_SIZE 32  // I have added this line to increase the payload size

#define TIMER_RELOAD_LSB (uint8_t)(0x10000-((SAMPLING_INTERVAL_US/3)*4))
#define TIMER_RELOAD_MSB (uint8_t)((0x10000 -((SAMPLING_INTERVAL_US/3)*4))>>8)

uint8_t adc_data_lsb, timer_set;
uint8_t rf_payload[PAYLOAD_SIZE], i;   //changing the Channel_number to payload_size


// ADC initialization
void adc_init()
{
  hal_adc_set_input_channel(HAL_ADC_INP_AIN0);
  hal_adc_set_reference(HAL_ADC_REF_VDD);
  hal_adc_set_input_mode(HAL_ADC_SINGLE);        // can be changed to differential
  hal_adc_set_conversion_mode(HAL_ADC_SINGLE_STEP);
  hal_adc_set_resolution(HAL_ADC_RES_8BIT);
  hal_adc_set_data_just(HAL_ADC_JUST_RIGHT);
}

void main()
{
        // Variable declarations.
        uint8_t j, i;
        //P3DIR = 0x00;

        // Initialize the ADC.
        adc_init();

        // 1. To use the radio the radio clock must be enabled.
        RFCKEN = 1;

        TMOD = 0x01;  // Timer 0 mode 1, 16-bit mode
        TR0 = 1;      // Start timer 0
        ET0 = 1;      // Enable timer 0 interrupt

        // 2. If the RF interrupt should be used, remember to set both the global interrupt enable
flag and the RF interrupt enable flag.
        RF = 1;
        EA = 1;
```

```
        // 3. By default the radio will be in PTX mode, and powered down. The last thing needed
is to power it up before it is ready for use.
        hal_nrf_set_power_mode(HAL_NRF_PWR_UP);

        P0DIR = 0xFE;
        P0 = 0;
        for(i = 0; i < 32; i++)
                rf_payload[i] = 128;
//      while(1)
        {
                while(!timer_set);
                hal_nrf_write_tx_payload(rf_payload, PAYLOAD_SIZE);
                CE_PULSE();
                timer_set = 0;
        }

        while(1)
        {
                for( j = 0; j < PAYLOAD_LUMPS; j++)
                {
                  //while(!timer_set);       //wait for another timer interrupt

                        for( i = 0; i < CHANNEL_NUMBER; i++ )
                        {
                                hal_adc_set_input_channel(i);
                                hal_adc_start();
                                while( hal_adc_busy() );

                                rf_payload[i + j*CHANNEL_NUMBER] = hal_adc_read_LSB();
                        }
                        timer_set = 0;
                }

                hal_nrf_write_tx_payload(rf_payload, PAYLOAD_SIZE);
                CE_PULSE();

        }
}
void timer0_irq() interrupt INTERRUPT_T0
{
        TL0 = TIMER_RELOAD_LSB;
        TH0 = TIMER_RELOAD_MSB;

        timer_set = 1;

}

// It is recommended to use an interrupt to receive data sent (TX_DS),
// data received (RX_DR) or max retransmit (MAX_RT) messages from the radio.
void rf_irq() interrupt INTERRUPT_RFIRQ
{
  // Read and clear IRQ flags from radio
```

```
  uint8_t irq_flags = hal_nrf_get_clear_irq_flags();
                      P0 ^= 0x01;
  switch(irq_flags)
  {
    // Transmission success
    case (1 << HAL_NRF_TX_DS):
      //radio_busy = false;
      // Data has been sent
      break;
    // Transmission failed (maximum re-transmits)
    case (1 << HAL_NRF_MAX_RT):
      // When a MAX_RT interrupt occurs the TX payload will not be removed from the TX FIFO.
      // If the packet is to be discarded this must be done manually by flushing the TX FIFO.
      // Alternatively, CE_PULSE() can be called re-starting transmission of the payload.
      // (Will only be possible after the radio irq flags are cleared)
      hal_nrf_flush_tx();
      //radio_busy = false;
      break;
  }
}
```

APPENDIX B

MICROCONTROLLER CODE FOR RECEIVER

```
/* Code for the receiver: should be a continuous receiver that transmit the received packets to a
PC through a UART communication. */
#include <stdio.h>
#include <Nordic\reg24le1.h>
#include <stdint.h>
#include "hal_nrf_hw.h"
#include "MyCustom.h"

#define CHANNEL_NUMBER 4
#define PAYLOAD_LUMPS 8
#define PAYLOAD_SIZE 32     // difining a payload size different than channel_number

// Variable declarations.
uint8_t rf_status;
uint8_t rf_payload[PAYLOAD_SIZE];
uint8_t dataready = 0;
bit write_to_uart = 0;

void main()
{
  uint8_t i;
        // Enable RF interrupt and activate the global interrupt flag.
        RF = 1;
        EA = 1;
        IP0 |= 0x10;
        IP1 |= 0x10;

        RFCKEN = 1;

        // 1. By default the radio will be in PTX mode. This means we need to active PRX mode
to use it as a receiver.
        hal_nrf_set_operation_mode(HAL_NRF_PRX);

        // 2. With the default settings Pipe 0 will be used to receive incomming packets. For the
radio to receive the packets sent by
        // project 03 it is important to configure the Pipe 0 with the right payload length (3
bytes).
        hal_nrf_set_rx_payload_width(0, PAYLOAD_SIZE);

        // Power up the radio.
        hal_nrf_set_power_mode(HAL_NRF_PWR_UP);

        // 3. To enable the receiver the Chip Enable signal should be set high permantently.
        RFCE = 1;

        //Setup the UART pins as outputs
        P0DIR = 0xDE;
        //Using the 24-pin variant chip, so there is no external P1 port
        //P1DIR = 0x00;

        // Init UART
        //custom function that sets the baud to 500k
```

```
        hal_uart_init();

        while(1)
        {
           if( write_to_uart )
           {
                        for( i = 0; i < CHANNEL_NUMBER*PAYLOAD_LUMPS; i++)
                                hal_uart_putchar(rf_payload[i]);
                    write_to_uart = 0;
           }
        }
}

// It is recommended to use an interrupt to receive data sent (TX_DS),
// data received (RX_DR) or max retransmit (MAX_RT) messages from the radio.
void rf_irq() interrupt INTERRUPT_RFIRQ
{
//      uint8_t i;
        //payload_counter = (payload_counter+1)%2;
        // 4. The status of the interrupt flags should be read out and stored in the "rf_status"
variable.
        rf_status = hal_nrf_get_clear_irq_flags();

        // It is common to use a switch to check which of the RF status bits were set.
        // Since this example will only be used as a receiver we should only expect RX_DR
interrupts, but the other interrupts
        // are included for reference.
        switch( rf_status )
        {
                case (1<<HAL_NRF_RX_DR):
                        // 5. The RF payload must be read out and put in a buffer.
                        //Toggle P0.0 high and low in order to time the length of
hal_nrf_read_rx_payload
                        //This was found to be ~200us using an oscilloscope
                        P0 |= 0x01;
                        hal_nrf_read_rx_payload(rf_payload);
                        P0 &= 0xFE;

                        write_to_uart = 1;
//                      P0 &= 0xFE;
                        break;

                // A packet was sent.
//              case (1<<HAL_NRF_TX_DS):
//                      break;

                // A packet was sent, but no acknowledge was received.
                case (1<<HAL_NRF_MAX_RT):
                        break;
        }
}
```

REFERENCES

[1.1] Sherrington CS. Flexion-reflex of the limb, crossed extension-reflex, and reflex stepping and standing. J Physiol. 40(1-2): 28-121, 1910.

[1.2] Walters ET. Injury-related behavior and neuronal plasticity: An evolutionary perspective on sensitization, hyperalgesia, and analgesia. Int Rev Neurobiol. 36:325-325, 1994.

[1.3] Merskey H, Albe-Fessard D, Bonica J, Carmon A, Dubner R, & Kerr F. Pain terms: A list with definitions and notes on usage: Recommended by the IASP subcommittee on taxonomy. Pain, 6(3): 249-252, 1979.

[1.4] Medical Data International, Market and Technology Reports, U.S. Markets For Pain Management Products, Report RP-821922, June 1999.

[1.5] King CR and Hinds PS. Quality of Life: From Nursing and Patient Perspectives. by Jones and Bartlett Publishers, Sudbury, Massachusetts, 1998.

[1.6] Ferrell BR, Cohen MZ, Rhiner M and Rozek A. Pain as a Metaphor for Illness. Part II: Family Caregivers' Management of Pain. Oncology Nursing Forum, 18(8):1315-1321, 1991.

[1.7] Juarez G, Ferrell BR. Family and Caregiver Involvement in Pain Management. Clinics in Geriatric Medicine, 12(3): 531-547, 1996.

[1.8] Ferrell BA, Ferrell BR. Pain management at home. Clin Geriatr Med. 7(4):765-76, 1991.

[1.9] Ferrell BR, Juarez G, Borneman T and Terveer A. Outcomes of pain education in community home care. Journal of Hospice and Palliative Nursing, 1(4):141-150, 1999.

[1.10] Cramer J and Spilker B. Quality of Life & Pharmacoeconomics: An Introduction," ISBN: 0-397-51845-5, published by Lippincott Williams & Wilkins, 1997.

[1.11] Phillips CJ. Pain management: health economics and quality of life considerations. Drugs, 63 (2): 47-50, 2003.

[1.12] The World Congress Leadership Summit on Manage Chronic Pain to Drive High Efficacy Rates and Increase Productvity, Atlanta, Georgia, Sept. 24, 2005.

[1.13] Zimmermann M. Behavioural investigations of pain in animals. Assessing Pain in Farm Animals, 16–27, 1986.

[1.14] Gibson TE and Paterson DA. The Detection and Relief of Pain in Animals. Proceedings of the Animal Welfare Foundation's Second Symposium, British Veterinary Association Animal Welfare Foundation, London, eds 1985.

[1.15] Morton, D. Griffiths PHM. Guidelines on the recognition of pain, distress and discomfort in experimental animals and an hypothesis for assessment. Veterinary Record, 116: 431-436, 1985.

[1.16]http://www.ninr.nih.gov/NR/rdonlyres/DC0351A6-7029-4FE0-BEEA-7EFC3D1B23AE/0/Pain.pdf

[1.17] Kuncel AM, and Grill WM. Selection of stimulus parameters for deep brain stimulation. Clin. Neurophysiol. 115(11): 2431 – 41, 2004.

[1.18] Chung J, Surmeier D, Lee K, Sorkin L, Honda C, Tsong Y and Willis W. Classification of primate spinothalamic and somatosensory thalamic neurons based on cluster analysis. J. Neurophysiol. 56(2): 308-27, 1986.

[1.19] Price DD. Central neural mechanisms that interrelate sensory and affective dimensions of pain. Molecular Interventions 2(6):392-403, 2002.

[1.20] Kandel ER, Schwartz JH, Jessell TM. Principles of Neural Science, 2000.

[1.21] Green A, Wang S, Stein J, Pereira E, Kringelbach M, Liu X, Brittain J, Aziz T. Neural signatures in patients with neuropathic pain. Neurology 72(6):569-71, 2009.

[1.22] Lee BH, Park SH, Won R, Park YG, Sohn JH. Antiallodynic effects produced by stimulation of the periaqueductal gray matter in a rat model of neuropathic pain. Neurosci. Lett. 291(1):29-32, 2000.

[1.23] Apkarian AV, Bushnell MC, Treede RD, Zubieta JK. Human brain mechanisms of pain perception and regulation in health and disease. Eur J Pain. 9(4):463-484, 2005.

[1.24] Chang JY. Brain stimulation for neurological and psychiatric disorders, current status and future direction. J. Pharmacol. Exp. Ther. 309(1):1-7, 2004.

[1.25] Marchand S, Kupers RC, Bushnell MC, Duncan GH. Analgesic and placebo effects of thalamic stimulation. Pain 105(3):481-488, 2003.

[1.26] Millan MJ. The induction of pain: An integrative review. Prog. Neurobiol. 57(1):1-164, 1999.

[1.27] Green A, Wang S, Stein J, Pereira E, Kringelbach M, Liu X, Brittain J, Aziz T. Neural signatures in patients with neuropathic pain. Neurology 72(6):569-71, 2009.

[1.28] Bandler R and Shipley MT. Columnar organization in the midbrain periaqueductal gray: Modules for emotional expression? Trends Neurosci. 17(9):379-389, 1994.

[1.29] Craig A. Pain mechanisms: Labeled lines versus convergence in central processing Annu. Rev. Neurosci. 26(1): 1-30, 2003.

[1.30] Jones E. Correlation and revised nomenclature of ventral nuclei in the thalamus of human and monkey. Stereotact. Funct. Neurosurg. 54(55):1–20, 1990.

[1.31] Mazars GJ. Intermittent stimulation of nucleus ventralis posterolateralis for intractable pain. Surg. Neurol., 4:93-95, 1975.

[1.32] Peschanski M. Trigeminal afferents to the diencephalon in the rat. Neuroscience 12:465-487, 1984.

[1.33] Mehler WR. Some neurological species differences-a posteriori Ann. N. Y. Acad. Sci. 167(1):424-468, 1969.

[1.34] Guilbaud G, Peschanski M, Gautron M and Binder D. Neurones responding to noxious stimulation in VB complex and caudal adjacent regions in the thalamus of the rat. Pain 8(3):303-318, 1980.

[1.35] Paxinos G and Watson C. The Rat Brain in Stereotaxic Coordinates, 2007.

[1.36] Diesch T, Mellor D, Johnson C, Lentle R. Electroencephalographic responses to tail clamping in anaesthetized rat pups. Lab Anim. 43(3), 224-31, 2009.

[1.37] Ritaccio A, Brunner P, Cervenka MC, Crone N, Guger C, Leuthardt E, Oostenveld R, Stacey W, Schalk G. Proceedings of the first international workshop on advances in electrocorticography. Epilepsy Behav. 19(3):204-15, 2010.

[1.38] Ball T, Kern M, Mutschler I, Aertsen A, Schulze-Bonhage A. Signal quality of simultaneously recorded invasive and non-invasive EEG. NeuroImage, 46(3):708-716, 2009.

[1.39] Sluka KA, Walsh D. Transcutaneous electrical nerve stimulation: basic science mechanisms and clinical effectiveness. J Pain 4(3):109-21, 2003.

[1.40] Rushton DN. Electrical stimulation in the treatment of pain. Disability and Rehabilitation. 24:407–15, 2002.

[1.41] Walsh DM. TENS: Clinical applications and related theory. Edinburgh: Churchhill Livingstone, 1997.

[1.42] Johnson MI. Trancutaneous electrical nerve stimulation (TENS). In: Watson T, ed. Electrotherapy, Evidence based practice, 11th ed. Edinburgh: Churchill Livingstone, 253-296, 2008.

[1.43] Ma YT, Sluka KA. Reduction in inflammation induced sensitization of dorsal horn neurons by transcutaneous electrical nerve stimulation in anesthetized rats. Exp Brain Res 137:94-102, 2001.

[1.44] Carroll D, Moore RA, McQuay HJ, Fairman F, Tramèr M, Leijon G. Transcutaneous electrical nerve stimulation (TENS) for chronic pain. Cochrane Database of Systematic Reviews 2000, Issue 4. Art. No.: CD003222.

[1.45] Simpson BA. Electrical stimulatin and the relief of pain. Elsevier, 2003.

[1.46] Weiner RL. The future of peripheral nerve stimulation. Neurol. Res., 22:299-303, 2000.

[1.47] Shealy C, Mortimer J, Teswick J. Electrical inhibition of pain by stimulation of dorsal columns: preliminary report. Anesth Analg. 46: 489-491, 1967.

[1.48] Stojanovic MP. Spinal cord stimulation: Mechanisms and clinical application; in Frontiers in pain research, edited by Lucas A., Ch. 5, 101-110, 2006.

[1.49] Brook AL, Georgy BA, Olan WJ. Spinal cord stimulation: A basic approach. Tech Vasc Interv Radiol 12: 64-70, 2009.

[1.50] Jeon Y, Huh BK. Spinal cord stimulation for chronic pain. Ann Acad Med Singapore 38: 998-1003, 2009.

[1.51] Rasche D, Rinaldi PC, Young RF, Tronnier VM. Deep brain stimulation for the treatment of various chronic pain syndromes. Neurosurg Focus 21: E8, 2006.

[1.52] Grover PJ, Pereira EAC, Green AL, Brittain JS, Owen SLF, Schweder P, Kringelbach ML, Davies PT, Aziz TZ. Deep brain stimulation for cluster headache. J Clin Neurosci 16: 861-866, 2009.

[1.53] Cameron T. Safety and efficacy of spinal cord stimulation for the treatment of chronic pain: A 20-year literature review. Journal of Neurosurgery: Spine 100(3):254-267, 2004.

[1.54] Marchand S, Kupers RC, Bushnell MC, Duncan GH. Analgesic and placebo effects of thalamic stimulation. Pain 105: 481-488, 2003.

[1.55] Gybels J. Thalamic stimulation in neuropathic pain: 27 years later. Acta Neurol Belg 101: 65-71, 2001.

[1.56] Gerhart KD, Yezierski RP, Wilcox TK, Willis WD. Inhibition of primate spinothalamic tract neurons by stimulation in periaqueductal gray or adjacent midbrain reticular formation. J Neurophysiol 51:450-466, 1984.

[1.57] Kringelbach ML, Jenkinson N, Owen SL, Aziz TZ. Translational principles of deep brain stimulation. Nat. Rev. Neurosci. 8(8):623-635, 2007.

[1.58] Andrews RJ, Neuroprotection for the new millennium. matchmaking pharmacology and technology Ann. N. Y. Acad. Sci. 939: 114-125, 2001.

[1.59] Breit S, Schulz JB, Benabid AL. Deep brain stimulation. Cell Tissue Res. 318(1):275-288, 2004.

[1.60] Akin T, and Najafi K. A telemetrically powered and controlled implantable neural recording circuit with CMOS interface circuitry. in Proceedings of IEEE 7th Mediterranean Electrotechnical Conf., 545–548, 1994.

[1.61] Akin T, Najafi K, and Bradley RM. A wireless implantable multichannel digital neural recording system for a micromachined sieve electrode. IEEE J. Solid-State Circuits, 33:109–118, 1998.

[1.62] Song HJ, Allee DR, and Speed KT. Single chip system for bio-data acquisition, digitization, and telemetry. in Proc. IEEE-ISCAS, 1848–1851, 1997.

[1.63] Mohseni P, Najafi K, Eliades S, and Wang X. Wireless multichannel biopotential recording using and integrated FM telemetry circuit. IEEE Trans. Neural Syst. Rehab. Eng., 13(3): 263–271, 2005.

[1.64] Harrison RR. A low-power integrated circuit for a wireless 100-electrode neural recording system. IEEE J. Solid-State Circuits 40:2796–2804, 2007.

[1.65] Chae M, Yang Z, Yuce M, Hoang L, Liu W. A 128-Channel 6mW Wireless Neural Recording IC with Spike Feature Extraction and UWB transmitter. IEEE Trans. Neural Syst. Rehabil. Eng., 17(4):312 – 321, 2009.

[1.66] Modarreszadeh M, and Schmidt RN. Wireless, 32-channel, EEG and epilepsy monitoring system. Proc. of the 19th International Conference of IEEE EMBS, Chicago, IL, 1157–1160, 1997.

[1.67] Irazoqui-Pastor P, Mody I, and Judy JW. In vivo recording using a wireless implantable neural transceiver. in Proc. 1st Int. IEEE-EMBS Conf. Neural Engineering, 622–625, 2003.

[1.68] Mollazadeh M, Murari K, Schwerdt H, Wang X, Thakor N, and Cauwenberghs G. Wireless multichannel acquisition of neuropotentials. IEEE Proc. Biomedical Circuits and Systems Conf. (BioCAS'2008), 49–52, 2008.

[1.69] Lapray D, Bergeler J, Dupont E, Thews O, Luhmann HJ. A novel miniature telemetric system for recording EEG activity in freely moving rats. J Neurosci Methods 168:119-126, 2008.

[1.70] Charvet G, Foerster M, Filipe S, Porcherot J, Bêche JF, Guillemaud R, Audebert P, Régis G, Zongo B, Robinet S, Condemine C, Têtu Y, Sauter F, Mestais C, Benabid AL. WIMAGINE: A wireless, low power, 64-channel ECoG recording platform for implantable BCI applications. Conf Proc Int IEEE EMBS Conf on Neural Engineering, 356-359, 2011.

[2.1] Ball T, Kern M, Mutschler I, Aertsen A, Schulze-Bonhage A. Signal quality of simultaneously recorded invasive and non-invasive EEG. Neuroimage 46:708-16, 2009.

[2.2] Engel AK, Moll CK, Fried I, Ojemann GA. Invasive recordings from the human brain: Clinical insights and beyond. Nat Rev Neurosci 6:35-47, 2005.

[2.3] Tang X, Orchard SM, Liu X, Sanford LD. Effect of varying recording cable weight and flexibility on activity and sleep in mice. Sleep 27:803-10, 2004.

[2.4] Farajidavar A, Seifert JL, Bell JE, Seo YS, Delgado MR, Sparagana S, Romero MI, Chiao JC. A wireless system for monitoring transcranial motor evoked potentials. Ann Biomed Eng. 39:517-23, 2011.

[2.5] Kant GJ, Pastel RH, Bauman RA, Meininger GR, Maughan KR, Robinson TN, Wright WL, Covington PS. Effects of chronic stress on sleep in rats. Physiol Behav 57:359-65, 1995.

[2.6] Kramer K, Kinter LB. Evaluation and applications of radiotelemetry in small laboratory animals. Physiol Genomics 13:197-205, 2003.

[2.7] Lapray D, Bergeler J, Dupont E, Thews O, Luhmann HJ. A novel miniature telemetric system for recording EEG activity in freely moving rats. J Neurosci Methods 168:119-126, 2008.

[2.8] Livezey G, Sparber S. Hyperthermia sensitizes rats to cocaine's proconvulsive effects and unmasks EEG evidence of kindling after chronic cocaine. Pharmacol Biochem Behav. 37:761-7, 1990.

[2.9] Williams P, White A, Ferraro D, Clark S, Staley K, Dudek FE. The use of radiotelemetry to evaluate electrographic seizures in rats with kainate-induced epilepsy. J Neurosci Methods. 155:39-48, 2006.

[2.10] Lin R, Lee RG, Tseng CL, Wu YF, Jiang JA. Design and implementation of wireless multi-channel EEG recording system and study of EEG clustering method. Biomed Eng-App Bas C 18: 276-83, 2006.

[2.11] Lin CT, Ko LW, Chiou JC, Duann JR, Huang RS, Liang SF, Chiu TW, Jung TP. Noninvasive neural prostheses using mobile and wireless EEG. Proc. IEEE, 96:1167-83, 2008.

[2.12] Zhu L, Chen H, Zhang X, Guo K, Wang S, Wang Y, Pei W, Chen H. Design of portable multi-channel EEG signal acquisition system. Conf Proc IEEE Biomed Eng & Info. 1-4, 2009.

[2.13] Cotugno M, Mandile P, D'Angiolillo D, Montagnese P, Giuditta A. Implantation of an EEG telemetric transmitter in the rat. Ital J Neurol Sci 17:131-4, 1996.

[2.14] Farajidavar A, McCorkle PG, Wiggins TW, Rao SMN, Haggains CE, Peng YB, Seifert JL, Romero MI, O'Grady G, Cheng LK, Sparagana S, Delgado MR, Tang S, Abell T, Chiao JC. A miniature power-efficient bidirectional telemetric platform for in-vivo acquisition of electrophysiological signals. Accepted to Conf Proc IEEE MTT-S Int. Microwave Symp. 2011.

[2.15] Zimmermann M. Ethical guidelines for investigations of experimental pain in conscious animals. Pain 16:109-10, 1983.

[2.16] Buzsaki G, Draguhn A. Neuronal oscillations in cortical networks. Science 304:1926-9, 2004.

[2.17] Fang G, Zhang C, Xia Y, Lai Y, Liu T, You Z, Yao D. The effect of different EEG derivations on sleep staging in rats: The frontal midline–parietal bipolar electrode for sleep scoring. Physiol Meas. 30:589-601, 2009.

[2.18] Hudetz AG. Effect of volatile anesthetics on interhemispheric EEG cross-approximate entropy in the rat. Brain Res, 954:123-131, 2002.

[2.19] Miller R. Theory of the normal waking EEG: From single neurones to waveforms in the alpha, beta and gamma frequency ranges. Int J Psychophysiol. 64:18-23, 2007.

[2.20] Vyazovskiy VV, Tobler I. Theta activity in the waking EEG is a marker of sleep propensity in the rat. Brain Res. 1050:64-71, 2005.

[3.1] Mendell LM. Physiological properties of unmyelinated fiber projection to the spinal cord. Exp Neurol 16: 316-332, 1966.

[3.2] Peng YB, Lin Q, Willis WD. Effects of GABA and glycine receptor antagonists on the activity and PAG-induced inhibition of rat dorsal horn neurons. Brain Res 736: 189-201, 1996.

[3.3] Ativanichayaphong T, He JW, Hagains CE, Peng YB, Chiao JC. A combined wireless neural stimulating and recording system for study of pain processing. J Neurosci Methods 170: 25-34, 2008.

[3.4] Chung J, Surmeier D, Lee K, Sorkin L, Honda C, Tsong Y and Willis W. Classification of primate spinothalamic and somatosensory thalamic neurons based on cluster analysis. J. Neurophysiol. 56(2):308-27, 1986.

[3.5] Palecek J, Dougherty P, Kim S, Paleckova V, Lekan H, Chung J, Carlton S and Willis W. Responses of spinothalamic tract neurons to mechanical and thermal stimuli in an experimental model of peripheral neuropathy in primates. J. Neurophysiol. 68(6): 1951-66, 1992.

[3.6] LINDBLOM U. Assessment of abnormal evoked pain in neurological pain patients and its relation to spontaneous pain: a descriptive and conceptual model with some analytical results. In: Advances in Pain Research and Therapy, edited by Fields HL, Dubner R, and Cervero F. New York: Raven, 1985, vol. 9, p.409-423.

[3.7] Zimmermann M. Ethical guidelines for investigations of experimental pain in conscious animals. Pain 16: 109-110, 1983.

[3.8] Bromm B. Modern techniques to measure pain in healthy man. Methods and Findings in Experimental and Clinical Pharmacology, 7(3): 161-169, 1985.

[3.9] Euchner-Wamser I, Meller S, Gebhart G. A model of cardiac nociception in chronically instrumented rats: Behavioral and electrophysiological effects of pericardial administration of algogenic substances. Pain, 58(1):117-128, 1994.

[3.10] Murrell J, Mitchinson S, Waters D, Johnson C. Comparative effect of thermal, mechanical, and electrical noxious stimuli on the electroencephalogram of the rat. Br J Anaesth. 98(3): 366-71, 2007.

[3.11] Farajidavar A, Hagains CE, Peng YB, Behbehani K, Chiao J.-C. Recognition and Inhibition of Dorsal Horn Nociceptive Signals within a Closed-loop System. Conf Proc IEEE Eng Med Biol Soc. 1535-8, 2010.

[3.12] Huang J, Chang JY, Woodward DJ, Baccalá LA, Han JS, Wang JY, et al. Dynamic neuronal responses in cortical and thalamic areas during different phases of formalin test in rats. Exp Neurol. 200(1):124-134, 2006.

[3.13] Jinks SL, Antognini JF, Carstens E. Isoflurane depresses diffuse noxious inhibitory controls in rats between 0.8 and 1.2 minimum alveolar anesthetic concentration. Anesth Analg. 97(1): 111-6, 2003.

[3.14] Engel AK, Moll CKE, Fried I, Ojemann GA. Invasive recordings from the human brain: Clinical insights and beyond. Nat Rev Neurosci. 6(1):35-47, 2005.

[3.15] Dzoljic E, van Leeuwen R, de Vries R, Dzoljic MR. Vigilance and EEG power in rats: Effects of potent inhibitors of the neuronal nitric oxide synthase. Naunyn Schmiedebergs Arch Pharmacol. 356(1): 56-61, 1997.

[3.16] Ichinose F, Miyazaki M, Goto T, Takahashi H, Terui K, Niimi Y, et al. Electroencephalographic responses to the formalin test in rats. Pain, 80(1-2):251-256, 1999.

[3.17] Kleinlogel H. Analysis of the vigilance stages in the rat by fast fourier transformation. Neuropsychobiology, 23(4):197-204, 1990.

[3.18] Handwerker HO and Brune K Deutschsprachige Klassiker der Schmerzforshung—Classical German Contributions to Pain Research, Tagblatt-Druckerei KG, Hassfurt, 1987.

[3.19] Kruger L. Methods in pain research. CRC press, Methods & new frontiers in neuroscience, 2001.

[3.20] Dubuisson D, Dennis SG. The formalin test: A quantitative study of the analgesic effects of morphine, meperidine, and brain stem stimulation in rats and cats. Pain, 4:161-174, 1978.

[3.21] Buzsaki G, Draguhn A. Neuronal oscillations in cortical networks. Science 2004;304:1926-9.

[4.1] Ativanichayaphong T, He JW, Hagains CE, Peng YB, Chiao JC. A combined wireless neural stimulating and recording system for study of pain processing. J Neurosci Methods 170: 25-34, 2008.

[4.2] Kandel ER, Schwartz JH, Jessell TM. Principles of neural science, 4th ed., McGraw-Hill, New York. 2000.

[4.3] Obeid I, Wolf PD. Evaluation of spike-detection algorithms for a brain-machine interface application. IEEE Trans Biomed Eng, 51: 905-911, 2004.

[4.4] Wheeler BC. Automatic discrimination of single units. In: Methods for neural ensemble recordings, edited by Nicolelis MAL, CRC press, New York, p. 61-77, 1999.

[4.5] Farajidavar A, Hagains CE, Peng YB, Behbehani K, Chiao JC. Recognition and Inhibition of Dorsal Horn Nociceptive Signals within a Closed-loop System. Conf Proc IEEE Eng Med Biol Soc 1: 1535-1538, 2010.

[4.6] Panzeri S, Petersen RS, Schultz SR, Lebedev M, Diamond ME. The role of spike timing in the coding of stimulus location in rat somatosensory cortex. Neuron 29: 769-777, 2001.

[4.7] Weidner C, Schmelz M, Schmidt R, Hammarberg B, Orstavik K, Hilliges M, Torebjörk HE, Handwerker HO. Neural signal processing: The underestimated contribution of peripheral human C-fibers. J Neurosci 22: 6704-6712, 2002.

[4.8] Kuncel AM, Grill WM. Selection of stimulus parameters for deep brain stimulation. Clin Neurophysiol 115: 2431-2441, 2004.

[4.9] Paxinos G, Watson C. The rat brain in stereotaxic coordinates. San Diego: Academic press, 1998, p.48.

[4.10] Senapati AK, Huntington PJ, Peng YB. Spinal dorsal horn neuron response to mechanical stimuli is decreased by electrical stimulation of the primary motor cortex. Brain Res 1036 (1-2): 173-179, 2005.

[4.11] Behbehani MM. Functional characteristics of the midbrain periaqueductal gray. Prog Neurobiol 46: 575-605, 1995.

[4.12] Peng YB, Lin Q, Willis WD. Involvement of alpha-2 adrenoceptors in the periaqueductal gray-induced inhibition of dorsal horn cell activity in rats. J Pharmacol Exp Ther 278(1):125-35, 1996.

[4.13] Peng YB, Lin Q, Willis WD. The role of 5-HT3 receptors in periaqueductal gray-induced inhibition of nociceptive dorsal horn neurons in rats. J Pharmacol Exp Ther 276(1):116-24, 1996.

[4.14] Sandkühler J, Gebhart GF. Relative contributions of the nucleus raphe magnus and adjacent medullary reticular formation to the inhibition by stimulation in the periaqueductal gray of a spinal nociceptive reflex in the pentobarbital-anesthetized rat. Brain Res 305: 77-87, 1984.

[4.15] Coimbra NC, Brandao ML. Effects of 5-HT2 receptors blockade on fear-induced analgesia elicited by electrical stimulation of the deep layers of the superior colliculus and dorsal periaqueductal gray. Behav Brain Res 87: 97-103, 1997.

[4.16] Gerhart KD, Yezierski RP, Wilcox TK, Willis WD. Inhibition of primate spinothalamic tract neurons by stimulation in periaqueductal gray or adjacent midbrain reticular formation. J Neurophysiol 51: 450-466, 1984.

[4.17] Mensah-Brown EP, Garey LJ. The superior colliculus of the camel: A neuronal-specific nuclear protein (NeuN) and neuropeptide study. J Anat 208: 239-250, 2006.

[4.18] Beitz AJ, Periaqueductal gray. In: Paxinos, G. Editor, 1995. The Rat Nervous System, 2nd ed. Academic Press, San Diego, 1995, pt. III, chapt. 10, p. 173–182.

[4.19] Hermann DM, Luppi PH, Peyron C, Hinckel P, Jouvet M. Afferent projections to the rat nuclei raphe magnus, raphe pallidus and reticularis gigantocellularis pars alpha demonstrated by iontophoretic application of choleratoxin (subunit b). J Chem Neuroanat 13: 1-21, 1997.

[4.20] Millan MJ. Descending control of pain. Prog Neurobiol 66: 355-474, 2002.

[4.21] Owen SL, Heath J, Kringelbach M, Green AL, Pereira EA, Jenkinson N, Jegan T, Stein JF, Aziz TZ. Pre-operative DTI and probabilisitic tractography in four patients with deep brain stimulation for chronic pain. J Clin Neurosci 15: 801-805, 2008.

[4.22] Zimmermann M. Ethical guidelines for investigations of experimental pain in conscious animals. Pain 16: 109-110, 1983.

[5.1] Gonzalez AA, Jeyanandarajan D, Hansen C, Zada G, and Hsieh PC. Intraoperative neurophysiological monitoring during spine surgery: A review. Neurosurg. Focus. 27:E6, 2009.

[5.2] Kothbauer K, Deletis V, and Epstein FJ. Intraoperative spinal cord monitoring for intramedullary surgery: An essential adjunct. Pediatr. Neurosurg. 26:247-254,1997.

[5.3] Wilder RT, Flick RP, Sprung J, Katusic SK, Barbaresi WJ, Mickelson C, Gleich SJ, Schroeder DR, Weaver AL, and Warner DO. Early exposure to anesthesia and learning disabilities in a population-based birth cohort. Anesthesiology. 110:796-804, 2009.

[5.4] Hu Y, Luk KD, Lu WW, Holmes A, and Leong JC. Prevention of spinal cord injury with time-frequency analysis of evoked potentials: An experimental study. J. Neurol. Neurosurg. Psychiatry. 71:732-740, 2001.

[5.5] McManus CD, Neubert KD, and Cramer E. Characterization and elimination of AC noise in electrocardiograms: A comparison of digital filtering methods. Comput. Biomed. Res. 26:48-67, 1993.

[5.6] Chimeno F, and Areny P. A comprehensive model for power line interference in biopotential measurements. IEEE Trans. Instrum. Meas. 49:535-540, 2000.

[5.7] Lapray D, Bergeler J, Dupont E, Thews O, and Luhmann HJ. A novel miniature telemetric system for recording EEG activity in freely moving rats. J. Neurosci. Methods 168:119-126, 2008.

[5.8] Lin CT, Ko LW, Chiou JC, Duann JR, Huang RS, Liang SF, Chiu TW, and Jung TP. Noninvasive neural prostheses using mobile and wireless EEG. Proc. IEEE. 96:1167-1183, 2008.

[5.9] Chae MS, Yang Z, Yuce MR, Hoang L and Liu W. A 128-channel 6 mW wireless neural recording IC with spike feature extraction and UWB transmitter. IEEE Trans. Neural Syst. Rehabil. Eng. 17:312-321, 2009.

[5.10] Sodagar AM, Wise KD, and Najafi K. A fully integrated mixed-signal neural processor for implantable multichannel cortical recording. IEEE Trans. Biomed. Eng. 54:1075-1088, 2007.

[5.11] Jovanov E, Milenkovic A, Otto C, and de Groen PC. A wireless body area network of intelligent motion sensors for computer assisted physical rehabilitation. J. Neuroeng. Rehabil. 2:6, 2005.

[5.12] Vehkaoja AT, Verho JA, Puurtinen MM, Nojd N, Lekkala JO and Hyttinen JA. Wireless head cap for EOG and facial EMG measurements. Conf. Proc. IEEE Eng. Med. Biol. Soc. 6:5865-5868, 2005.

[5.13] Mahfouz MR, Kuhn MJ, To G, Fathy AE. Integration of UWB and wireless pressure mapping in surgical navigation. IEEE Trans. Microwave Theory Tech. 57:2550-2564, 2009.

[5.14] Di Lazzaro V, Oliviero A, Pilato F, Saturno E, Dileone M, Mazzone P, Insola A, Tonali PA and Rothwell JC. The physiological basis of transcranial motor cortex stimulation in conscious humans. Clin. Neurophysiol. 115:255-266, 2004.

[5.15] Tinazzi M, Valeriani M, Moretto G, Rosso T, Nicolato A, Fiaschi A, and Aglioti SM. Plastic interactions between hand and face cortical representations in patients with trigeminal neuralgia: A somatosensory-evoked potentials study. Neuroscience. 127:769-776, 2004.

[5.16] Deletis V, and Sala F. Intraoperative neurophysiological monitoring of the spinal cord during spinal cord and spine surgery: A review focus on the corticospinal tracts. Clin. Neurophysiol. 119:248-264, 2008.

[5.17] Journee HL, Polak HE and De Kleuver M. Conditioning stimulation techniques for enhancement of transcranially elicited evoked motor responses. Neurophysiol. Clin. 37:423-430, 2007.

[5.18] Macdonald DB. Intraoperative motor evoked potential monitoring: Overview and update. J. Clin. Monit. Comput. 20:347-377, 2006.

[5.19] Langeloo DD, Journee HL, de Kleuver M, and Grotenhuis JA. Criteria for transcranial electrical motor evoked potential monitoring during spinal deformity surgery: A review and discussion of the literature. Neurophysiol. Clin. 37:431-439, 2007.

[5.20] Langeloo DD, Lelivelt A, Louis Journee H, Slappendel R and de Kleuver M. Transcranial electrical motor-evoked potential monitoring during surgery for spinal deformity: A study of 145 patients. Spine (Phila Pa 1976). 28:1043-1050, 2003.

[5.21] Quinones-Hinojosa A, Lyon R, Zada G, Lamborn KR, Gupta N, Parsa AT, McDermott MW, and Weinstein PR. Changes in transcranial motor evoked potentials during intramedullary spinal cord tumor resection correlate with postoperative motor function. Neurosurgery. 56:982-993, 2005.

[5.22] Ativanichayaphong T, He JW, Hagains CE, Peng YB and Chiao J.C. A combined wireless neural stimulating and recording system for study of pain processing. J. Neurosci. Methods. 170:25-34, 2008.

[5.23] Du P, O'Grady G, Egbuji JU, Lammers WJ, Budgett D, Nielsen P, Windsor JA, Pullan AJ, Cheng LK, “High-resolution mapping of in vivo gastrointestinal slow wave activity using flexible printed circuit board electrodes: methodology and validation,” Ann Biomed Eng. 37(4): 839-846, 2009.

BIOGRAPHICAL INFORMATION

Aydin Farajidavar received his B.Sc. and M.Sc. degrees in Biomedical Engineering (Bioelectric), from Shahed University and Amirkabir University of Technology (Tehran Polytechnic) in 2003 and 2006, respectively. During his Master's education, he worked on modeling of biological systems and neural disorders in the Neuromuscular Laboratory. In 2008, he joined *iMEMS* group, to pursue his Ph.D. in Bioengineering at the University of Texas Arlington under the supervision of Dr. J.C. Chiao His research focused on the design and fabrication of wireless systems and computer algorithms for neural signal acquisition and processing. Aydin received his Ph.D. in Bioengineering at the University of Texas Arlington (UTA) in 2011. He is the recipient of various awards, including the 2011 Alfred and Janet Potvin Outstanding Bioengineering Student; the 2010 Graduate Dean's Award in Annual Celebration of Excellence by Students (ACES); and the Outstanding Poster Award in UT Metroplex Day (2009). Aydin has authored/co-authored 12 peer-reviewed conference and journal publications, and 14 abstracts. He is a member of International Neural Network Society (INNS), Society for Neuroscience (SfN), Biomedical Engineering Society (BMES) and student member of IEEE.